

**Synthesis and physicochemical evaluation of a series
of boron dipyrromethene dye derivatives for
potential utility in antimicrobial photodynamic
therapy and nonlinear optics**

**A thesis submitted in fulfilment of the requirements
for the degree of**

MASTERS OF SCIENCE

of

RHODES UNIVERSITY

by

Gugu Patience Kubheka

February 2016

Dedication

My dad

Mduduzi Nicholas Kubheka

My grandmother

Nomanzi Idah Kubheka

My son and fiancé

Tlhangga Mvuyelwa and Khethobole Cassius Sekgota

Acknowledgements

“Mbonge uJehova mphefumulo wami, nakho konke okuphakathi kwami makulibonge igama lakhe elingcwele, ungakhohlwa imisebenzi yakhe akwenzela yona emihle”.(Amahubo 103)

All praises go to God Almighty for being my Shepherd and my source of strength.

I would like to express my heartfelt gratitude to my supervisor Dr John Mack for his continued assistance, patience and support throughout this project. I have learnt a lot from your supervision and it was a great pleasure working with you.

I am deeply grateful to Professor Tebello Nyokong “the golden girl” for the opportunity to work under her co-supervision as well as the international opportunity she afforded me. You are an inspiration and amazing.

I must also acknowledge Professor Kimura and Professor Kobayashi from Shinshu University for the scientific knowledge they shared with me and for the opportunity to work with them and in their laboratory.

My gratitude also go to Dr Edith Amuhaya, Dr Entunes and Dr Imran Uddin for their assistance and inputs throughout this project.

My thanks also go to S22, F22 and Kimura labs for the great time and for forever willing to help and share their scientific knowledge with me. I consider it a privilege and an honour to have worked with brilliant people like you.

A special thanks to my friends Dr Mthethwa, Dr Mkhize, Dr Nyoni, Dr Maringa, Munya, Nokwanda and the Saturday bible study group (David, Maureen, Sister Bola, Sister Rachel,

etc) for keeping me sane throughout this research by your encouraging words, love and support. Much love for you guys.

It gives me great pleasure to also acknowledge my fiancé (Khethobole Sekgota) for sharing his organic chemistry skills, knowledge and for making my project fun. You are the best *monna wa ka*.

This work was supported by the DST/NRF South African Research Chairs Initiative for Professor of Medicinal Chemistry and Nanotechnology, and by the South Africa/Japan Joint Science and Technology Research Collaboration (uid: 92425) promoted by the Japanese Society for the Promotion of Science and the National Research Foundation (NRF) (to Prof. Tebello Nyokong). Financial support for the research was also provided by NRF through a CUSR grant (uid: 93627) and a China-South Africa joint research program in cooperation with The National Natural Science Foundation of China (NSFC) (uid: 95421) (to Dr. John Mack). This work was also supported by the CSIR National Laser Centre, Rental Pool Programme, and the theoretical calculations were carried out at the Centre for High Performance Computing in Cape Town, South Africa.

Last but not least I am deeply grateful to my family in East London and KwaZulu Natal for the encouragement, patience and for their endless love and support.

ABSTRACT

A series of new BODIPY dye derivatives have been synthesized and characterized using various characterization tools such as $^1\text{H-NMR}$, MALDI-TOF mass spectrometry, FT-IR, UV-visible spectrophotometry and elemental analysis. The aniline-substituted BODIPY derivative was further coordinated with gold nanorods and the characterization was achieved by transmission electron microscopy (TEM), X-ray diffractometry (XRD) and X-ray photoelectron spectroscopy (XPS). In addition to this dye, quaternized BODIPY dyes were also synthesized and investigated for their potential utility as photosensitizers in antimicrobial photodynamic therapy (APDT). BODIPY dyes with pyrene substituted styryl groups were embedded in polymer thin film using poly(bisphenol A carbonate) (PBC) to study their optical limiting properties. The optical limiting values of these BODIPY dyes once embedded in thin films were found to be greatly improved and the limiting intensity of each film was well below the maximum threshold which is set to be $0.95 \text{ J}\cdot\text{cm}^{-2}$. The physicochemical properties and NLO parameters of all of the synthesized dyes were investigated.

Title Page.....	i
Dedication	ii
Acknowledgements.....	iii
Abstract.....	v
Table of Contents.....	vi
List of Abbreviations	x
List of Symbols	iii
List of Figures	v
List of Schemes.....	ii
List of Tables	iii
<i>Chapter1</i>	1
1. INTRODUCTION	2
1.1. BODIPY	4
1.1.1. <i>History and structure</i>	4
1.1.2. <i>Synthetic methodologies</i>	7
1.1.2.1. <i>Synthesis of the parent BODIPY core</i>	8
1.1.2.2. <i>Synthesis of asymmetrical and symmetrical BODIPY dyes</i>	9
1.1.3. <i>Derivatization of the BODIPY framework</i>	11
1.1.4. <i>physicochemical properties of BODIPY dyes</i>	14
1.1.4.1. <i>Absorption spectra of BODIPY dyes</i>	16

1.1.4.2. Fluorescence quantum yields and lifetimes of BODIPY dyes	17
1.1.4.3. Singlet oxygen quantum yield of BODIPY dyes	19
1.1.5. Application of BODIPY dyes.....	20
1.2. BODIPY dyes in antimicrobial photodynamic therapy (APDT).....	21
1.2.1. BODIPY dyes synthesised	23
1.3. BODIPY dyes in nonlinear optics (NLO).....	25
1.3.1. Mechanisms in optical limiting	28
1.3.2. Optical limiting parameters	30
1.3.3.. BODIPY dyes synthesised	32
1.4. Summary of aims	33
Chapter 2.....	35
2. EXPERIMENTAL SECTION	36
2.1. Materials	36
2.1.1. Synthesis of BODIPYs 1-8	36
2.1.2. Synthesis of goldnanorods (AuNRs).....	36
2.1.3. Synthesis of BODIPY 9	36
2.2. Instrumentation	37
2.3. Synthesis	40
2.4. Summary	52
Chapter 3.....	53

3. RESULTS AND DISCUSSION	54
3.1. Synthesis and characterization	54
3.1.1. Syntheses.....	54
3.1.2. Characterization.....	58
3.1.3. Optical spectroscopy.....	66
3.2. Physicochemical properties.....	72
3.2.1. Fluorescence studies	72
3.2.2. Photochemical studies	78
Chapter 4.....	81
4.1. Nonlinear optical (NLO) parameters.....	82
4.1.1. Nonlinear absorption coefficients (β_{eff}) and sequential photon (RSA) mechanism	83
4.1.2. Second-order hyperpolarizability (γ) and third-order nonlinear susceptibility ($Im[\chi^{(3)}]$).....	88
4.1.3. Optical limiting threshold (I_{lim}).....	89
4.4. Summary.....	91
Chapter 5.....	92
5.1. Introduction	93
5.2. experimental section.	98
5.2.1. Materials.....	98
5.2.2. Instrumentation	98
5.2.3. Preparation of BODIPY-cyclodextrin inclusion complexes	99

5.3. Results and discussion	99
5.3.1. <i>Uv-visible absorption studies</i>	99
5.3.2. <i>Fluorescence studies</i>	105
5.3.3. <i>Circular dichroism studies</i>	107
5.4. Summary	114
Chapter 6.....	116
6. GENERAL CONCLUSIONS AND FUTURE PROSPECTS.....	117
6.1. <i>Conclusions</i>	117
6.2. <i>Future prospects</i>	118
REFERENCES	119

List of Abbreviations

2PA	Two-photo absorption
A. A.	Ascorbic acid
APDT	Antimicrobial photodynamic therapy
AuNRs	Gold nanorods
$\text{BF}_3 \cdot \text{OEt}_2$	boron trifluoride diethyl etherate
BODIPY	Borondipyrromethene
CTAB	Cetyltrimethylammonium bromide
CD	Circular dichroism
CDx	Cyclodextrin
DCM	Dichloromethane
DMF	Dimethylformamide
DMSO	Dimethylsulfoxide
DPBF	Diphenylisobenzofuran
ESI-MS	Electrospray ionization mass spectrometry
ESA	Excited state absorption
edtm	electric dipole transition moment
F	Fluorescence
FT-IR	Fourier transform-infrared

HOMO	Highest occupied molecular orbital
IC	Internal conversion
ICD	Induced circular dichroism
ISC	Intersystem crossing
LUMO	Lowest unoccupied molecular orbital
MALDI-TOF-MS spectrometry	Matrix-assisted laser desorption/ionization time of flight mass
NIR	Near infra-red
NMR	Nuclear magnetic resonance
NLO	Nonlinear optics
NRs	Nanorods
PDT	Photodynamic therapy
P	Phosphorescence
<i>p</i> -chloranil	tetrachloro-1,4-benzoquinone
PBC	poly(bisphenol A carbonate)
Ps	Photosensitization
PTT	Photothermal therapy
RSA	Reverse saturable absorption
SPR	Surface plasmon resonance

TD-DFT	Time dependent Density-Functional Theory
TEM	Transmission electron microscopy
TCSPC	Time correlated single photon counting
TFA	trifluoroacetic acid
TEA	triethylamine
UV-Vis	Ultraviolet-visible
XRD	X-ray diffraction
XPS	X-ray photoelectron spectroscopy
VR	Vibrational relaxation

List of Symbols

ΔA	Change in absorbance
β_{eff}	Nonlinear absorption coefficients
ϵ	Molar extinction coefficient
h	Planck's constant
$h\nu$	Light
I	Light intensity
I_{lim}	Limiting intensity
$I_{\text{m}}[\chi^{(3)}]$	Imaginary third order susceptibility
γ	Second order hyperpolarizability
M	Concentration in molarity
m/z	Mass to charge ratio
η	Refractive indexes of solvent
S_0	Ground singlet state
S_1	Excited singlet state
Φ_{F}	fluorescence quantum yield
Φ_{Δ}	Singlet oxygen quantum yield
$^1\text{O}_2$	Singlet oxygen
$^3\text{O}_2$	Ground state triplet oxygen

τ_0	Radiative lifetime
τ_F	Fluorescence lifetime
λ	Wavelength

List of Figures:

- Figure 1.1.: (a) – (c) Generic structure of common fluorophores; (d) BODIPY core and its IUPAC numbering system.
- Figure 1.2. Molecular structure of i) BODIPY core, *meso*-unsubstituted ii) asymmetrical and iii) symmetrical BODIPY dyes.
- Figure 1.3. Jablonski diagram for a molecule upon excitation. A = Absorption; F = Fluorescence; P = Phosphorescence; Ps = Photosensitization; IC = Internal conversion; ISC = Intersystem crossing, K_{nr} = non-radiative decay.
- Figure 1.4. Typical molecular orbitals and Absorption (blue line) and Emission (red line) spectrum of BODIPY dye.
- Figure 1.5. Typical fluorescence decay curve of BODIPY dyes.
- Figure 1.6. Schematic diagram showing cell death after APDT.
- Figure 1.7. BODIPY dyes reported in literature for APDT (i and ii) and PDT (iii, iv, and v).
- Figure 1.8. BODIPY dyes synthesised in this work for APDT.
- Figure 1.9. (A) A typical open-aperture z-scan curve showing a RSA behaviour of an optical limiter, and (B) A schematic representation of the ideal functioning of a BODIPY dye optical limiter under normal and high intensity light.
- Figure 1.10. The behaviour of an ideal optical limiter, I_{in} = incident intensity, I_{out} = transmitted intensity, T = transmittance.
- Figure 1.11. BODIPY dyes reported in literature for NLO.

- Figure 1.12. Energy level diagram for (A) one photon absorption (OPA), two photon absorption (2PA) and emission and (B) excited-state absorption (ESA).
- Figure 1.13. BODIPY dyes synthesised in this work for NLO studies.
- Figure 2.1. Synthesis of gold nanorods through continuous secondary growth.
- Figure 3.1. Chemical structure of BODIPY **1**.
- Figure 3.2. Chemical structure of BODIPY **2** and **3**.
- Figure 3.3. Chemical structure of BODIPY **4**.
- Figure 3.4. Chemical structure of BODIPY **5**.
- Figure 3.5. Chemical structure of BODIPY **6**.
- Figure 3.6. IR spectra of BODIPY dyes (i) **1(a)**, (ii) **4** (Chapter 2) and (iii) **3** showing the disappearance of the nitro group and the appearance of the amino group and the presence of the methyl group.
- Figure 3.7. (A) XRD pattern of (i) **3**, AuNRs (ii) and **3**-AuNR (iii). And (B) TEM images of (i) AuNRs in aqueous and (ii) **3**-AuNR in aqueous-DMSO (1:1) solution.
- Figure 3.8. XPS spectra of (A) wide scan for (i) BODIPY **3** and (ii) **3**-AuNRs and (B) and (C) expanded wide scan for (i) BODIPY **3** and (ii) **3**-AuNRs, wide scan for (i) BODIPY **3** and (ii) **3**-AuNRs.
- Figure 3.9. A: IR spectra of BODIPY dyes (i) **2(b)**, (ii) **4(a)** and (iii) **4(b)** showing the presence of aromatic and aliphatic alkanes, aromatic amines and the SO₂ group. B: MALDI-TOF mass spectrum of **4(a)** highlighting the expected mass.

- Figure 3.10. MALDI-TOF mass spectrum of A: **5(a)** and B: **5(b)** highlighting the expected mass.
- Figure 3.11. IR spectra of BODIPY dyes (i) **2(c)**, (ii) **2(a)** (iii) **6(a)** and (iv) **6(b)** showing the presence and absence of the OH group.
- Figure 3.12. Normalized absorption spectra of A: (i) **3**-AuNR in DMSO: H₂O (1:1), (ii) BODIPY **3** in DMSO and (iii) AuNRs in H₂O; B: (i) **1(b)**, (ii) **2(b)** in DCM (iii) BODIPY **4(a)** and (iv) BODIPY **4(b)** in acetone.
- Figure 3.13. The HOMO and LUMO of the B3LYP optimized geometry of **3** at an isosurface values of 0.02 a.u. MO energies in TD-DFT calculations (Bottom) at the CAM-B3LYP/6-31G(d) level of theory for the B3LYP/6-31G(d) optimized geometries of 1,3,5,7-tetramethyl-meso-phenyl-BODIPY (BDY), **2** (**0**), its 2,6-dibromo-analogue (**2**), tri- and tetra-bromo analogues with bromines added at the meta-positions of the phenyl ring (**3** and **4**), **3** (**5**) and **4** (**6**). The HOMO and LUMO for each compound are highlighted with thicker black lines. The calculated HOMO-LUMO gaps and energies for the main BODIPY absorption bands are plotted against a secondary axis.
- Figure 3.14. . Normalized absorption spectra of BODIPY A: (i) **1(a)**, (ii) **1(c)**, (iii) **5(a)** and (iv) **5(b)** in DCM; B: (i) **5(b)**, (ii) **5(a)** embedded in PBS as a thin film, (iii) **5(b)** and (iv) **5(a)**.
- Figure 3.15. Normalized absorption spectra of BODIPY A: (i) **1(d)**, (ii) **2(c)** and (iii) **6(b)**; B: (i) **1(a)**, (ii) **2(a)** and (iii) **6(a)** in DCM.

- Figure 3.16. Normalized absorption spectra of BODIPY (i) **3**-AuNRs in DMSO:H₂O (1:1) and (ii) **3** in DMSO and emission spectra of BODIPY (iii) **3** in DMSO and (iv) **3**-AuNRs in DMSO:H₂O (1:1).
- Figure 3.17. Normalized absorption spectra of BODIPY (i) **4(a)** and (ii) **4(b)** and emission spectra of BODIPY (iii) **4(a)** and (iv) **4(b)** in DMSO.
- Figure 3.18. Normalized absorption spectra of BODIPY (i) **5(b)** and (ii) **5(a)** and emission spectra of BODIPY (iii) **5(b)** and (iv) **5(a)** in DMSO.
- Figure 3.19. Normalized absorption spectra of BODIPY (i) **6(b)** and (ii) **6(a)** and emission spectra of BODIPY (iii) **6(b)** and (iv) **6(a)** in DCM.
- Figure 3.20. Figure 3.20. Fluorescence decay curve of (i) BODIPY**3** in DMSO and (ii) **3**-AuNRs in DMSO:H₂O (1:1).
- Figure 3.21. Fluorescence decay curve of BODIPY (i) **5(b)** and (ii) **5(a)** in DMSO
- Figure 3.22. Photodegradation of DPBF in the presence of BODIPY**3** in DMSO in an interval of 3 min.
- Figure 3.23. Photodegradation of DPBF in the presence of BODIPY (i) **4(a)** and (ii) **4(b)** in DMSO in an interval of 3 min.
- Figure 4.1. Open aperture z-scan profiles of BODIPY (i) **5(a)** and (ii) **5(b)** in DMSO.
- Figure 4.2. Z Open aperture z-scan profiles of BODIPY (A) **5(a)** and (B) **5(b)** in DMSO in different concentrations.
- Figure 4.3. Open aperture z-scan profiles of BODIPY (i) **5(b)** and (ii) **5(a)** embedded in PBS as a thin film.

Figure 4.4. Open aperture z-scan profiles of BODIPY (i) **5(a)**, (ii) **5(b)** in DMSO, (iii) **5(a)** and (iv) **5(b)** embedded in PBS as a thin film.

Figure 4.5. Open aperture z-scan profiles of BODIPY (i) **6(b)** and (ii) **6(a)** in DCM.

Figure 4.6. A: Input intensity vs output intensity plot for BODIPY (i) **6(a)** and (ii) **6(b)** in DCM. B: Transmittance vs input fluence (I_0) curves for (i) **6(a)** and (ii) **6(b)** in DCM. The black solid line represents linear transmission.

Figure 4.7. A: Input intensity vs output intensity plot for BODIPY (i) **5(a)**, (ii) **5(b)** embedded in PBS as thin films, (iii) **5(b)** and (iv) **5(a)** in DMSO. B: Transmittance vs input fluence (I_0) curves for (i) **5(b)**, (ii) **5(a)** embedded in PBS as thin films, (iii) **5(a)** and (iv) **5(b)** in DMSO. The black solid line represents linear transmission.

Figure 5.1. The structures of α , β , and γ -CDXs and their molecular dimensions.

Figure 5.2. BODIPY dyes synthesised in this work to form inclusion complexes with CDXs.

Figure 5.3. Absorption spectra of BODIPY **i** in aqueous solution in the absence (a) and (g) and in the presence of alpha (A) and beta (B) CDXs: (b) $[\alpha\text{-CDx}] = 0.014$, (c) 0.028, (d) 0.056, (f) 0.112 and (h) $[\beta\text{-CDx}] = 0.012$, (i) 0.024, (j) 0.048, (k) 0.096, (l) 0.192 mol dm⁻³.

Figure 5.4. Absorption spectra of BODIPY **ii** in aqueous solution in the absence (a) and (g) and in the presence of alpha (C) and beta (D) CDXs: (b) $[\alpha\text{-CDx}] = 0.014$, (c) 0.028, (d) 0.056, (f) 0.112 and (h) $[\beta\text{-CDx}] = 0.012$, (i) 0.024, (j) 0.048, (k) 0.096, (l) 0.192 mol dm⁻³.

Figure 5.5. Absorption spectra of BODIPY **iii** in aqueous solution in the absence (a), (g) and (m) in the presence of alpha (E), beta (F) and gamma (G) CDXs: (b) $[\alpha\text{-CDx}] =$

0.011 (c) 0.022 , (d) 0.044, (f) 0.088; (h) [β -CDx] = 0.009, (i) 0.018, (j) 0.036, (k) 0.072, (l) 0.144 and (m) [γ -CDx]= 0.008 (n) 0.016 , (o) 0.032, (p) 0.064, (q) 0.128 mol dm⁻³.

Figure 5.6. Absorption spectra of BODIPY **iv** in aqueous solution in the absence (a), (g) and (m) in the presence of alpha (E), beta (F) and gamma (G) CDxs: (b) [α -CDx] = 0.011 (c) 0.022 , (d) 0.044, (f) 0.088 and (h) [β -CDx] = 0.009, (i) 0.018, (j) 0.036, (k) 0.072 mol dm⁻³.

Figure 5.7. Fluorescence spectra of BODIPY **i** (A) and **ii** (B) in aqueous solution in the absence (a) in the presence of alpha (b) and beta (c) CDx rings (0.112 and 0.192 mol dm⁻³, respectively).

Figure 5.8. .Fluorescence spectra of BODIPY **i** (C) and **ii** (D) in aqueous solution in the absence (a) in the presence of alpha (b), beta (c) and gamma (d) CDx rings (0.088, 0.144 and 0.128 mol dm⁻³, respectively).

Figure 5.9. (A) Absorption (i) and CD spectra of BODIPY **i** in the presence of (ii) β -CDx and (iii) α -CDx (0.0615 and 0.07 mol.dm⁻³, respectively). (B)Schematic configurations of **i**-CDx inclusion complex.

Figure 5.10. (A) Absorption (i) and CD spectra of BODIPY **ii** in the presence of (ii) β -CDx and (iii) α -CDx (0.0615 and 0.07 mol.dm⁻³, respectively). (B)Schematic configurations of **ii**-CDx inclusion complex.

Figure 5.11. (A) Absorption (i) and CD spectra of BODIPY **iii** in the presence of (ii) β -CDx, (iii) γ -CDx and (iv) α -CDx (0.04655, 0.0399 and 0.0532 mol.dm⁻³, respectively) (B)Schematic configurations of **iii**-CDx inclusion complex.

Figure 5.12. (A) Absorption (i) and CD spectra of BODIPY **ii** in the presence of (ii) β -CDx and (iii) α -CDx. (0.0458 and 0.0528 mol.dm⁻³, respectively) (B) Schematic configurations of **ii**-CDx inclusion complex.

List of Schemes

Scheme 1.1. Different pathways for the synthesis of the BODIPY core.

Scheme 1.2. General synthetic route for asymmetrical and symmetrical BODIPY dyes.

Scheme 1.3. Synthesis of symmetrical BODIPY dyes using different aldehyde derivatives.

Scheme 2.1. Synthesis of BODIPYs **2(a-d)**.

Scheme 2.2. Synthesis of BODIPYs **3(a-c)**.

Scheme 2.3. Synthesis of BODIPYs **4** and **5**.

Scheme 2.4. Functionalization of AuNRs with BODIPY **5**.

Scheme 2.5. Synthesis of BODIPY **7**.

Scheme 2.6. Synthesis of BODIPY **8**.

Scheme 2.7. Synthesis of BODIPY **9**.

Scheme 5.1. Simplified equilibria of CDx/BODIPY systems (K_a values reported in Table 4.1).

Scheme 5.2. Schematic representation of inclusion types showing electronic transitions parallel to the molecular axis of CDxs to produce positive ICD, and those normal to the axis producing negative ICD.

List of Tables

Table 3.1. TEM size of AuNRs and **3**-AuNRs.

Table 3.2. Calculated and observed electronic excitation wavelengths of 1,3,5,7-tetramethyl-meso-phenyl-BODIPY (BDY), 1-4 and calculated oscillator strengths and wavefunctions.

Table 3.3. Absorption wavelengths of BODIPY dyes **1-6** in respective solvents and molar extinction coefficient ($\log \epsilon$) values for the targeted BODIY dyes.

Table 3.4. Physicochemical properties of short wavelength BODIPY dye photosensitizers

Table 3.5. Physicochemical properties of distyryl BODIPY dye derivatives.

Table 4.1. Nonlinear Optical limiting parameters for distyryl BODIPY dye derivatives at 532 laser excitation.

Table 5.1. Photophysical data of the BODIPY-CDx inclusion complexes and their binding constant (K_a).

Chapter 1

1. INTRODUCTION

Fluorescent organic dyes have been intensively studied in various scientific disciplines. Their photophysical properties have inspired successful applications as the active media for tuneable lasers, in the development of photoelectronic devices, as fluorescent probes, and in chemical sensors for monitoring the physicochemical characteristics of the surrounding chemical environment [1-7]. Despite their favourable photophysical properties in this regard; properties such as their high fluorescent quantum yields and their strong absorption in the visible region limit the utility of many types of fluorescent dyes for use in other applications, such as photosensitizers in photodynamic therapy (PDT) and antimicrobial photodynamic therapy (APDT), and as optical limiting (OL) materials in nonlinear optics (NLO). The focus of this study is on the preparation of dyes that are suitable for use in these applications.

PDT is a non-invasive therapeutic technique that uses a photosensitizer dye for triplet state formation, incident laser light and molecular oxygen to provide an alternative cancer treatment through the generation of cytotoxic singlet oxygen ($^1\text{O}_2$). Compared to the traditionally used cancer treatments, PDT is attractive because it provides scope for specificity and selectivity in the destruction of malignant tumour cells [8]. Moreover, the principles of PDT have also become useful in APDT, which is an alternative therapy to the conventionally used antibiotics for the treatment of microorganisms, which have developed resistance in this regard. The success of this treatment is based on the inactivation of the microorganisms using singlet oxygen and other reactive species. This makes microorganism resistance to this treatment improbable compared to the issues that are currently being faced with

conventional antibiotics [9-11], which led to the need for alternative antimicrobial approaches [12].

The study of NLO provides the ability to control the intensity of light in a predictable and predetermined manner. This manipulation of light is useful in applications ranging from optical communications to OL [12]. Optical limiting materials are of particular interest in this case due to the need to protect sensitive optical devices and the human eye from high intensity light sources such as lasers [13]. These materials when exposed to very intense light, limit the output energy of the emerging beam [13].

Since PDT, APDT and NLO are of importance particularly in the eradication of cancer cells and harmful microorganisms, or in the protection of sensitive optics and sensory organs such as the human eye, from dangerous laser light, the design of novel fluorescent dyes for use in these applications is an obvious research goal. This requires an in-depth understanding of the photophysical properties of these dyes, and the synthetic strategies that can provide the most appropriate modifications of the molecular structure of the chromophore (e.g. substituent effects) along with the influence of the environment conditions (e.g. the solvent effect, incorporation in rigid solid material, *etc*).

BODIPY dyes have emerged as one of one of the most promising classes of organic fluorescent dyes. The BODIPY structure can be modified to obtain the desired set of photophysical properties [14]. The main objective of this thesis is to evaluate the physicochemical properties of several series of novel BODIPY dyes and their suitability for use in APDT and to

study their NLO behaviour for subsequent use as optical limiting materials. The study is primarily motivated by their relative physicochemical stability and structural versatility of these dyes, since they are readily functionalized by using various synthetic routes to form a series of BODIPY derivatives for use in a wide range of applications.

1.1. BODIPY

1.1.1. *History and structure*

Boron dipyrromethene (4,4-difluoro-4-bora-3a,4a-diaza-s-indacene) dyes, abbreviated hereafter as BODIPY, form part of the dipyrin class of complexes that have recently garnered a large amount of interest as one of the most versatile heterocyclic skeleton fluorophores, since they provide a possible alternative to established nonradiative fluorescent organic dyes such as fluoresceins, rhodamines and cyanines (Figure 1.1) [15,16]. Their characteristic features include intense absorption and fluorescence bands in the visible region [17–25], high lasing efficiency [26–29], structural diversity, chemical robustness, and high thermal and photochemical stability [30-32].

The first synthesis of BODIPY dyes was reported in 1968 by Treibs and Keuzer [16]. It was only in the 1990s, however, when reports by Boyer and Pavlopoulos showed their potential utility as tuneable lasers, and as a new candidate for fluorescence markers, that they began to attract attention from the wider scientific community [33–36]. The promising results obtained in their lasing behaviour inspired further research on their use in other fields such as biomedical applications [37–41]. The strong focus on these dyes has been related to their

outstanding properties compared with other fluorophore shown in Figure 1.1A-C. These properties include their facile synthesis and structural versatility, excellent spectroscopic properties (narrow Gaussian-shaped absorption and emission bands), high molar extinction coefficients (usually $\epsilon > 80\,000\text{ M}^{-1}\text{ cm}^{-1}$), and high fluorescence quantum yields (ϕ_f) (commonly $\phi > 0.50$). In addition, BODIPY dyes have moderate redox potentials, negligible triplet-state formation, and negligible sensitivity to solvent polarity, excellent photothermal stability, and high solubility in commonly used organic solvents of differing polarities [42].

The use of BODIPYs as fluorescent probes or chemical sensors has been described in many biomedicine and biochemistry reports. In this context, the photophysics of BODIPYs have to be sensitive to the environmental properties [43–47] or to the presence of an analyte in the surrounding medium [48–58]. Usually, these probes or sensors are achieved by the incorporation of specific functional groups on the BODIPY core, promoting new deactivation processes sensitive to environmental conditions (*e.g.* photoinduced charge transfer). These processes quench the fluorescence of the dye, and the sensor behaves as a fluorescent on/off switch system depending on the environmental conditions [59].

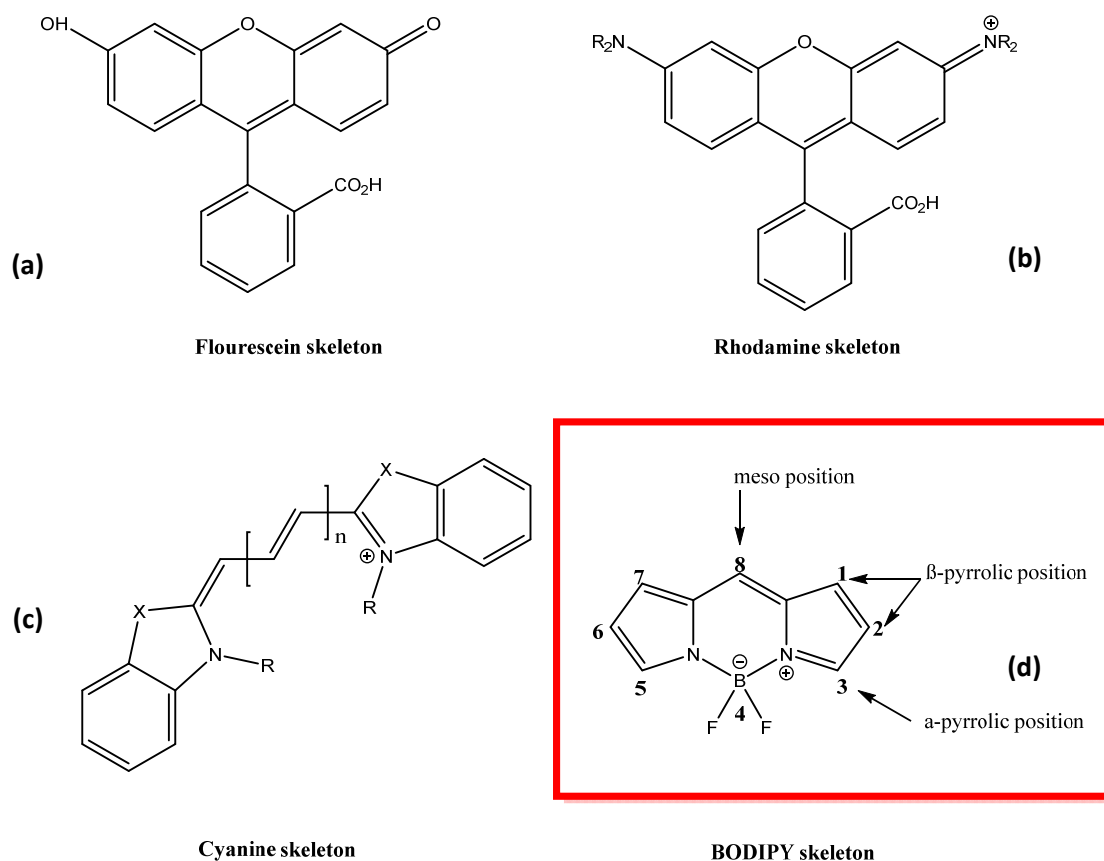


Figure 1.1. (a) – (c) Generic structure of common fluorophores; (d) BODIPY core and its IUPAC numbering system.

The structure of BODIPY consists of a dipyrromethene ligand complexed with a disubstituted boron atom, generally a BF_2 moiety (Figure 1.1). The dipyrromethene ligand is formed by joining two pyrrole units via an interpyrrolic methine bridge. Due to the BF_2 complexation, the BODIPY fluorophore can be viewed as a “constrained” cross-conjugated cyanine-type dye [60]. The rigidity introduced by the boron complexation-prevents the *cis-trans* isomerization and interpyrrolic methine chain-twisting, commonly associated with the more flexible cyanine dyes.

BODIPY dyes can also be compared to indacene dyes, since the coordination of the boron atom holds the dipyrromethene ligand in a rigidly planar conformation, but BODIPY dyes do not formally fit Hückel's $4n+2$ rule for aromaticity. Indacene dyes are heteroaromatic due to the properties of the π -MOs associated with the indacene plane that can be compared to those of an aromatic $C_{12}H_{12}^{2-}$ cyclic perimeter, which has MOs arranged in a $M_L = 0, \pm 1, \pm 2, \pm 3, \pm 4, \pm 5, 6$ sequence in ascending energy terms, where the magnetic quantum number is concerned [42]. Although the angular nodal patterns for the π -MOs of an unsubstituted BODIPY dye follow a similar sequence, the introduction of the BF_2 moiety disrupts the indacene cyclic perimeter, and the cross links and pyrrole nitrogen atoms lift all of the MO degeneracies in the π -system due to the C_{2v} symmetry. The HOMO and LUMO are well separated in energy terms from the other π -system MOs and this results in the main visible region spectral band being dominated by the HOMO \rightarrow LUMO transition [42].

1.1.2. Synthetic methodologies

Synthetic approaches to the BODIPY framework are generally based on the well-known chemistry of pyrroles and dipyrromethanes, which have been studied previously as synthetic precursors for porphyrins and related macrocyclic compounds [61,62]. It is relatively easy to produce a wide variety of dipyrromethene ligands by using readily available pyrroles and highly electrophilic carbonyl compounds as the precursors, which after complexation with BF_2 in the presence of a base affords a BODIPY complex, usually in reasonable and reproducible yields. There are different synthetic routes that can be utilised to synthesise the parent BODIPY core as well as the asymmetrical and symmetrical BODIPY dyes depicted in Figure 1.2.

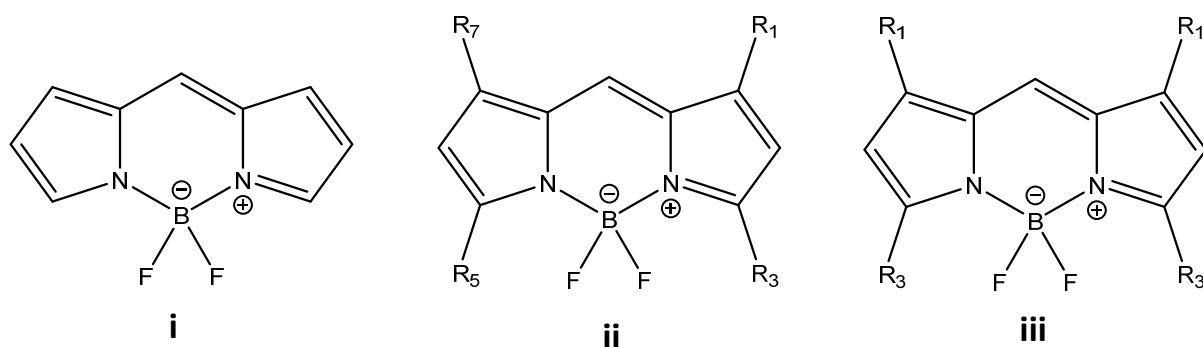
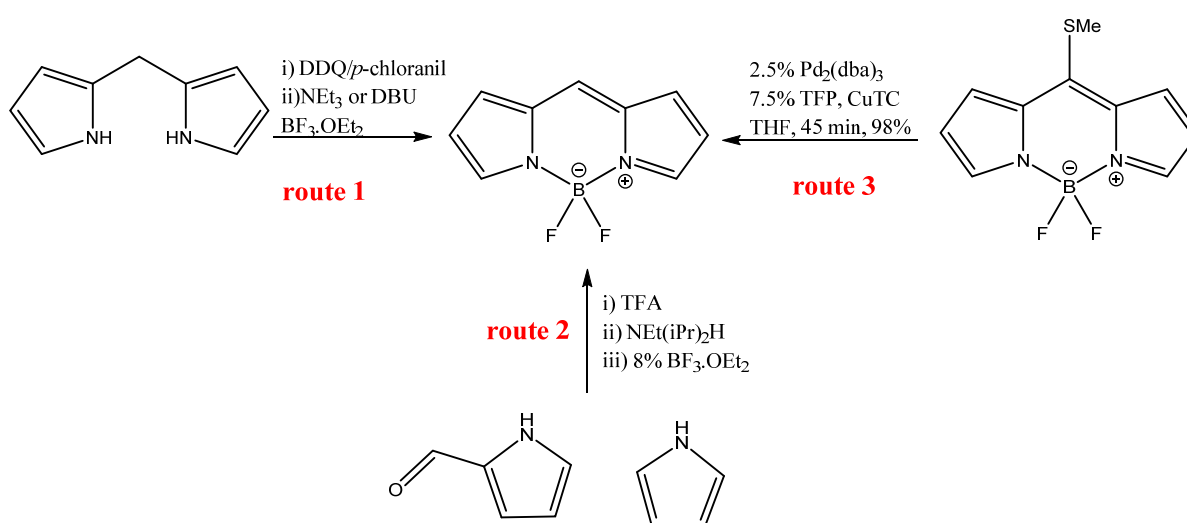


Figure 1.2. Molecular structure of i) BODIPY core, *meso*-unsubstituted ii) asymmetrical and iii) symmetrical BODIPY dyes.

1.1.2.1. Synthesis of the parent BODIPY core

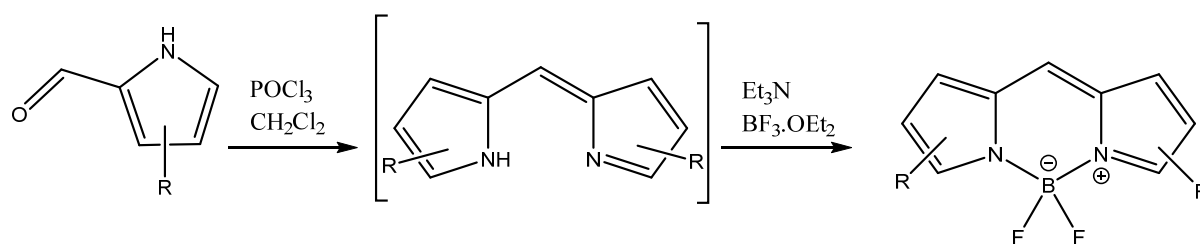
The synthesis of the parent unsubstituted BODIPY chromophore proved to be highly challenging due to the reactivity of the dipyrromethene precursor [63-65,15b]. Bruce and co-workers (route 1) [63], Wild and co-workers (route 2) [65], Pena-Cabrera and co-workers (route 3), [64] independently developed facile and reproducible synthetic routes to the BODIPY core (Scheme 1.1). Its spectroscopic properties are now well-established.



Scheme 1.1. Different pathways for the synthesis of the BODIPY core.

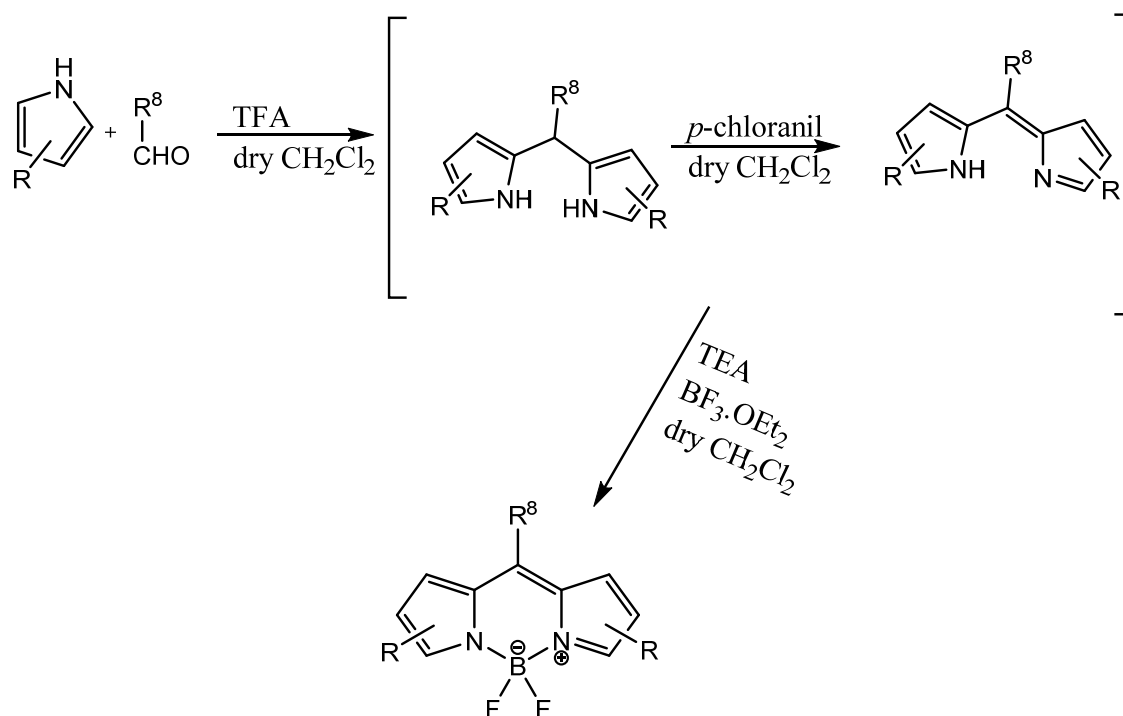
1.1.2.2. Synthesis of asymmetrical and symmetrical BODIPY dyes

The synthetic route outlined in Scheme 1.2 can be utilized for the synthesis of both symmetrical and asymmetrical BODIPY dyes. Asymmetric BODIPY dyes, substituted or unsubstituted at the meso-position are usually obtained by the MacDonald coupling approach, i.e. via acid-catalyzed condensation of a pyrrole-2-carbaldehyde with an α -free pyrrole [66]. Yields for these reactions are generally very high but are reduced drastically when an electron-deficient α -free pyrrole is used. Under these conditions, self-condensation of pyrrole-2-carbaldehyde is favored and this yields a symmetrical BODIPY as the major product instead. The main advantage of this method lies in its ability to afford a BODIPY scaffold with different functional moieties for further structural elaboration [67].



Scheme 1.2. General synthetic route for asymmetrical and symmetrical BODIPY dyes.

On the other hand, symmetric BODIPY dyes with substituents at the meso- or 8-position can be prepared by a Lewis acid, typically trifluoroacetic acid (TFA), catalyzed condensation of pyrroles with acid chlorides, anhydrides or aldehydes to generate the dipyrromethene (or dipyrromethanes for aldehydes which are subsequently oxidized) intermediate [67]. Scheme 1.3 shows a one pot synthetic route to a BODIPY dye that involves the use of various aldehydes and pyrrole derivatives.



Scheme 1.3. Synthesis of symmetrical BODIPY dyes using various aldehydes and pyrrole derivatives.

In order to avoid polymerization, pyrroles are usually substituted at the 3 and 5-positions [67]. The dipyrromethene intermediate are then converted to BODIPY dyes through a reaction with a tertiary base and $\text{BF}_3 \cdot \text{OEt}_2$. Yields for this reaction are generally greater than 50% with high purity and reproducibility readily achieved. BODIPY dyes bearing substituents at the meso-position often display enhanced stability in contrast to their meso-unsubstituted counterparts. Since a large range of functional groups are compatible with these reaction conditions, this method has emerged as the most popular route for forming BODIPYs, and is often referred to as the “classical one-pot two/three-step reaction” [67]. The major advantage of this reaction lies in its ability to use the meso-substituent as a point of elaboration to build larger molecular structures. Symmetric BODIPY dyes that are

unsubstituted at the meso-position can be obtained by the self-condensation of an appropriate pyrrole carbinyl cation precursor under acidic conditions, which include use of *p*-toluenesulfonic acid and Montmorillonite clay, followed by BF₂ complexation [68]. The focus in this study, however involved the synthesis of symmetrical BODIPY dyes using the acid catalysed condensation reaction and derivatization thereof.

1.1.3. Derivatization of the BODIPY framework

BODIPY dyes are electron-deficient compounds which are relatively easy to synthesize and derivatize. Derivatized BODIPY dyes can be formed either by functionalising the core at nearly any of the available positions or through the use of already substituted pyrroles in the initial synthesis. Many research groups including those of Vicente [69-71], Burgess [72], Ziesel [73], Boens and Dehaen [73,74], Nagano [75], Akkaya [76], O'Shea [77], Rurack and Daub [78], and Carreira [79] have explored various strategies for modifying the optoelectronic properties and applications of BODIPY dyes. Possible modifications on the BODIPY core include:

- i) *Electrophilic substitutions at the 2, 6-positions.* The 2, 6-positions can readily undergo electrophilic aromatic substitution reactions due to their electron deficiency. Hence, sulfonate groups can be substituted to improve the water solubility of the typically hydrophobic core without impacting the optical properties of the BODIPY core so that they become useful for biological purposes [80-82]. Furthermore, the introduction of halogens, usually Br or I, can red shift the main absorption and emission bands and quench the fluorescence intensity relative to the parent dye [83] due to the heavy atom effect [15b].

- ii) *Addition of styryl derivatives at the 3, 5-positions via a base-catalyzed Knoevenagel condensation reaction.* The introduction of styryl groups was first achieved by reacting a 3, 5-dimethylBODIPY with an aromatic aldehyde [84, 85]. The protons attached to the methyl groups are acidic enough to undergo condensation reactions. Extension of the π -conjugation and the addition of functionality is most frequently accomplished through the methyl groups at the 3, 5-positions, since this generally produces a greater red shift (ca. 50–100 nm) than is observed upon extending the π -conjugation through the 2, 6- [15b] or 1, 7-positions [71].
- iii) *Nucleophilic substitution at the 3, 5-positions.* The presence of good leaving groups, such as chlorine or iodine atoms at the 3, 5-positions enables the electron-deficient BODIPY structure to undergo nucleophilic substitution reactions. Various nucleophiles, including carbon, nitrogen, oxygen, and sulfur atoms, have been used to add functionality or to extend conjugation and shift the main absorption and emission bands of the BODIPY chromophore to the red [80]. The presence of halogens at the 3, 5-positions also allows the use of palladium mediated couplings for the incorporation of ethynyl, ethenyl, and aryl-substituents to form long wavelength BODIPY-based fluorescent biosensing materials and biolabels [86].
- iv) *Functionalization at the C-8 position via acid-catalyzed condensation of pyrrole with a specifically substituted aryl-aldehyde or acyl-chloride* [87]. This point of attachment remains the most utilized given its versatility for incorporating groups such as ion capture ligands [88, 89], donor-acceptor groups [90, 91], chiral auxiliaries [92, 93], water solubilizing groups [94, 95], and biomolecules [96] for applications such as pH probes, chemosensors, light-harvesting devices and biological labels.

- v) *Replacement of the meso-carbon with nitrogen to form aza-BODIPY dyes.* Aza-BODIPY dyes can be formed via Michael addition reactions [97] or through the reaction of phthalonitrile and an arylmagnesium bromides [98]. Incorporation of the electronegative nitrogen atom greatly influences the HOMO–LUMO energy gap through stabilization [88]. Enhanced stability of the LUMO results in a red-shift of the main absorption and emission bands into the 650–850 nm region [59]. Aza-BODIPYs have high molar extinction coefficients and moderate fluorescence quantum yields (ca. 0.20–0.40) [88].
- vi) *Fusion of aromatic rings to the pyrrole units.* This structural modification results in the formation of BODIPY dyes with red shifted absorption and emission bands. Red and near-IR emitting dyes can be used for biological imaging. Strategies such as the use of aryl-fused pyrroles, 2-acetyl phenols [99], and retro Diels-Alder syntheses of norbornane-derived pyrroles [100,101] have been employed to form these extensively π -conjugated systems [102].
- vii) *Replacement of the pyrrole moiety with an isoindole or indole ring* [103, 105]. This approach has enabled the development of brighter emitting fluorophores with more red-shifted band than their unconstrained analogs.
- viii) *Nucleophilic substitution of the fluorine at the boron center.* Replacement of the fluorines by carbon, ethynyl, and oxygen nucleophiles has led to a family of photostable, highly luminescent redox-active complexes that are referred to as C-BODIPYs, E-BODIPYs, and O-BODIPYs, respectively [15b].
- ix) *Modification of the boron chelate.* Substitution of the fluorine atoms requires the use of organometallic compounds, typically an organolithium or Grignard complex [84, 105, 106].

1.1.4. Physicochemical properties of BODIPY dyes

Figure 1.3 provides a Jablonski diagram illustrating the possible photophysical processes that take place once a BODIPY dye is excited by the absorption of an incident photon [107]. Following photon absorption, an electron is promoted to a S_n excited state. This excited state rapidly relaxes to the lowest vibrational level of the S_1 state through a process called internal conversion and this generally occurs within 10^{-12} s. The S_1 state then relaxes to the ground state by releasing a photon via fluorescence or by nonradiative decay. According to Kasha's rule the emission spectra and the fluorescence quantum yields are generally independent of the excitation wavelength, since the fluorescence process occurs exclusively from the lowest vibrational level of the S_1 state. As a result, the fluorescence spectrum obtained is usually a mirror image of the $S_0 \rightarrow S_1$ absorption band and not of the total absorption spectrum.

The S_1 state can also undergo a spin forbidden conversion to the first triplet state, T_1 , which is referred to as intersystem crossing. This transition is favoured by the presence of a heavy atom on the BODIPY dye due to the effect of spin-orbit coupling. Photon emission from the T_1 state is known as phosphorescence, and is generally shifted to longer wavelengths relative to fluorescence. Also, the BODIPY dye in the T_1 state can transfer its energy to ground state molecular dioxygen to produce singlet oxygen and other radicals. In this thesis, three major photophysical processes of BODIPY dyes were consistently measured, the electronic excitation, fluorescence emission and singlet oxygen generation (the latter was only for those dyes that were functionalised with heavy atoms).

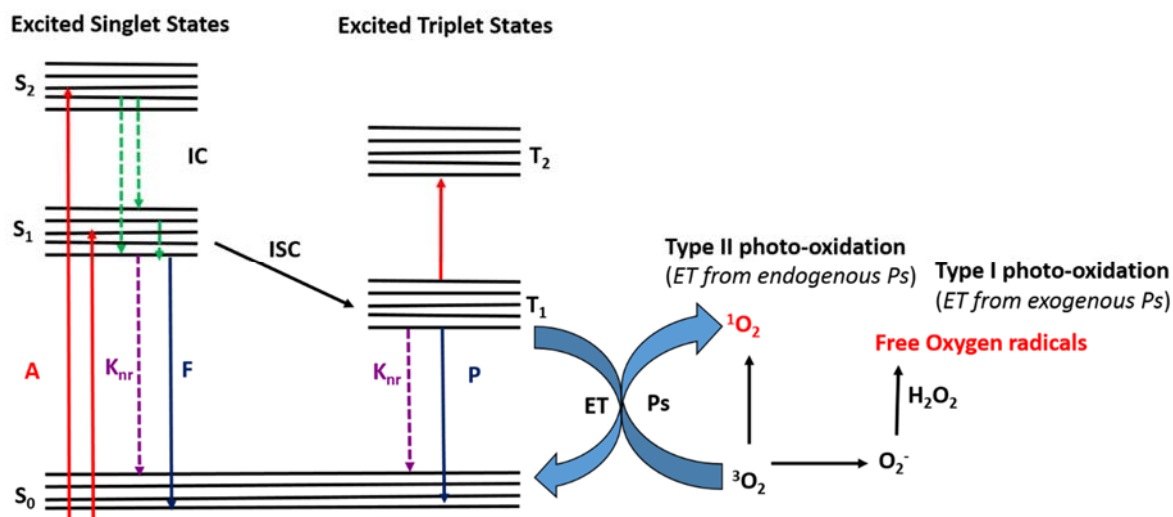


Figure 1.3. Jablonski diagram for a molecule upon excitation. A = Absorption; F = Fluorescence; P = Phosphorescence; Ps = Photosensitization; IC = Internal conversion; ISC = Intersystem crossing, K_{nr} = non-radiative decay.

1.1.4.1. Absorption spectra of BODIPY dyes

Typical UV-visible absorption and fluorescence spectra of BODIPYs are shown in Figure 1.4. The lowest energy absorption band corresponding to the electronic transition from the ground to the first excited states (the $S_0 \rightarrow S_1$ transition) is characterized by a high transition probability with high molar absorption coefficients ($\epsilon \sim 10^5 \text{ M}^{-1}\text{cm}^{-1}$) and oscillator strengths ($f \approx 0.5$). A shoulder of intensity is observed at higher energy (ca. 1100 cm^{-1} from the absorption maximum) which has been attributed to out-of-plane vibrations of the heterocyclic structure [108, 109]. Other less intense absorption bands arising from transitions to higher singlet excited states ($S_2, S_3 \dots S_n$) lie in the UV region [108, 109]. Theoretical calculations have demonstrated that the main spectral band at ca. 500 nm can be assigned almost exclusively to the promotion of an electron from the HOMO to the LUMO (Figure 1.4),

resulting in a transition that is polarized along the long molecular axis of the chromophore [110]. The morphology of this absorption band is nearly independent of the dye concentration (at least up to 2×10^{-3} M) suggesting the absence of any intermolecular dye-dye interaction, such as dye aggregation [108]. The low tendency of BODIPYs to self-associate is a very important advantage of these dyes with respect to other fluorescent dyes such as rhodamines since the formation of non- or poorly fluorescent aggregates drastically reduces the fluorescent capacity in concentrated solutions [19].

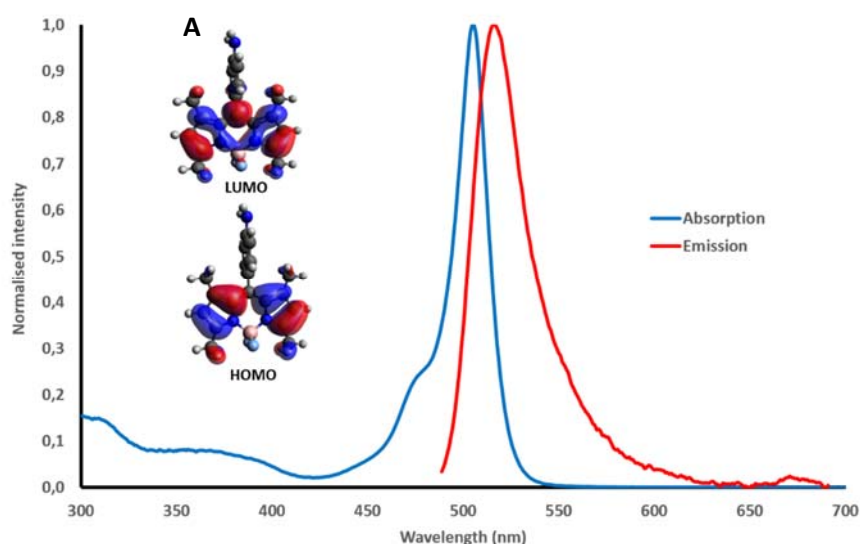


Figure 1.4. (A) Typical molecular orbitals showing nodal plane patterns of the HOMO and LUMO, and the absorption (blue line) and emission (red line) spectra of BODIPY dye.

1.1.4.2. Fluorescence quantum yields and lifetimes of BODIPY dyes

The fluorescence spectrum of most BODIPYs are practically the mirror image of the $S_0 \rightarrow S_1$ absorption band (Figure 1.4). This suggests that the potential energy surfaces are similar in both electronic states. Consequently, the fluorescent band is characterized by a small Stokes

shift in the range of 500 cm⁻¹. The shape of the fluorescence band is independent of the excitation wavelength indicating that the emission is from the lowest vibrational level of the S₁ excited state [108], due to very fast internal conversion process from higher energy excited states. The fluorescence quantum yields (Φ_F) can be very high, reaching values close to the unity for some BODIPYs in certain media [108, 109]. The determination of the quantum yield is generally accomplished by comparison of the integrated intensity of the BODIPY dye with that of a standard [111]. The quantum yield is given by Equation (1) in this context.

$$\Phi_F = \frac{F A_{std} \eta^2}{F_{std} A \eta_{std}^2} \quad (1)$$

F and F_{Std} are the integrated areas under the fluorescence curves for the sample and standard; A and A_{Std} are the absorbance values of the sample and reference at the excitation wavelength; while η and η_{std} are the refractive indices of the solvents in which the sample and reference were dissolved. Rhodamine 6G and ZnPc can be used as standards for the determination of fluorescence quantum yields in ethanol and DMSO, respectively, with Φ_F = 0.95 and 0.20 [112,113].

The time profile of the fluorescence emission of BODIPYs can be analyzed with monoexponential decay curves (Figure 1.5) and fluorescence lifetime (τ) values of ca. 4–6 ns are typically observed. The lifetime is defined by the average time the BODIPY dye stays in its excited state and is described by Equation (2) [114].

$$\tau_0 = \tau_F / \Phi_F \quad (2)$$

τ_F radiative lifetime and Φ_F the fluorescence quantum yield. The lifetime is typically independent of the excitation and the emission wavelengths, confirming that the emission is from a locally excited state [108].

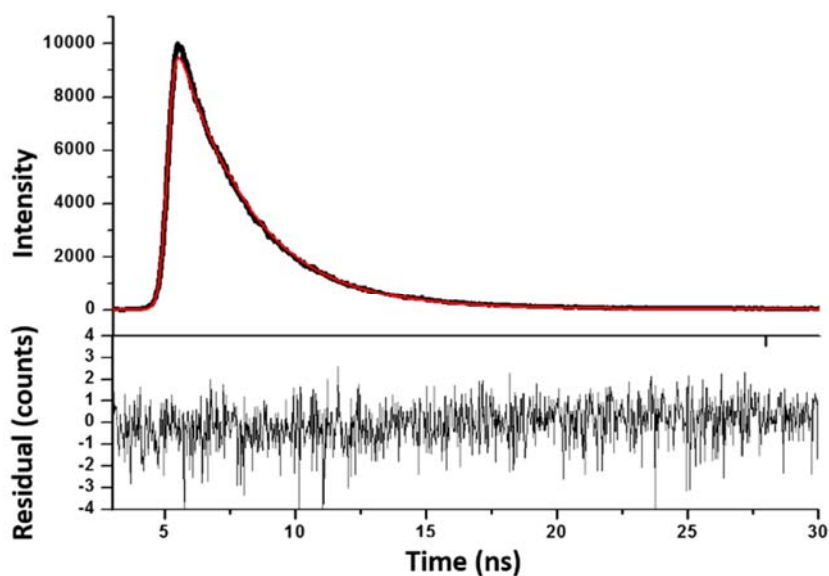


Figure 1.5. Typical fluorescence decay curve of BODIPY dyes.

1.1.4.3. Singlet oxygen quantum yield of BODIPY dyes

BODIPY dyes are known to be highly fluorescent, because the BF_2 group acts as a linking bridge, providing a rigid delocalized π -system. The BF_2 moiety disrupts the aromaticity of the π -system, since it eliminates any cyclic electron flow around the outer perimeter of the indacene ring structure [115]. Consequently, BODIPY dyes can be classified as quasi-aromatic dyes and are characterized by a low or no intersystem crossing probability by means of the “Drexhage’s loop rule” [116]. The low population of the triplet state [117] usually limits their utility for applications that require singlet oxygen generation. However, incorporation of a

heavy atom can permit the intersystem process to occur and hence facilitates the production of singlet oxygen. In this study, a series of BODIPY dyes were functionalised with bromines at the 2, 6-positions. These positions are more susceptible to electrophilic attack because they are less positively charged due to the mesomeric structures of the BODIPY core [118].

There are two methods that can be used to quantify singlet oxygen; the use of a germanium detector to study singlet oxygen phosphorescence and a comparative chemical method. The latter method was employed in this work. This method requires the use of a singlet oxygen quencher [1, 3-diphenylisobenzofuran (DPBF) in this case] that will react with singlet oxygen as soon as it is produced in an oxygenated solution. UV-visible absorption spectroscopy is then used to monitor the production of singlet oxygen by observing the change in the intensity of the main absorption peak of the quencher. Equation (3), shown below, is used for calculating singlet oxygen quantum yields (Φ_{Δ}) [119, 120].

$$\Phi_{\Delta} = \Phi_{\Delta}^{std} \cdot \frac{R^{sample} \cdot I^{std}}{R^{std} \cdot I^{sample}} \quad (3)$$

Φ_{Δ}^{std} is the singlet oxygen quantum yield for the standard (Rose Bengal, $\Phi_{\Delta}^{std} = 0.76$ in DMSO) [121]. R^{sample} and R^{std} are the DPBF photobleaching rates in the presence of the sample under investigation and the standard and; and I^{sample} and I^{std} are the rates of light absorption by the sample and the standard.

1.1.5. Applications of BODIPY dyes

BODIPY dyes are highly favored for their fundamental properties and applications in various disciplines such as molecular biolabelling, cell imaging, chemical sensing, solar cells and two photon absorption [15b, 122, 123]. One of the main goals of the study was to investigate

their potential application in APDT by studying the physicochemical properties as well as their optical limiting parameters due to their potential use as optical limiters.

1.2. BODIPY dyes in antimicrobial photodynamic therapy (APDT)

APDT provides a non-antibiotic approach to inactivate microorganisms [124-128]. It has proven to be a potential alternative for microbial control to microorganisms that are resistant to conventional antibiotics. APDT follows similar principles to those of PDT which is well known for the treatment of cancerous cells. As shown in Figure 1.6, APDT involves the eradication of target cells by reactive oxygen species (such as singlet oxygen, $^1\text{O}_2$) produced by the interaction of a chemical photosensitizer (PS) and laser light of appropriate wavelength (ideally at the maximum absorption of the PS) [129]. As has been highlighted previously, the bacteria resistance to APDT is improbable [130-131], since they are inactivated by the highly reactive $^1\text{O}_2$ and other radical species.

A good PS possesses the ability to absorb visible light becoming excited to the triplet state and then transfer its energy efficiently to molecular oxygen. For a PS to be suitable for APDT, a water soluble charged structure is required to ensure a good degree of interaction between the bacterial cell wall and the PS itself. Dyes possessing such characteristics are typically rigid planar structures with a high degree of conjugation [132]. Macrocyclic photosensitizers such as porphyrins and phthalocyanines have been widely used for APDT [132-134]. However, there are major drawbacks associated with porphyrins and phthalocyanines, such as their

weak absorption in the visible region or at shorter wavelengths, a lack of tumour specificity, and a tendency to aggregate at high concentrations [135].

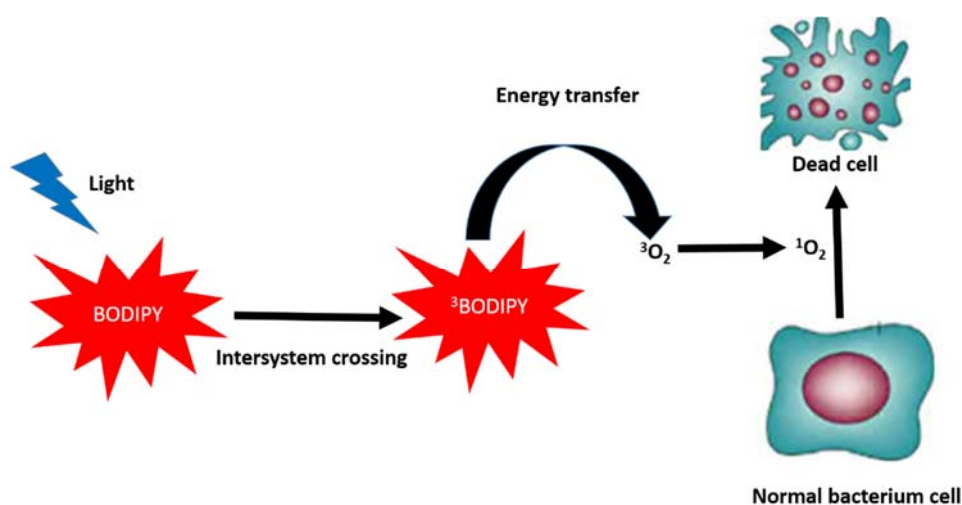


Figure 1.6. Schematic diagram showing cell death after APDT.

The low intersystem crossing rates [136] and insolubility of most BODIPY dyes in water make them inappropriate for use in PDT and APDT. However, some studies have shown that extending the π -conjugation through styryl, aryl and ethynylaryl substitution at the 1, 3, 5, and/or 7-positions, aromatic ring fusion, azaBODIPY formation and appropriate combinations thereof can significantly shift the absorption band to longer wavelengths that are for use in PDT in the optical window for tissue penetration in the 650–1000 nm region [137]. Incorporation of heavy atoms to the BODIPY dye can enhance the rate of intersystem crossing and decrease the fluorescence quantum yield thereby enhancing triplet state absorption and the production of singlet oxygen [138, 139]. In addition, water soluble BODIPYs have been reported in which the hydrophilicity was ensured by the presence of sulfonic groups [140], phosphonates [141], sulfonated peptide chains [81] or oligo-ethyleneglycol chains [142, 143].

1.2.1. BODIPY dyes synthesised

Only a limited range of BODIPY dyes have been studied for use in APDT. Cationic BODIPY dyes based photosensitizers **i** and **ii** shown in Figure 1.7 have been reported by Caruso et al. [144]. In recent years, O'Shea and co-workers [145] reported the preparation of an azaBODIPY dye **iii** as a potential photodynamic therapy agent. Nagano [146], Akkaya and co-workers [147] also introduced some BODIPY derivatives **iv** and **v** which are appropriate for PDT (Figure 1.7).

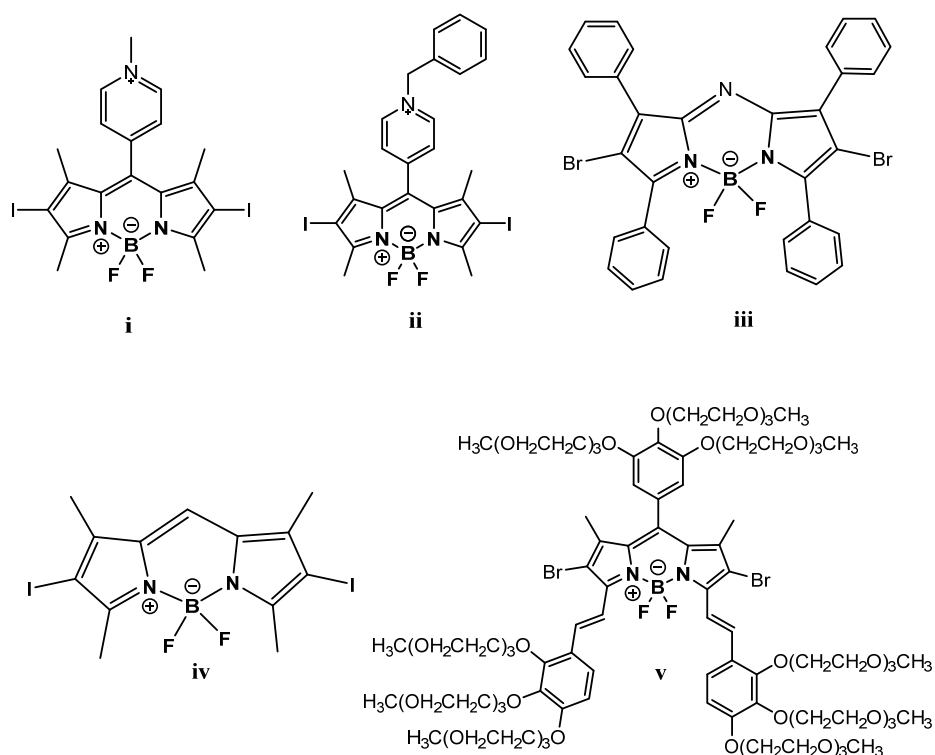


Figure 1.7. BODIPY dyes reported in literature for APDT (**i** and **ii**) and PDT (**iii**, **iv**, and **v**).

The main focus of this study is to synthesize short wavelength BODIPY photosensitizers (i.e. those that absorb < 600 nm) with improved singlet oxygen production, water solubility and cell penetration. A meso-(*p*-aminophenyl)-2,6-dibromo BODIPY **1** was conjugated with gold nanorods (AuNRs) to afford gold conjugates **2**. The amino group of **1** was also quaternised to

afford compounds **3** and **4** (Figure 1.8). Generally, the 2, 6-positions of the BODIPY core are prone to electrophilic substitution [16], and halogenation at these positions converts the highly fluorescent molecule to a potent PS with efficient intersystem crossing.

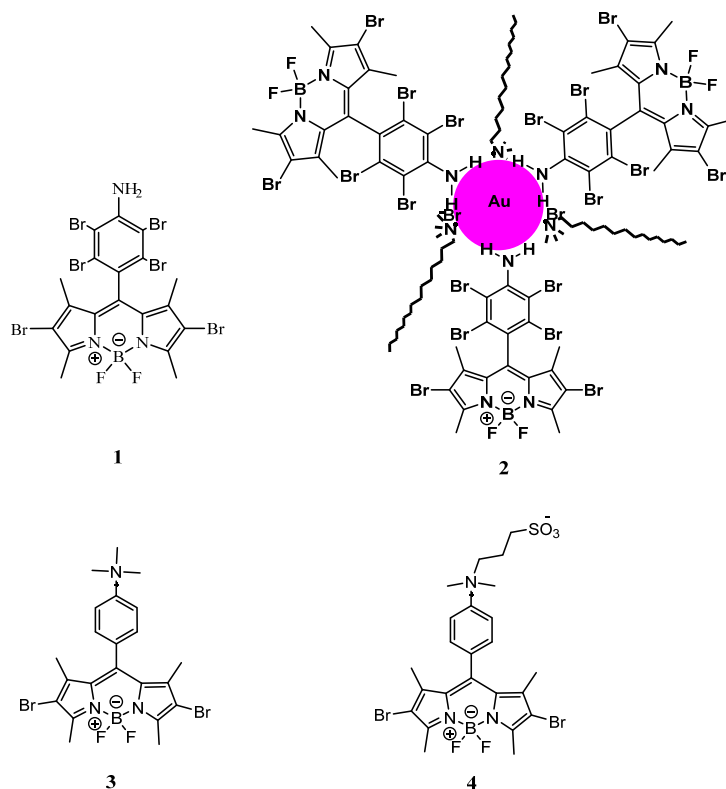


Figure 1.8. BODIPY dyes synthesised in this work for possible use in APDT.

The heavy atom effect can be described as the enhancement of a spin-forbidden process induced by the presence of an atom of a high atomic number, either internal or external to the excited molecule [148]. Photosensitisers conjugated to AuNPs have demonstrated improved necrosis and/or apoptosis [149-151]. AuNPs can increase the solubility of photosensitiser and offer the benefits of hydrophilicity [152]. In addition to these properties, AuNPs can bind to bacteria enhancing photo-inactivation and this facilitates the binding of the photosensitizer to the bacteria [153]. AuNPs can also enhance the production of singlet oxygen quantum yields as a result of the heavy atom effect, which is a necessity for PACT.

AuNPs also have the ability to absorb light and rapidly convert it to heat through non-radiative processes. For this reason, AuNPs have potential as photothermal agents in photothermal inactivation of bacteria [154]. In addition, BODIPY dyes have also been quaternized to improve water solubility. On the other hand, hydrophobic groups are introduced to BODIPY dyes to enhance the amphiphilicity of the compounds and this has proven to increase cell penetration [155, 156], hence the use of propanesultone for quaternization in the case of BODIPY 4 (Figure 1.8).

1.3. BODIPY dyes in nonlinear optics (NLO)

Nonlinear optics (NLO) is associated with changes in the optical properties of a material when it interacts with incident light of differing intensity. Several optical devices or technologies such as optical rectifiers, optical switches, dynamic holography, optical data recording and optical limiters are based on nonlinear effects [157]. Optical limiters are devices that strongly reduce the transmission of light at high incident light intensities, while remaining largely transparent in ambient light conditions (Figure 1.9). These devices have become crucial in the protection of light sensitive elements such as optical sensors, the human eye and other sensitive materials, since the emergence of intense light sources based on the laser mechanism in the 1960s. In addition, modern warfare is often based on laser weapons, and laser pointers are often used maliciously to impede the vision of civil pilots on their landing approaches. Furthermore, since sensors currently used in the South African military do not cover the complete range of laser threats including effectively protecting the eyes of pilots, aviation safety in this regard currently relies on pilot training and on laser illumination warning

systems [158]. This has motivated researchers to pursue research in this field, so that novel efficient and stable optical limiting materials can be identified. The second harmonic of Nd/YAG lasers at 532 nm and the 1064 nm fundamental beam in the infrared region are of most pressing interest [159, 160]. Accordingly, BODIPY dyes can be modified in such a way that their main absorption bands lie at longer wavelengths, so that second harmonic wavelength of 532 nm falls below the maximum absorption band and there is limited absorption under ambient light conditions.

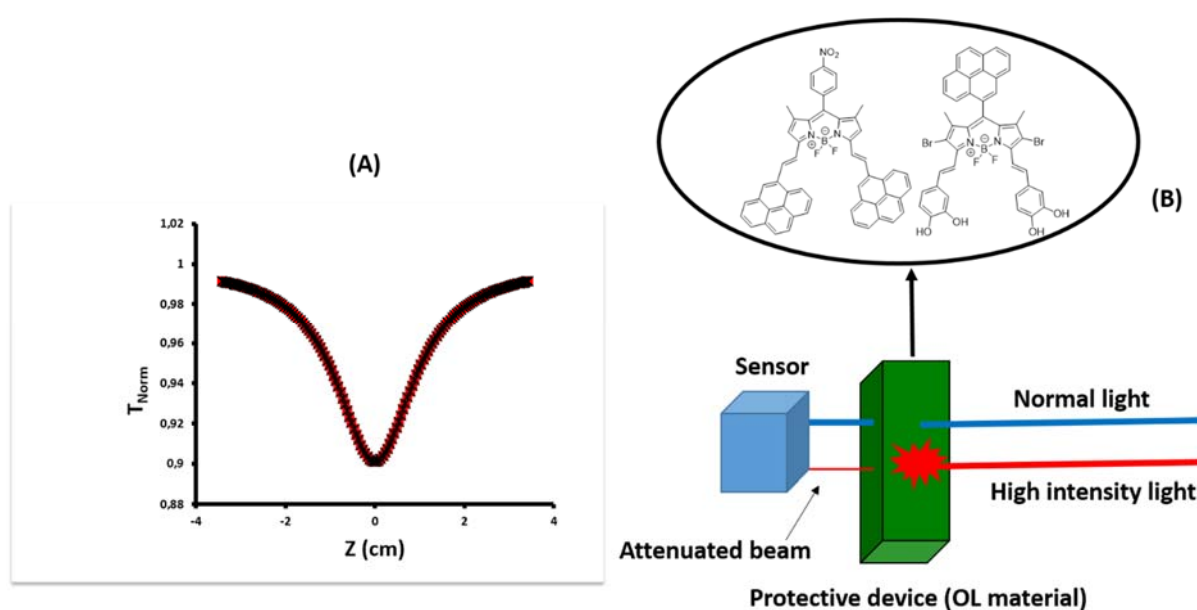


Figure 1.9. (A) A typical open-aperture z-scan curve showing the RSA behaviour of an optical limiter, and (B) a schematic representation of the ideal functioning of a BODIPY dye optical limiter under normal and high intensity light.

As shown in Figure 1.10, the ideal behaviour of an optical limiter involves transmitted intensity remaining constant (or decreasing) above a certain illumination intensity (A), with a linear decrease of the initial constant transmittance above a threshold value (B) [161]. The

key structural requirement for an optical limiting material tends to be a delocalized π -conjugation system, since the conjugated structure affords high polarizability and thus rapid charge redistribution upon interaction with intense incident laser radiation.

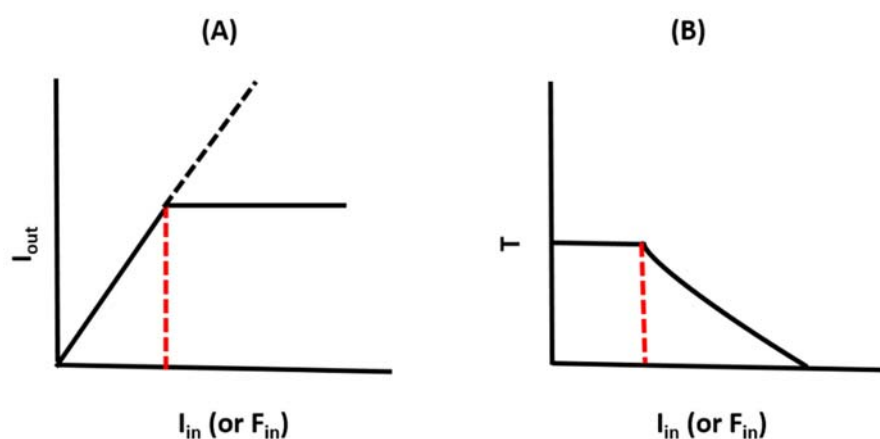


Figure 1.10. The behaviour of an ideal optical limiter, I_{in} = incident intensity, I_{out} = transmitted intensity, T = transmittance.

BODIPY dyes have potential in this regard due to their structural versatility, photochemical stability and high molar extinction coefficients. Comparatively little research has been carried out on BODIPY dyes to investigate their potential utility as optical limiting materials. The two-photon absorption and third-order nonlinear optical properties of functionalized BODIPY dyes **vi** [162], **vii** [163] and **viii**, **ix**, and **x** [164], respectively) have been investigated in the near infrared region, (Figure 1.11). The nonlinear optical properties of novel poly(aryleneethynylene) films containing BODIPY dyes have also been investigated [165].

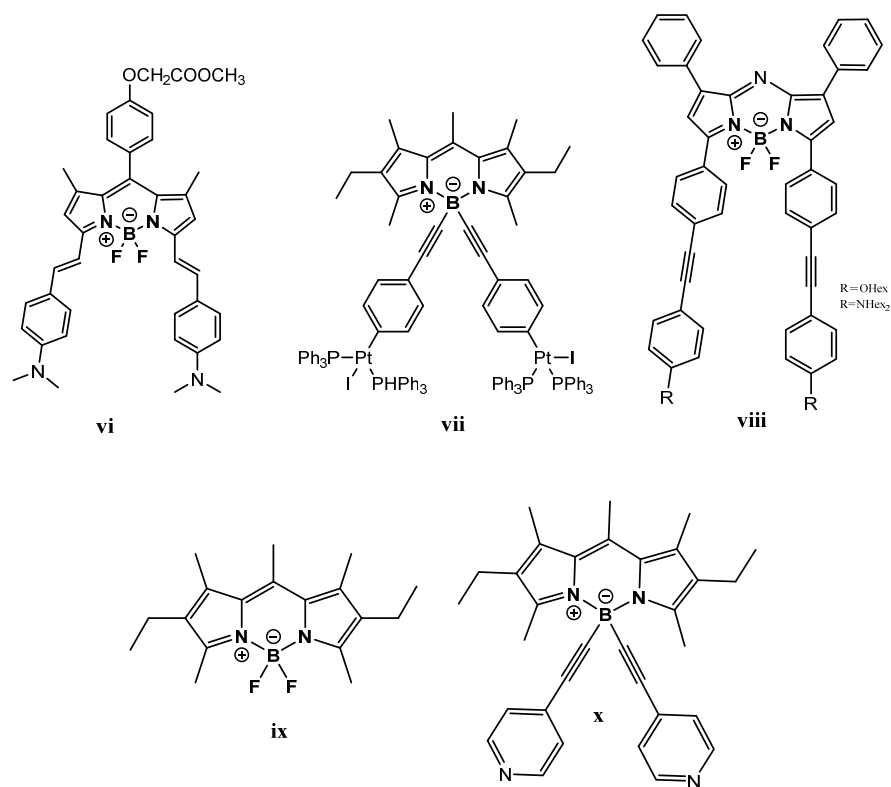


Figure 1.11. BODIPY dyes reported in literature for NLO.

1.3.1. Mechanisms in optical limiting

The main mechanisms involved in achieving optical limiting are nonlinear absorption (NLA), nonlinear refraction (NR) and nonlinear light scattering (NLS). The focus in this study was on the optical limiting that results from NLA processes. Materials with a positive NLA coefficient exhibit reverse saturable absorption (RSA) with a decrease in transmittance at high-intensity levels, and so function as optical limiters (Figure 1.9A). Two photon absorption (2PA) is described by the imaginary part of the third order susceptibility ($\chi^{(3)}$), and this accounts for OL in optical limiting materials [161]. 2PA is a resonant third-order nonlinear optical (NLO) process in which an excited state is formed by the simultaneous absorption of two photons

of half-energy, Figure 1.12A, in an intense focused light beam such as that generated by a laser source.²

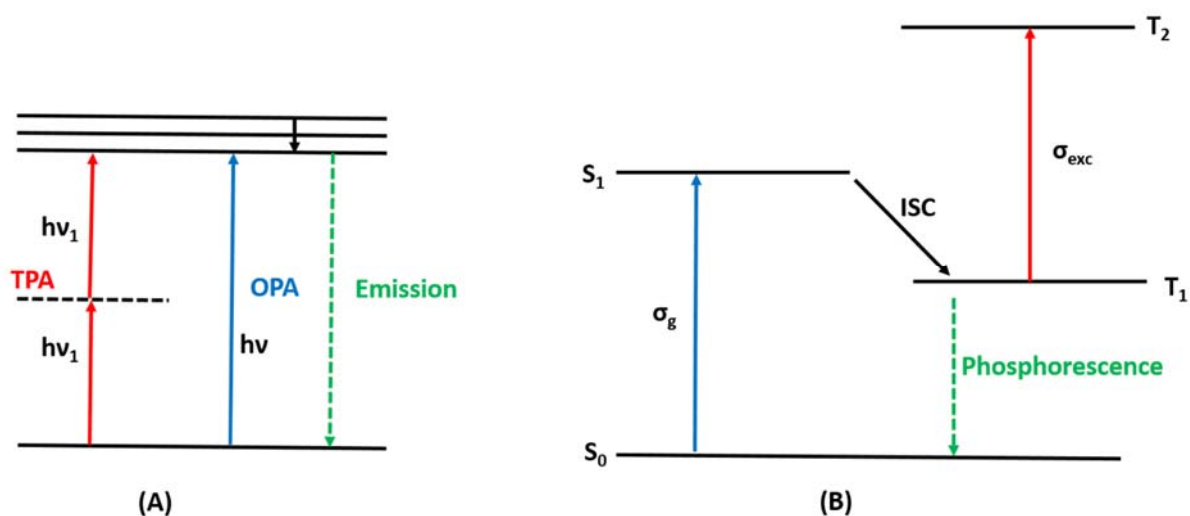


Figure 1.12. (A) Energy level diagram for one photon absorption (OPA), two photon absorption (2PA) and emission and (B) excited-state absorption (ESA).

Excited-state absorption (ESA), which results from an increase in absorption in the excited states relative to the ground state, constitutes the fundamental mechanism for RSA and OL for many materials with high triplet state quantum yields [161]. This process depends on the presence of an intense triplet-triplet absorption band at the wavelength of the incident laser light (Figure 1.12B).

1.3.2. Optical limiting parameters

The z-scan technique is the most common method for determining optical limiting parameters. This technique can be used to make nonlinear refraction and absorption measurements. The z-scan experiment was performed according to the method described by Sheik Bahae [166-168]. Assuming a Gaussian-shaped spatial and temporal pulse and using the open aperture z-scan theory for multi-photon absorption (nPA) [169], the general expression for open aperture normalized transmittance can be written as Equation (4).

$$T_{OA(TPA)} = \frac{1}{1 + \beta_2 L_{eff} (I_{00} / (1 + (z/z_0)^2))} \quad (4)$$

I_{00} is the on-focus intensity (peak input intensity), β_2 is the two photon nonlinear absorption coefficient, L_{eff} , z and z_0 are the effective pathlength in the sample of length L , the translation distance of the sample relative to the focus, and the Rayleigh length, respectively.

The Rayleigh length is defined as $\pi w_0^2 / \lambda$ where λ is the wavelength of the laser and w_0 is the beam waist at the focus, ($z = 0$). L_{eff} is given by Equation (5):

$$L_{eff} = \frac{1 - e^{-\alpha L}}{\alpha} \quad (5)$$

where α is the linear absorption coefficient.

The limiting intensity (I_{lim}), which is the intensity at which the optical limiting response begins to occur, can be calculated using Equation (6) [170, 171]:

$$I_{lim} = \frac{h\omega^*}{2\pi\sigma_{13}\tau_{21}} \quad (6)$$

where ω^* , σ_{13} , h and τ_{21} are the frequency at which the system absorbs, the singlet state absorption cross section, Planck's constant and triplet lifetimes, respectively. There is no

specified optimal range for I_{lim} values, however, lower values provide a better optical limiter because the optical limiting behaviour occurs at lower light intensities. The imaginary component of the third order susceptibility is also representative of the nonlinear absorption, Equation (7):

$$Im[\chi^{(3)}] = \frac{\eta^2 \epsilon_0 c \lambda \beta_2}{2\pi} \quad (7)$$

where η and c are the linear refractive index and the speed of light, respectively, ϵ_0 is the permittivity of free space, and λ is the wavelength of the laser beam. β_2 has been described in the context of Equation (4).

The optimal range for $Im[\chi^{(3)}]$ lies in the 10^{-9} – 10^{-11} range [172].

The real component is representative of the nonlinear refraction of the compound. It is usually not possible to calculate the real component ($Re[\chi^{(3)}]$) of the third-order susceptibility directly, Equation (8) [170]:

$$Re[\chi^{(3)}] = \frac{c\eta_0^2 \eta_2'}{120\pi} \times 10^{-20} \quad (8)$$

The nonlinear refraction term (η^2) is difficult to measure directly. Although $Re[\chi^{(3)}]$ can be measured by the z-scan technique, it is not essential because the imaginary component described in Equation (7) usually yields more meaningful data on how effective an optical limiter the compound [170].

Another term to consider is the hyperpolarizability, which describes the nonlinear absorption per mole of the compound, which is useful when comparing the effectiveness of a series of compounds for NLO applications. Hyperpolarizability can be determined by using Equation (9) [170, 173]:

$$\gamma = \frac{\text{Im}\{\chi^{(3)}\}}{f^4 c_{\text{mol}} N_A} \quad (9)$$

where N_A is Avogadro's constant, C is the concentration of the active species in the triplet state and f is Lorentz local field factor, $f = (\eta^2 + 2)/3$. Optimal values of γ lie between 10^{-29} – 10^{-34} .

1.3.3. BODIPY dyes synthesized

Four distyryl-BODIPY dyes functionalised at the 3, 5-positions were synthesized to assess their potential for this particular application, Figure 1.13. For the first two compounds, pyrene groups were added to extend the π -conjugation system (5 and 6). The other two were functionalised with bromine atoms at the 2, 6-positions to enhance the rate of intersystem crossing and the π -conjugation system was extended with phenol rings (7 and 8).

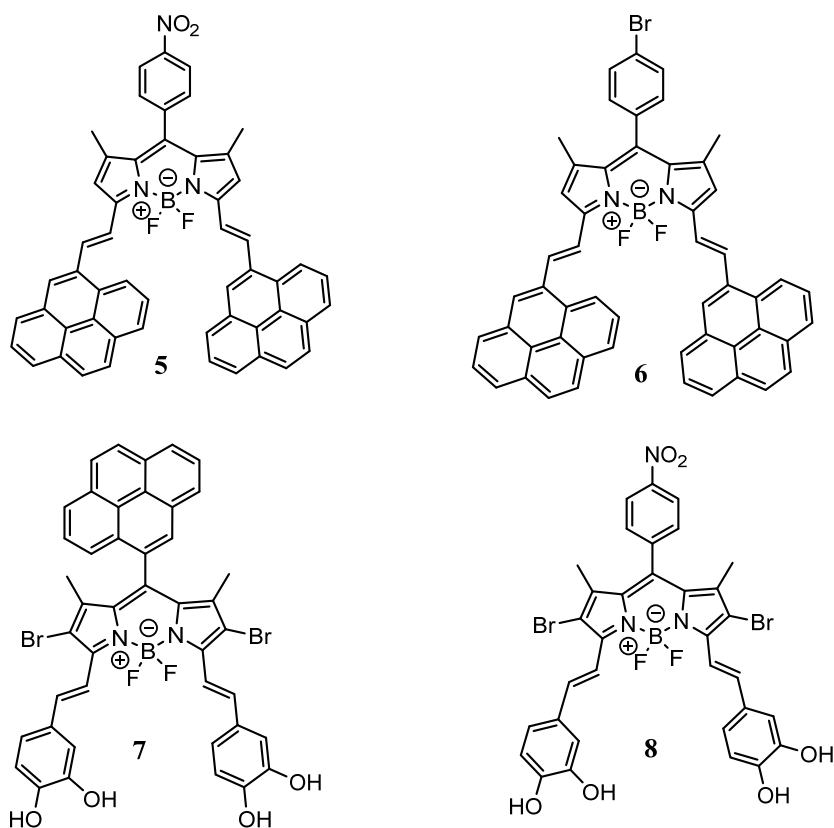


Figure 1.13. BODIPY dyes synthesised in this work for NLO studies.

1.4. Summary of aims

The aims of this thesis are summarised below:

1. Synthesis and photophysical studies of BODIPY dye conjugated to gold nanorods and an assessment of their utility for antimicrobial photodynamic therapy.
2. Synthesis and photophysical studies of water soluble BODIPY dyes through quaternization with iodomethane and propanesultone for antimicrobial photodynamic therapy.

3. A study of the synthesis and photophysical properties and nonlinear optical behaviour in solution and thin films of distyryl-BODIPY dyes functionalised with pyrene groups to extend their π -conjugation systems.
4. A study of the synthesis and photophysical properties and nonlinear optical behaviour of 2,6-dibromo-3,5-distyryl-BODIPY dyes (this extends π -conjugation system) functionalised with phenol groups (this influences the dipole moment for induced polarizability) on the styryl moieties
5. An exploratory study on the UV-visible absorption, fluorescence, and circular dichroism spectroscopy of BODIPY dye inclusion complexes with cyclodextrins in aqueous solution.

Chapter 2

2. EXPERIMENTAL SECTION

2.1. Materials

2.1.1. *Synthesis of BODIPYs 1-8*

2,4-Dimethylpyrrole, 4-nitrobenzaldehyde reagentplus (98%), 4-dimethylaminobenzaldehyde (99%), 1-pyrenecarboxaldehyde reagentplus (99%), 4-bromobenzaldehyde reagentplus (99%), trifluoroacetic acid (TFA), tetrachloro-1,4-benzoquinone (*p*-chloranil), triethylamine (TEA), boron trifluoride diethyl etherate (BF₃·OEt₂), sodium sulfide nanohydrate (98%), liquid bromine, sodium thiosulfate, diphenylisobenzofuran (DPBF), iodomethane, 1,3-propanesultone, acetic acid (glacial), magnesium sulphate anhydrous (MgSO₄), piperidine and Rhodamine 6G were purchased from Sigma-Aldrich. Hydrochloric acid (32%) was purchased from Merck, and Bengal Rose B was purchased from Fluka Chemika. All solvents were dried using molecular sieves before use.

2.1.2. *Synthesis of gold nanorods (AuNRs)*

Potassium bromide (KBr), gold (III) chloride trihydrate, cetyltrimethylammonium bromide (CTAB), sodium borohydride (≥99.0%), L-ascorbic acid (AA) and silver nitrate (>99.8%) were purchased from Sigma-Aldrich.

2.1.3. Synthesis of BODIPY 9

2,4-Dimethylpyrrole and boron trifluoride diethyl etherate ($\text{BF}_3 \cdot \text{OEt}_2$) were purchased from Tokyo chemical industry (TCI), *p*-nitrobenzaldehyde reagentplus (99%), 1-pyrenecarboxaldehyde, trifluoroacetic acid (TFA), tetrachloro-1,4-benzoquinone (*p*-chloranil), triethylamine (TEA), acetic acid superdehydrated (99.9%), ethanol (99.5%), piperidine (98%) sodium hydrogen carbonate (NaHCO_3), β - and α -cyclodextrin were purchased from Wako. 3,4-dihydroxybenzaldehyde purchased in Kanto Chemical Co. Highly purified γ -cyclodextrin was provided by Prof. Nagao Kobayashi of Shinshu University and was used as received.

2.2. Instrumentation

- i. ^1H -NMR spectra were recorded at room temperature in chloroform- d_1 or DMSO- d_6 on Bruker AMX 600 and 400 instruments operating at 600 and 400 MHz, respectively
- ii. Mass spectrometric measurements were performed on a Bruker AutoFLEX III Smartbeam TOF/TOF Mass spectrometer. The instrument was operated in positive ion mode over a 400–3000 m/z range. The voltage of the ion sources were set at 19.0 and 16.7 kV for ion sources 1 and 2 respectively, while the lens was set at 8.50 kV. The reflector 1 and 2 voltages were set at 21 and 9.7 kV, respectively. The spectra were acquired using dithranol as the MALDI matrix, using a 337 nm nitrogen laser.
- iii. An electron spray ionization mass spectrometer (ESI-MS) was operated in positive ion mode using an Advion Expression CMS over a 0–1200 m/z range.

- iv. Fourier Transform Infrared spectra (FT-IR) were recorded on a Perkin Elmer Spectrum 100 FT-IR spectrometer.
- v. Elemental analyses were carried out on a Vario EL III MicroCube CHNS Analyzer.
- vi. Ultraviolet-visible (UV-vis) spectra were measured at room temperature on a Shimadzu UV-2550 spectrophotometer using a 1 cm pathlength quartz cuvette for solution studies. The UV-Vis spectra of thin films were measured by placing them on a glass slide.
- vii. Fluorescence emission spectra were measured on a Varian Eclipse spectrofluorimeter.
- viii. Fluorescence lifetimes were measured using a time correlated single photon counting (TCSPC) setup (FluoTime 200, Picoquant GmbH) (Figure 2.1). The excitation source was a diode laser (LDH-P-670 driven by PDL 800-B, 670 nm, 20 MHz repetition rate, 44 ps pulse width, Picoquant GmbH). Fluorescence was detected under the magic angle with a Peltier cooled photomultiplier tube (PMT) (PMA-C 192-N-M, Picoquant) and integrated electronics (PicoHarp 300E, Picoquant GmbH). A monochromator with a spectral width of about 8 nm was used to select the required emission wavelength band. The response function of the system, which was measured with a scattering Ludox solution (DuPont), had a full width at half-maximum (FWHM) of about 300 ps. The ratio of stop to start pulses was kept low (below 0.05) to ensure good statistics. All luminescence decay curves were measured at the maximum of the emission peak. The data were analysed with the FluoFit program (Picoquant, GmbH).
- ix. X-ray photoelectron spectroscopy (XPS) analysis was carried out with an AXIS Ultra DLD (supplied by Kratos Analytical) using Al (monochromatic) anode equipped with a

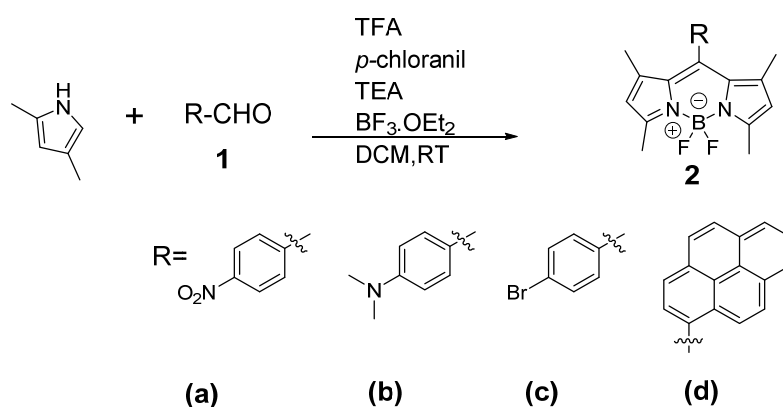
charge neutralizer. The following parameters were used: the emission was 10 mA, the anode (HT) was set at 15 kV and the operating pressure was kept below 5×10^{-9} torr. A hybrid lens was used and the resolution to acquire scans was set at a 160 eV pass energy in slot mode. The center used for the scans was at 520 eV (width of 1205 eV) with steps of 1 eV and a dwell time of 100 ms. The high resolution scans were acquired using an 80 eV pass energy in slot mode. The chemically distinct species were resolved using a nonlinear least squares curve fitting procedure. The core level binding energies (BEs) were aligned with respect to the C_{1s} binding energy (BE) of 285 eV.

- x. Transmission electron microscope (TEM) images were obtained using a JEOL TEM 1210 transmission electron microscope at 100 kV accelerating voltage. TEM samples were prepared by placing a drop of conjugate or nanoparticle solution on the sample grid and allowing it to dry prior to measurements.
- xi. X-ray powder diffraction (XRD) patterns were recorded on a Bruker D8, Discover instrument equipped with a Lynx Eye Detector, using $Cu\ K\alpha$ radiation ($\lambda = 1.5405\ \text{\AA}$, nickel filter). Data were collected over the $2\theta = 5^\circ$ to 100° range, scanning at $1^\circ\ \text{min}^{-1}$ with a filter time-constant of 2.5 s per step and a slit width of 6.0 mm. Samples were placed on a zero background silicon wafer slide. The X-ray diffraction data were treated using Eva (evaluation curve fitting) software. A baseline correction was performed on each diffraction pattern by subtracting a spline fitted to the curve background and the full width at half maximum values reported in this study were obtained from the fitted curves.
- xii. All z-scan experiments described in this study were performed using a frequency doubled Nd:YAG laser (Quanta-Ray, 1.5 J / 10 ns FWHM pulse duration) as the

excitation source. The laser was operated in a near Gaussian transverse mode at 532 nm (second harmonic), with a pulse repetition rate of 10 Hz and energy range of 0.1 μJ – 0.1 mJ, limited by the energy detectors (Coherent J5-09). The low repetition rate of the laser prevents cumulative thermal nonlinearities. The beam was spatially filtered to remove the higher order modes and tightly focused with a 15 cm focal length lens. No damage was detected between runs since the sample was moved or replaced.

- xiii. Circular dichroism (CD) spectra were recorded on a Jasco J-720 spectrodichrometer in water at room temperature. All samples were prepared from aqueous stock solutions. The following conditions were used: bandwidth, 1.0 nm; slit width, 1.0 nm; autosensitivity, 10 mdeg; time constant, 1.0 s; step resolution, 0.2 nm; scan speed, 20 $\text{nm}\cdot\text{min}^{-1}$; number of scans, 4.

2.3. Synthesis



Scheme 2.1. Synthesis of BODIPYs **2(a-d)**.

BODIPYs **2(a-d)** were synthesized by modified versions of a method previously described [174] (Scheme 2.1). 2,4-Dimethylpyrrole (2 g, 21.02 mmol) and the appropriate benzaldehyde (10.51 mmol) were dissolved in dry DCM (117.4 ml) under argon. TFA (0.2 ml) was added and the reaction mixture was stirred at room temperature. When the aldehyde was consumed (monitored by TLC), a solution of *p*-chloranil (3.88 g, 15.77 mmol) in dry DCM (5 ml) was added via syringe at 0 °C. After stirring for 20 min at room temperature, TEA (10.64 g, 105.10 mmol) and BF₃·OEt₂ (17.90 g, 126.12 mmol) were added dropwise at 0 °C over a period of 10 min, and the mixture was stirred at room temperature for 18 h. The mixture was then filtered and washed with water (6 x 60 ml), dried over anhydrous sodium sulphate and evaporated in a rotavapor. The residue was purified by flash column chromatography eluting with 1:4 DCM:ethyl acetate to yield the pure product as an orange crystalline solid.

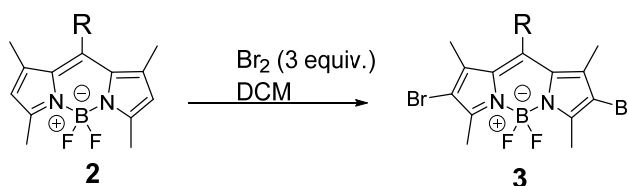
BODIPY **2(a)** obtained in 41% yield (0.65 g); IR (v_{max}/cm⁻¹): 3106 (Ar C-H), 2920-2851 (Aliph C-H), 1604 (Ar C-C), 1525 (Ar N-O); ¹H NMR (600 MHz; CDCl₃): ppm 1.33 (6H, s, 2 × CH₃), 2.53 (6H, s, 2 × CH₃), 6.01 (2H, s, 2 × CH), 7.51 (2H, d, *J* = 12 Hz, 2 × Ar-H), 8.34 (2H, d, *J* = 12 Hz, 2 × Ar-H); ESI-MS Anal. calc. m/z 369.15; Found: [M]⁺ 369.12; Anal. Calc. for C₁₉H₁₈BF₂N₃O₂: C, 61.82; H, 4.91; N, 11.38; Found: C, 61.80.96; H, 4.50; N, 10.98.

BODIPY **2(b)** obtained in 59% yield (0.43 g); IR (v_{max}/cm⁻¹): 3179 (Ar C-H), 2919-2850 (Aliph C-H), 1603 (Ar C-C), 1310 (Ar C-N); ¹H NMR (600 MHz; CDCl₃): ppm 2.07 (6H, s, 2 × CH₃), 2.20 (6H, s, 2 × CH₃), 2.85 (3H, s, CH₃), 2.92 (3H, s, CH₃), 6.01 (2H, s, 2 × CH), 7.16 (2H, d, *J* = 12 Hz, 2 × Ar-H), 7.31 (2H, d, *J* = 12 Hz, 2 × Ar-H); ESI-MS Anal. calc. m/z 367.20; Found: [M]⁺ 367.18; Anal. calc for C₂₁H₂₄BF₂N₃: C, 68.68; H, 6.59; N, 11.44; Found: C, 68.70; H, 6.40; N, 11.43.

BODIPY **2(c)** obtained in 48% yield (0.94 g); IR (v_{max}/cm⁻¹): 2960 (Ar C-H), 2923-2850 (Aliph C-H), 1589 (Ar C-C); ¹H NMR (600 MHz; CDCl₃): ppm 1.38 (6H, s, 2 × CH₃), 2.52 (6H, s, 2 × CH₃),

5.96 (2H, s, 2 × CH), 7.14 (2H, d, $J = 12$ Hz, 2 × Ar-H), 7.62 (2H, d, $J = 12$ Hz, 2 × Ar-H); ESI-MS Anal. calc. m/z 403.07; Found: $[M]^+$ 403.12; Anal. calc for $C_{19}H_{18}BBrF_2N_2$: C, 56.62; H, 4.50; N, 6.95; Found: C, 56.55; H, 4.61; N, 7.03.

BODIPY **2(d)** obtained in 63% yield (0.63 g); IR (ν_{max}/cm^{-1}): 3179 (Ar C-H), 2920-2850 (Aliph C-H), 1600 (Ar C-C); 1H NMR (600 MHz; $CDCl_3$): ppm 1.20 (3H, s, CH_3), 1.42 (3H, s, CH_3), 2.55 (3H, s, CH_3), 2.75 (3H, s, CH_3), 5.95 (2H, s, 2 × CH), 7.76 (H, s, Ar-CH), 7.84 (H, s, Ar-CH), 7.98 (H, s, Ar-H), 8.12 (2H, d, $J = 18$ Hz, 2 × Ar-H), 8.35 (2H, d, $J = 24$ Hz, 2 × Ar-H), 8.47 (2H, d, $J = 18$ Hz, 2 × Ar-H); ESI-MS Anal. calc. m/z 448.32; Found: $[M]^+$ 448.35; Anal. calc for $C_{29}H_{23}BF_2N_2$: C, 77.69; H, 5.17; N, 6.25; Found: C, 77.62; H, 5.13; N, 6.20.



Scheme 2.2. Synthesis of BODIPYs **3(a-c)** (refer to scheme 2.1 for the R-group).

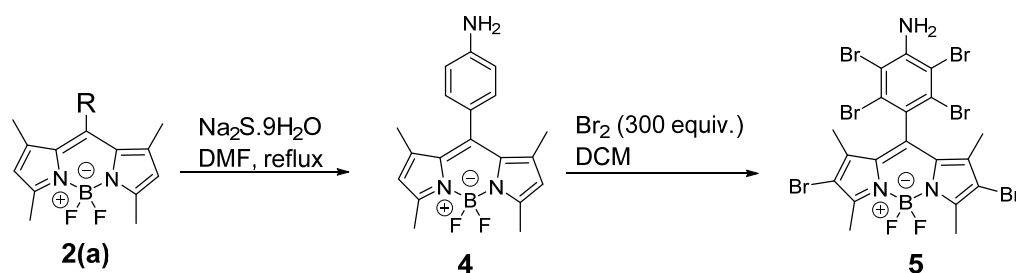
BODIPYs **3(a,b,d)** were prepared by following modified versions of a procedure reported previously [118]. To a solution of BODIPY **2(a)**, **2(b)** or **2(d)** (0.33 mmol) in 62 mL of dry DCM, liquid bromine (24 μ l, 0.48 mmol) in DCM (6 mL) was added at 0 °C over a period of 2 h, and the mixture was left to stir at room temperature overnight. The mixture was washed with an aqueous solution of sodium thiosulfate, and extracted by DCM. The organic layers were combined, dried over Na_2SO_4 , and evaporated to dryness. Purification was performed by

column chromatography on silica gel using DCM:hexane (8:1) as eluent, and the desired product was obtained as a red solid.

BODIPY **3(a)** obtained in 78% yield (0.091g); IR ($\nu_{\max}/\text{cm}^{-1}$): 3111 (Ar C-H), 2922-2852 (Aliph C-H), 1599 (Ar C-C), 1521 (Ar N-O); ^1H NMR (400 MHz; CDCl_3): ppm 1.26 (6H, s, $2 \times \text{CH}_3$), 1.36 (3H, s, CH_3), 1.39 (3H, s, CH_3), 7.55 (2H, d, $J = 8.0$ Hz, $2 \times \text{Ar-H}$), 8.45 (2H, d, $J = 8.0$ Hz, $2 \times \text{Ar-H}$); MALDI-TOF Anal. calc. m/z 524.97; Found: $[\text{M}]^+$ 524.33; Anal. calc for $\text{C}_{19}\text{H}_{16}\text{BBr}_2\text{F}_2\text{N}_3\text{O}_2$: C, 43.31; H, 3.06; N, 7.97; Found: C, 48.01; H, 4.10; N, 7.79.

BODIPY **3(b)** obtained in yield 95% (0.089 g); IR ($\nu_{\max}/\text{cm}^{-1}$): 3179 (Ar C-H), 2952-2850 (Aliph C-H), 1603(Ar C-C), 1229(Ar C-N); ^1H NMR (600 MHz, CDCl_3): ppm 1.58 (6H, s, $2 \times \text{CH}_3$), 2.10 (6H, s, $2 \times \text{CH}_3$), 2.92 (6H, s, $2 \times \text{CH}_3$), 7.20 (2H, d, $J = 12$ Hz, $2 \times \text{Ar-H}$), 7.33 (2H, d, $J = 12$ Hz, $2 \times \text{Ar-H}$); MALDI-TOF Anal. calc. m/z 525.04; Found: $[\text{M}]^+$ 525.73; Anal. calc for $\text{C}_{21}\text{H}_{22}\text{BBr}_2\text{F}_2\text{N}_3$: C, 48.04; H, 4.22; N, 8.00; Found: C, 48.01; H, 4.10; N, 7.79.

BODIPY **3(d)** obtained in yield 89% (0.098 g) IR ($\nu_{\max}/\text{cm}^{-1}$): 3293 (Ar C-H), 2921-2851 (Aliph C-H), 1600 (Ar C-C); ^1H NMR (CDCl_3): ppm 1.22 (3H, s, CH_3), 1.52 (3H, s, CH_3), 2.65 (3H, s, CH_3), 2.95 (3H, s, CH_3), 7.88 (H, s, CH), 7.95 (H, s, CH), 7.99 (H, s, CH), 8.24 (2H, d, $J = 18$ Hz, $2 \times \text{Ar-H}$), 8.42 (2H, d, $J = 24$ Hz, $2 \times \text{Ar-H}$), 8.56 (2H, d, $J = 18$ Hz, $2 \times \text{Ar-H}$); MALDI-TOF Anal. calc. m/z 604.01; Found: $[\text{M-F}]^+$ 589.20; Anal. calc for $\text{C}_{29}\text{H}_{21}\text{BBr}_2\text{F}_2\text{N}_2$: C, 57.47; H, 3.49; N, 4.62; Found: C, 57.50; H, 3.43; N, 4.55.



Scheme 2.3. Synthesis of BODIPYs **4** and **5** (refer to scheme 2.1 for the R-group).

The reduction of BODIPY **2(a)** was achieved following a modified version of a procedure reported previously [175]. To a solution of BODIPY **2(a)** (0.5208 g, 1.41 mmol) in 11.5 ml DMF, sodium sulfide nanohydrate was added in excess (ca. 0.217 g). The mixture was refluxed overnight. Upon reaction completion, the product was washed with water to remove excess sodium sulfide nanohydrate and DMF, and was extracted with DCM. The organic layers were combined, dried over Na_2SO_4 , and evaporated to dryness under vacuum. The residue was purified by flash column chromatography by eluting with DCM to yield **4** as a bright orange solid in 68% yield (0.3552 g); IR (cm^{-1}): 3493 and 3396 (Ar N-H), 3230 (Ar C-H), 2922-2852 (Aliph C-H), 1610 (Ar C-C); ^1H NMR (600 MHz; CDCl_3): ppm 1.49 (6H, s, CH_3), 2.54 (6H, s, CH_3), 3.82 (2H, s, Ar- NH_2), 5.97 (2H, s, 2 \times CH), 6.78 (2H, d, $J = 12$ Hz, 2 \times Ar-H), 7.01 (2H, d, $J = 12$ Hz, 2 \times Ar-H); ESI-MS Anal. calc. m/z 339.17; Found. 339.20; Anal. calc for $\text{C}_{19}\text{H}_{20}\text{BF}_2\text{N}_3$: C, 67.28; H, 5.94; N, 12.39. Found: C, 67.02; H, 5.53 N, 12.11.

BODIPY **5** was formed following a modified version of a procedure reported previously [118]. To a solution of BODIPY **4** (113.30 mg, 0.33 mmol) in 62 mL of dry DCM, liquid bromine (2 mL, 0.099 mol) in DCM (16 mL) was added dropwise overnight at 0 °C. The mixture was left stirring

until most of the starting material had been converted to the desired product, was washed with an aqueous solution of sodium thiosulfate, and extracted by DCM. The organic layers were combined, dried over Na_2SO_4 , and evaporated to dryness under vacuum. The residue was purified by flash column chromatography by eluting with 1:9 ethyl acetate:hexane to yield **5** as a dark red solid. BODIPY **5** was obtained in 89% yield (101.23 mg); IR (cm^{-1}): 3480 and 3381 (Ar N-H), 2922-2851 (Aliph C-H), 1615 (Ar C-C); ^1H NMR (600 MHz; CDCl_3): ppm 2.62 (12H, s, $4 \times \text{CH}_3$), 3.49 (2H, s, Ar- NH_2); ESI-MS Anal. calc. m/z 806.63; Found [M+H] 808.60; Anal. calc for $\text{C}_{19}\text{H}_{14}\text{BBBr}_6\text{F}_2\text{N}_3$: 806.63; C, 28.08; H, 1.74; N, 5.17. Found: C, 28.40; H, 2.01 N, 5.20. . UV-Vis (DMSO): λ_{max} nm (log ϵ): 532 (4.45), 495 (3.97), 390 (3.61).

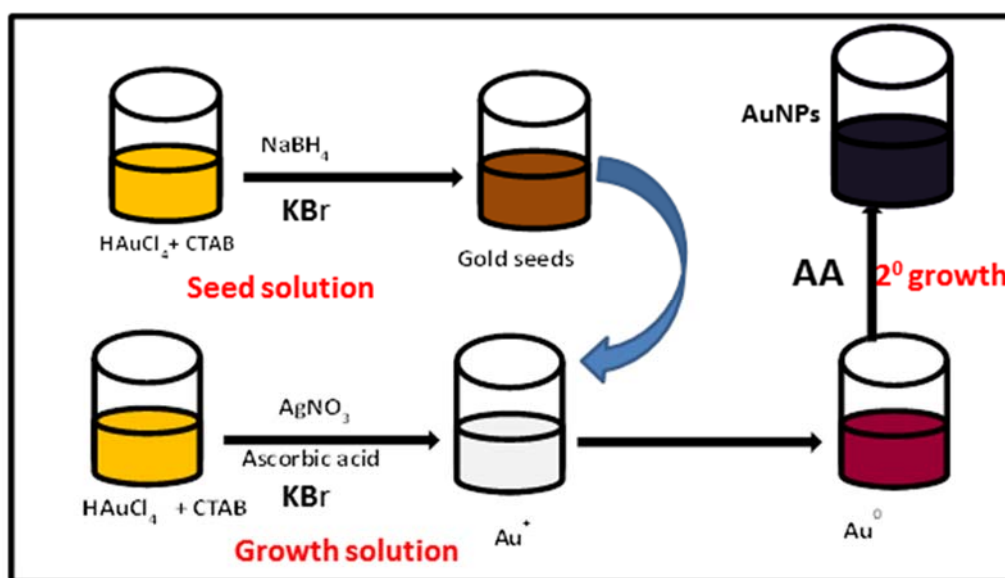


Figure 2.1. Synthesis of gold nanorods through continuous secondary growth.

AuNRs were synthesized following a method reported previously in the literature [176]. A 100 mL solution of AuNRs, a seed solution, a primary growth solution (GS), and a secondary

GS were prepared. The deionised water (DIW) used to prepare all of the solutions was preheated to 30 °C before the addition of any reagents.

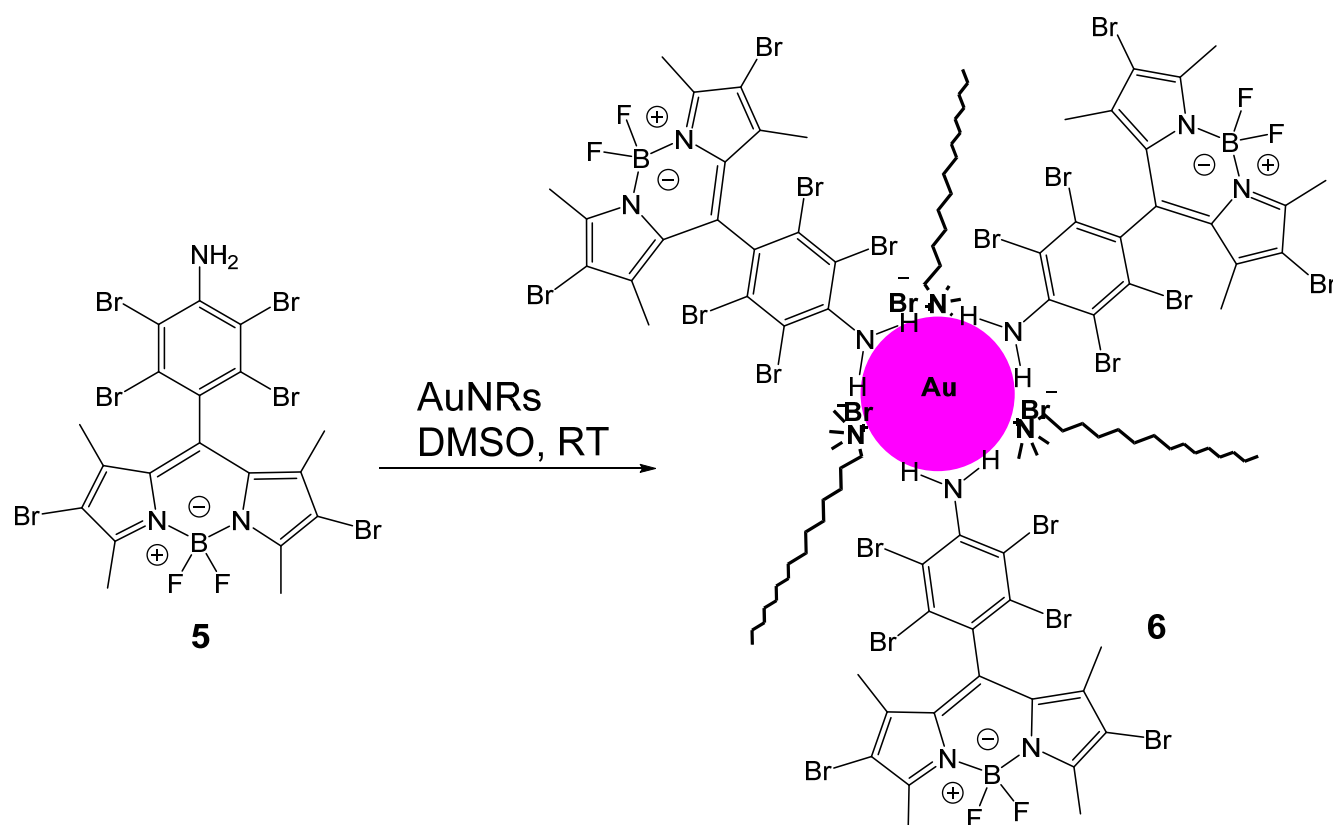
Preparation of seed solution

0.3640 g of CTAB (0.9988 mmol) was dissolved in 8 mL of DIW. Solutions of 11.9 mg (0.10 mmol) of KBr in 1 mL of DIW and 1.0 mg (2.54 μ mol) of H₂AuCl₄·3H₂O in 1 mL of DIW were added to the CTAB solution. 1 mL/37.8 mg of ice cold NaBH₄ was added into the stirring solution of precursors. The seed solution was stirred for two minutes after adding NaBH₄ and then left still for three minutes before addition into the primary growth solution.

Preparation of primary growth solution

3.4309 g of CTAB (9.4139 mmol) was dissolved in 77 mL of DIW. The mixture was kept in a water bath set to 30 °C. 0.1120 g of KBr (0.9412 mmol) in 1 mL of DIW was added to the CTAB solution, giving 0.1 mol of KBr per mol of CTAB. A solution containing 3.26 mg (0.0192 mmol) of AgNO₃ in 1 mL of DIW was then added. A light yellow solution containing 37.9 mg (0.0962 mmol) of H₂AuCl₄·3H₂O was dissolved in 20 mL of DIW and was then added to the CTAB solution, which became a deep orange color. Finally, 18.6 mg (0.105 mmol) of ascorbic acid dissolved in 1 mL of DIW was added to this mixture, causing it to become colorless. 0.1358 mL of the seed solution was rapidly added by micropipette into the primary GS, after which the primary GS was completely inverted seven times to homogenize any seed solution caught in the foam, while taking care to avoid excessive foaming. The solution was then left still for one hour in a water bath at 30 °C, to allow the seeded primary GS to evolve into nanorods

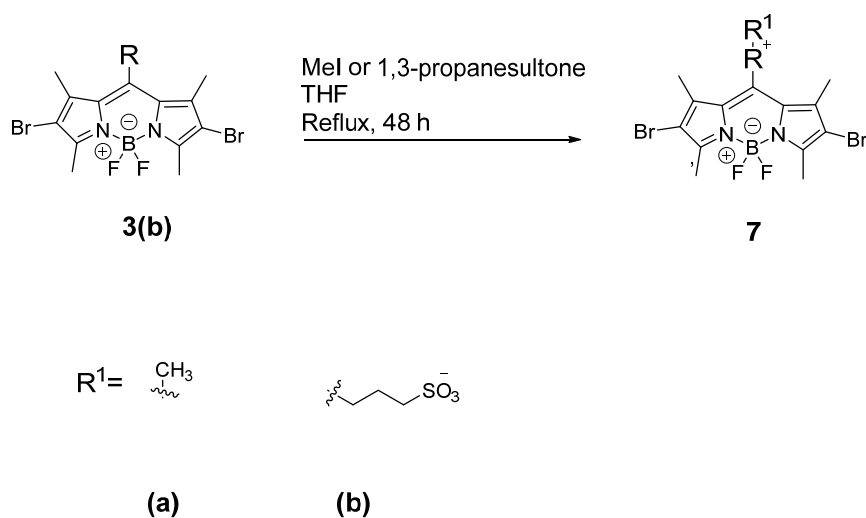
(NRs). A secondary GS comprised of 16.7 mg (0.0948 mmol) of AA in 10 mL of DIW was prepared to commence and sustain the secondary growth phase. An amount of 5 mL of the secondary GS was added into 100 mL of vigorously stirring NRs.



Scheme 2.4. Functionalization of AuNRs with BODIPY 5.

BODIPY 5 was functionalised following a modified version of a procedure reported in the literature [177]. To a solution of BODIPY 5 (0.2 mg, 26 μ M) in DMSO (15 mL), AuNRs (20 mL) were added, and the mixture was stirred at room temperature for 24 h. The solutions of

functionalized AuNRs were centrifuged for 30 min and redispersed in aqueous solution after the supernatant was removed.

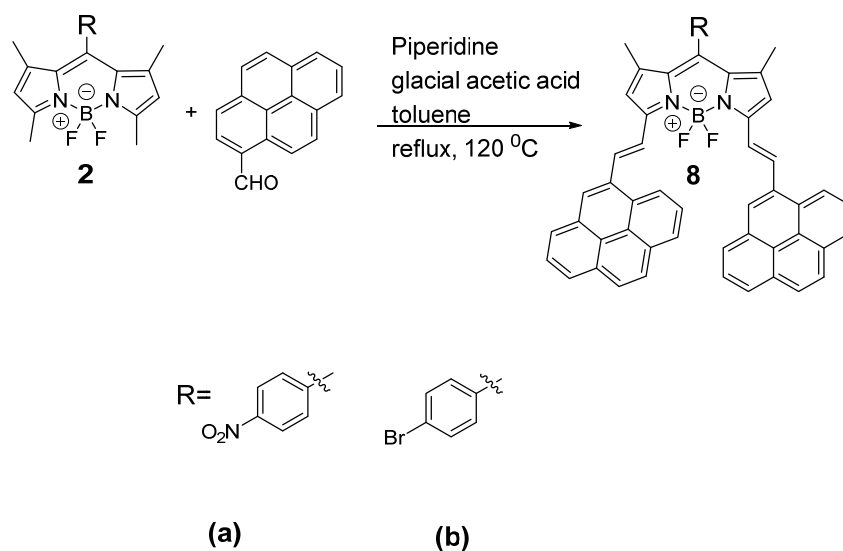


Scheme 2.5. Synthesis of BODIPY **7**.

BODIPYs **7(a)** and **7(b)** were synthesized following a modified version of a procedure reported in the literature [178]. To solutions of BODIPY **3(b)** (79.6 mg, 0.15 mmol) in 10 mL of THF, were added either CH_3I or 1,3-propanesultone (94 μL , 0.15 mmol). The solutions were kept under reflux and stirred for 48 h. The products were precipitated by the addition of 30 mL of Et_2O and filtered. Upon cooling, the precipitate was thoroughly washed with diethyl ether to give **7(a)** and **7(b)** as dark red solids.

BODIPY **7(a)** obtained in 88% (70.5 mg); IR ($\nu_{\text{max}}/\text{cm}^{-1}$): 3299 (Ar C-H), 2918-2850 (Aliph C-H), 1600 (Ar C-C); ^1H NMR (400 MHz, DMSO-d_6): ppm 1.58 (6H, s, $2 \times \text{CH}_3$), 2.10 (6H, s, $2 \times \text{CH}_3$), 2.88 (3H, s, CH_3), 2.92 (3H, s, CH_3), 2.97 (3H, s, CH_3), 7.20 (2H, d, $J = 12$ Hz, $2 \times \text{Ar-H}$), 7.33 (2H, d, $J = 12$ Hz, $2 \times \text{Ar-H}$); MALDI-TOF Anal. calc. m/z 540.08; Found: $[\text{M}+\text{H}]^+$ 541.77; Anal. calc. for $\text{C}_{22}\text{H}_{25}\text{BBr}_2\text{F}_2\text{N}_3^+$: C, 48.93; H, 4.67; N, 7.78; Found: C, 48.75; H, 4.70; N, 7.83. UV-Vis (EtOH): λ_{max} nm (log ϵ): 532 (4.52), 360 (4.48).

BODIPY **7(b)** obtained in, 62% (31 mg); IR ($\nu_{\max}/\text{cm}^{-1}$): 3225 (Ar C-H), 2934-2870 (Aliph C-H), 1600 (Ar C-C), 1142 (S=O); ^1H NMR (400 MHz, DMSO- d_6): ppm 1.24 (3H, s, CH_3), 1.71 (2H, s, 2 \times CH), 1.91 (6H, s, 2 \times CH_3), 2.33 (2H, s, 2 \times CH), 2.44 (2H, s, 2 \times CH), 2.54 (9H, s, 3 \times CH_3), 2.67 (2H, s, 2 \times CH), 6.98 (2H, d, $J = 12$ Hz, 2 \times Ar-H), 7.10 (2H, d, $J = 12$ Hz, 2 \times Ar-H); MALDI-TOF Anal. calc. m/z 647.18; Found: $[\text{M}]^+$ 647.04; Anal. calc. for $\text{C}_{24}\text{H}_{28}\text{BBr}_2\text{F}_2\text{N}_3\text{O}_3\text{S}$: C, 44.54; H, 4.36; N, 6.49; S, 4.95; Found: C, 45.02; H, 4.21; N, 6.65, S, 5.22. UV-Vis (EtOH): λ_{\max} nm (log ϵ): 525 (4.71), 312 (4.73).



Scheme 2.6. Synthesis of BODIPY **8**.

BODIPYs **8(a)** and **8(b)** were synthesized following a modified version of the Knoevenagel condensation method [179] (Scheme 1). In a round-bottomed flask equipped with a Dean-Stark apparatus, 1-pyrenecarboxaldehyde (0.54g, 2.61 mmol), glacial acetic acid (0.83 ml) and piperidine (0.83 mL) were added to a stirred solution of BODIPY **2(d)** (0.50 g, 1.3 mmol)

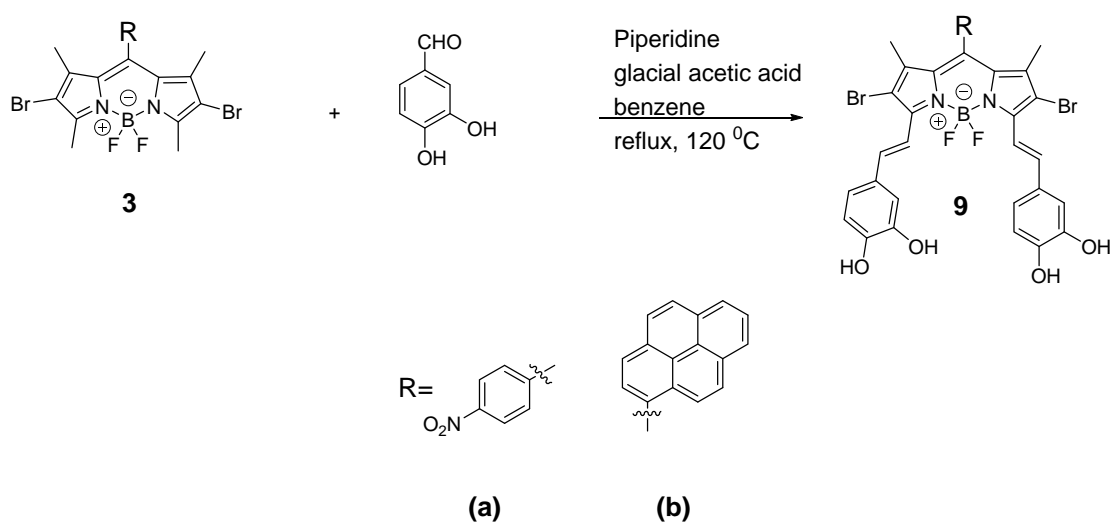
dissolved in 83 mL of toluene. The solution was heated at its boiling point until it had evaporated to dryness. The resulting solid was washed with 1% hydrochloric acid three times and extracted with DCM. The organic phase was dried over MgSO_4 , and the solvent was evaporated under reduced pressure. The residue was purified by flash column chromatography on SiO_2 , by eluting with 1:9 ethyl acetate:DCM, to yield a green solid as the product.

BODIPY **8(a)** obtained in 61% yield (0.30g); IR ($\nu_{\text{max}}/\text{cm}^{-1}$): 3011 (Ar C-H), 2922-2852 (Aliph C-H), 1605 (Ar C-C), 1513 (Ar N-O); ^1H NMR (600 MHz, CDCl_3): ppm 1.99 (6H, s, 2 \times CH_3), 6.05 (2H, s, 2 \times CH), 7.53 (2H, d, $J = 12$ Hz, 2 \times Ar-H), 7.65 (2H, d, $J = 12$ Hz, 2 \times Ar-H); 7.70 (2H, d, $J = 12$ Hz, 2 \times Ar-H), 7.80 (2H, d, $J = 6$ Hz, 2 \times Ar-H), 8.00 (2H, t, 2 \times Ar-H), 8.17 (8H, m, 8 \times Ar-H), 8.46 (6H, m, 6 \times Ar-H), 8.58 (2H, d, $J = 6$ Hz, 2 \times Ar-H); MALDI-TOF Anal. calc. m/z 793.68; Found: $[\text{M}+2\text{H}]^+$ 795.81; Anal. calc. for $\text{C}_{53}\text{H}_{34}\text{BF}_2\text{N}_3\text{O}_2$: C, 80.21; H, 4.32; N, 5.29; Found: C, 79.13; H, 5.07; N, 5.11. UV-Vis (DMSO): λ_{max} nm (log ϵ): 709 (4.76), 653 (4.53), 441 (4.31), 414.5 (4.37), 338.5 (4.46).

BODIPY **8(b)** obtained in 70% yield (0.42g); IR (cm^{-1}): 2995 (Ar C-H), 2920-2832 (Aliph C-H), 1602 (Ar C-C); ^1H NMR (600 MHz; CDCl_3): ppm 2.58 (6H, s, 2 \times CH_3), 6.05 (2H, s, 2 \times CH), 7.61 (2H, d, $J = 15$ Hz, 2 \times Ar-H), 7.69 (2H, d, $J = 6$ Hz, 2 \times Ar-H); 7.78 (2H, d, $J = 12$ Hz, 2 \times Ar-H), 7.87 (2H, d, $J = 6$ Hz, 2 \times Ar-H), 7.99 (2H, d, 2 \times Ar-H), 8.06 (4H, m, 4 \times Ar-H), 8.18 (8H, m, 8 \times Ar-H), 8.49 (4H, m, 4 \times Ar-H), MALDI-TOF Anal. calc. m/z 827.58; Found: $[\text{M}+2\text{H}]^+$ 830.17; Anal. calc. for $\text{C}_{53}\text{H}_{34}\text{BBrF}_2\text{N}_2$: C, 76.92; H, 4.14; N, 3.39; Found: C, 76.82; H, 5.86; N, 4.22. UV-Vis (DMSO): λ_{max} nm (log ϵ): 705.5 (5.21), 648 (4.95), 421.5 (4.78), 410.5 (4.83), 345 (5.10), 329.5 (5.05).

Preparation of thin films of **8(a)** and **8(b)**

To 2.5 mL of BODIPY **8(a)** (0.0134 M) and BODIPY **8(b)** (0.00166 M) solutions in DCM, 100 mg of poly(bisphenol A carbonate) (PBC) was added to form PBC-BODIPY **8(a)** and PBC-BODIPY **8(b)** thin films, respectively. The film was prepared by placing 200 μ L of these solutions on a glass slide and left to dry in the oven at 60 $^{\circ}$ C. The thickness of the thin films obtained were 0.065 and 0.083 mm for PBC/BODIPY **8(a)** and PBC/BODIPY **8(b)**, respectively.



Scheme 2.7. Synthesis of BODIPY **9**.

BODIPYs **9(a)** and **9(b)** were synthesized following a modified version of the Knoevenagel condensation method [180]. A mixture of BODIPY **3(a)** or **3(b)** (120 mg, 0.14 mmol), 3,4-dihydroxybenzaldehyde (59 mg, 0.2 mmol), glacial acetic acid (0.4 mL), piperidine (0.4 mL), was refluxed in toluene (50 mL) until the aldehyde was consumed. The water formed during

the reaction was removed azeotropically with a Dean-Stark trap apparatus. The mixture was concentrated under reduced pressure. Then the residue was purified by silica gel column chromatography using DCM:MeOH (97:3) as the eluent. The green fraction was collected and isolated with a rotary evaporator to afford the desired product as a green solid.

BODIPY **9(a)** obtained in 35% yield (0.042 g); IR ($\nu_{\max}/\text{cm}^{-1}$): 3322 (O-H), 2955 (Ar C-H), 2916-2849 (Aliph C-H), 1463 (Ar C-C), 1306 (Ar N-O); $^1\text{H NMR}$ (600 MHz, DMSO- d_6): ppm 1.96 (6H, s, 2 \times CH₃), 6.91 (4H, d, $J = 6.0$ Hz, 4 \times Ar-H), 7.24 (6H, m, 6 \times Ar-H); 7.27 (2H, d, $J = 6.0$ Hz, 2 \times Ar-H), 7.29 (2H, d, $J = 6.0$ Hz, 2 \times Ar-H), 9.70 (4H, s, 4 \times Ar-OH), MALDI-TOF Anal. calc. m/z ; 767.18 Found: $[\text{M}+2\text{H}]^+$ 770.03; Anal. calc. for C₃₃H₂₄BBr₂F₂N₃O₆: C, 51.66; H, 3.15; N, 5.48; Found: C, 51.76; H, 4.02; N, 5.60. UV-Vis (EtOH): λ_{\max} nm (log ϵ): 700 (4.98), 635 (4.74), 508 (4.35), 407 (4.68), 323 (4.02).

BODIPY **9(b)** obtained in 55% yield (0.055 g); IR ($\nu_{\max}/\text{cm}^{-1}$): 3204 (O-H), 3053 (Ar C-H), 2920-2875 (Aliph C-H), 1591 (Ar C-C); $^1\text{H NMR}$ (600 MHz, DMSO- d_6): ppm 2.65 (6H, s, 2 \times CH₃), 6.98 (4H, d, $J = 6.0$ Hz, 4 \times Ar-H), 7.30 (6H, m, 6 \times Ar-H), 8.27 (3H, m, 3 \times Ar-H), 8.45 (4H, m, 4 \times Ar-H), 8.66 (2H, d, $J = 18$ Hz, 2 \times Ar-H), 9.84 (4H, s, 4 \times Ar-OH); MALDI-TOF Anal. calc. m/z ; 846.33 Found: $[\text{M}]^+$ 847.10; Anal. calc. for C₄₃H₂₉BBr₂F₂N₂O₄: C, 61.03; H, 3.45; N, 3.31; Found: C, 61.23; H, 4.01; N, 3.35. UV-Vis (EtOH): λ_{\max} nm (log ϵ): 690 (4.89), 620 (4.42), 503 (4.24), 419 (4.48), 356 (4.81), 320 (4.12).

2.4. Summary

All of the target BODIPY dyes were successfully synthesized following modified versions of previously reported literature procedures, and were fully characterized. The dyes were all obtained in reasonable yield.

Chapter 3

3. RESULTS AND DISCUSSION

3.1. Synthesis and characterization

This chapter reports on the synthesis and structural characterization of a series of novel BODIPY dye derivatives and BODIPY-gold nanorod conjugates. The characterization techniques employed include $^1\text{H-NMR}$, FT-IR and UV-visible absorption spectroscopy, fluorimetry, MALDI-TOF-MS, CHNS elemental analysis, XRD and TEM. Optical limiting properties of some of the BODIPY dyes were also studied using a Z-scan apparatus.

3.1.1 Synthesis

The reaction schemes for compounds synthesized in this work are shown in chapter 2. Following the commonly used three-step one-pot acid catalysed condensation reaction, a series of BODIPY dyes (**1(a)-(d)**) were synthesized from commercially available 2, 4-dimethylpyrrole and aldehyde derivatives (Figure 3.1) [181]. The desired products were obtained in moderate to high yields. The synthesis of BODIPY dyes **1(a)-(d)** shown in Figure 3.1 began with the condensation of two pyrrole units with a different aldehyde derivatives in anhydrous DCM. TFA was used as a catalyst to promote condensation through protonation or chelation to the carbonyl oxygen. Thus, enhancing the partial positive charge on the carbonyl carbon and ensuring nucleophilic attack by the pyrrole.

In all of the syntheses reported herein, under inert conditions, TFA was used to facilitate the synthesis of the intermediate dipyrromethanes which were subsequently oxidized to more stable dipyrromethenes using *p*-chloranil. Once formed, the dipyrromethenes were first

deprotonated under basic conditions using Et_3N , before being exposed to excess $\text{BF}_3 \cdot \text{OEt}_2$ to yield the BF_2 -complexed BODIPY structures.

In order to form BODIPY dyes that are suitable for use as photosensitizers for APDT and as NLO materials, the goal was to incorporate three structural modifications. First, to facilitate the intersystem crossing via the heavy atom effect, BODIPY dyes **1(a),(b),(d)** were functionalised with bromines in the 2, 6-positions following electrophilic substitution reaction previously reported in literature [118] to form BODIPY dyes **2(a)-(c)**. The addition of excess bromine resulted in the bromination of the phenyl ring at the 8-position to form BODIPY **3** (Figure 3.2).

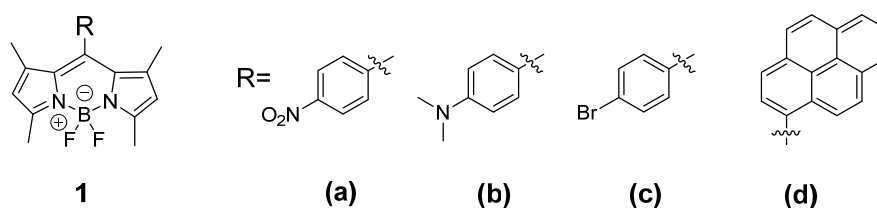


Figure 3.1. Molecular structures of BODIPYs **1a-d**.

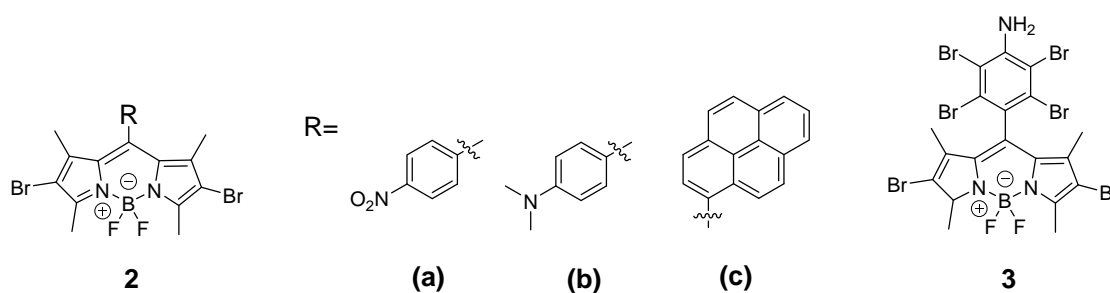


Figure 3.2. Molecular structures of BODIPYs **2a-c** and **3**.

Secondly, to improve the water solubility, without compromising the organic solubility which is essential for chromatographic manipulations, quaternized BODIPYs **4(a)-(b)** were synthesized according to the established literature procedures [178] (Figure 3.3). BODIPY **2(b)** was treated with excess iodomethane as a quaternising agent in DMF to obtain the water soluble quaternized BODIPY **4(a)**. Quaternization of **2(b)** with an excess of 1, 3-propanesultone led to the formation of zwitterionic BODIPY **4(b)**.

Finally, to shift the main spectral bands of BODIPY dyes **5** and **6** to longer wavelengths, the π -conjugation was extended at the 3, 5-positions. BODIPY dyes with methyl substituents on the 3- (or 5-) position have been shown previously to undergo Knoevenagel condensation reactions with aldehydes to yield longer wavelength absorbing dyes (red shifts of ca. 100 nm are possible) with intramolecular charge transfer (ICT) characteristics [182].

For APDT purposes, gold nanorods were synthesized following a synthetic procedure previously reported in literature [176], using CTAB as both the phase transfer agent and the protecting ligand. The gold nanorods were further functionalized with BODIPY **3** to improve the intersystem crossing and water solubility. The nitrobenzene moiety of BODIPY **2(a)** was reduced to an aniline group following a procedure that has been reported previously for an analogous phthalocyanine synthesis [183], which involved the use sodium sulfide nanohydrate and dry K_2CO_3 as a base in anhydrous DMF.

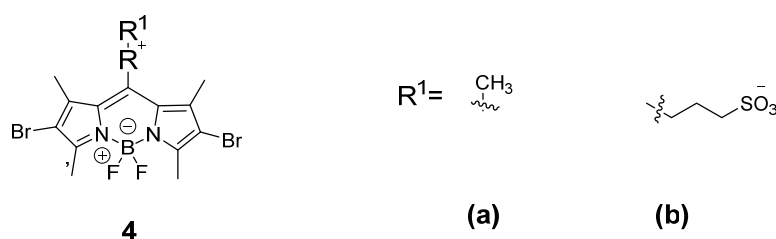


Figure 3.3. Chemical structure of BODIPY **4**.

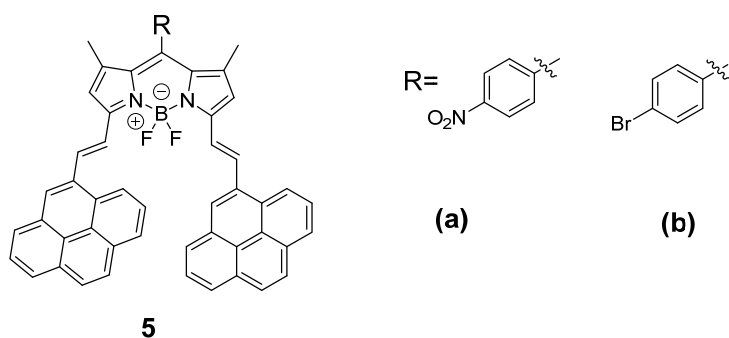


Figure 3.4. Chemical structure of BODIPY **5**.

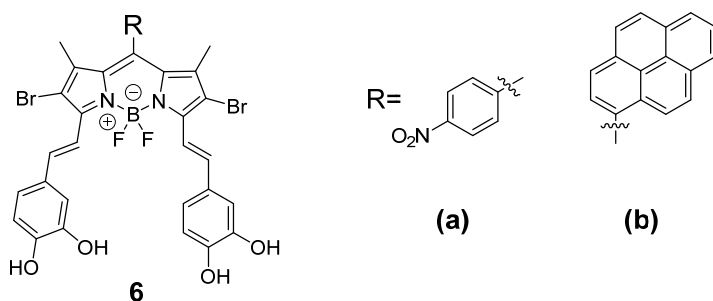


Figure 3.5. Chemical structure of BODIPY **6**.

BODIPY **3** was attached to gold nanorods through a ligand exchange method, where loosely bound CTAB ligands were partially exchanged by BODIPY **3**. To attach BODIPY **3** to the gold nanorods surface, BODIPY **3** was derivatized with an aniline moiety, which provided a direct linkage to the nanorods surface via self-assembly. The partial presence of CTAB is important since the presence of the bromine atom adds to the enhancement of spin-orbit coupling via the heavy atom effect [184]; hence increasing the population of the triplet state and increasing generation of singlet oxygen.

3.1.2 Characterization

Characterization of BODIPY **3** was achieved using ^1H NMR spectroscopy to confirm the number of bromines substituted and FTIR spectroscopy to confirm the conversion of the NO_2 to NH_2 group (Figure 3.6). As anticipated, the ^1H NMR spectrum of BODIPY **3** showed complete disappearance of proton signals in the aromatic region. ESI-MS showed molecular ion peaks consistent with the target BODIPY compounds.

The characterization of the AuNRs was achieved by transmission electron microscopy (TEM) and X-ray diffraction (XRD). The TEM images reveal the presence of rod and bone shaped structures in aqueous and aqueous-DMSO (1:1) mixtures, respectively (Figure 3.8B) with a narrow size distribution. The nanocrystalline appearance was maintained as shown by the XRD pattern in Figure 3.9A. Functionalization of AuNRs with BODIPY **3** was confirmed by XRD. An increase in the crystalline size of 0.6 nm was calculated from the XRD measurements (Figure 3.9A). In the TEM image, an increase in the aspect ratio of the AuNRs from 2.0 to 2.6 nm is observed upon conjugation (Table 3.1 and Figure 3.9B) along with increased clustering of the AuNRs upon functionalisation.

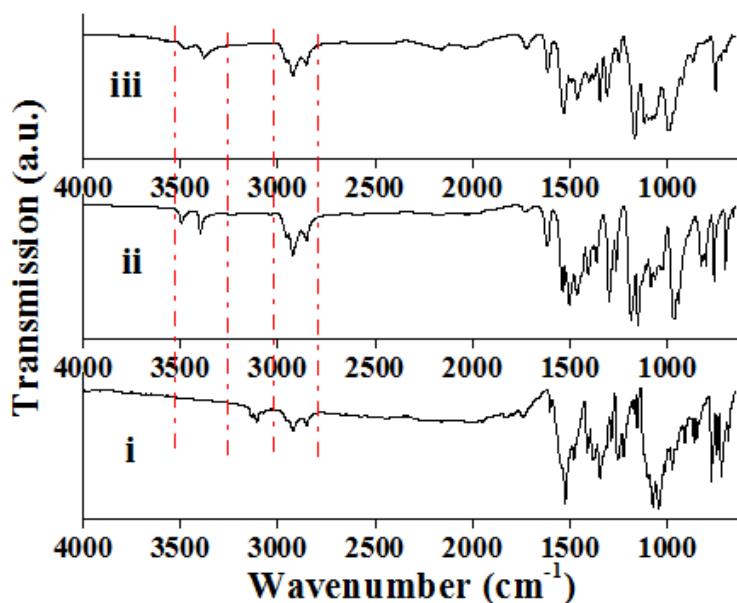


Figure 3.6. FTIR spectra of BODIPY dyes (i) **1(a)**, (ii) **4** (Chapter 2) and (iii) **3** showing the disappearance of the nitro group and the appearance of the amino group and the presence of the methyl group.

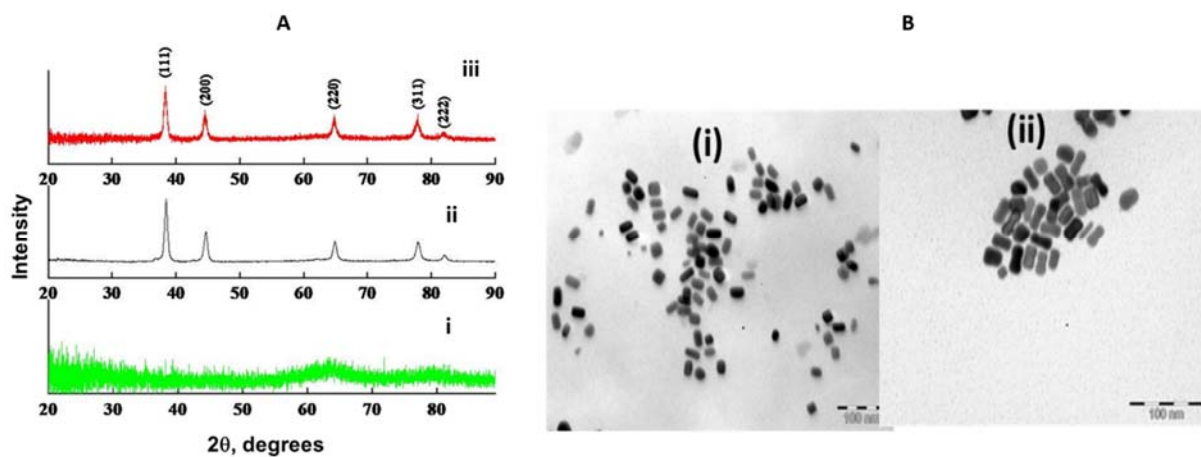


Figure 3.7. (A) The XRD patterns of, (i) **3**, AuNRs (ii) and **3**-AuNR (iii), and (B) TEM images of (i) AuNRs in aqueous solution and (ii) **3**-AuNR in aqueous-DMSO (1:1) solution.

Table 3.1. TEM size of AuNRs and **3**-AuNRs.

Sample	Average aspect ratio	Crystalline size
AuNRs	2.0	28.0
3 -AuNRs	2.6	28.8

X-ray photoelectron spectroscopy (XPS) was used to confirm the chemical composition of the **3**-AuNR conjugates and the results were compared to those obtained for BODIPY **3**. The wide scan XPS spectrum of the conjugate (Figure 3.8) demonstrated the anticipated presence of C, O, N, and Br in the **3**-AuNR sample. The core level high-resolution N_{1s} XPS spectrum of BODIPY **3** contains two characteristic peaks at 399.6 and 401.40 eV. These peaks can be attributed to the C=N and/or C-N and N-H bands, respectively. Figure 3.8 shows the N_{1s} XPS spectrum of **3**-AuNR, which can be deconvoluted into three chemically distinct components centered at 400.0, 402.1 and 406.5 eV corresponding to the C=N and/or N-C, N-H and N-Au bonds. The presence of the N-Au peak as shown in Figure 3.8 demonstrates the participation of the nitrogen atom in the **3**-AuNR conjugate. The core level high-resolution C_{1s} XPS spectra for BODIPY **3** and the **3**-AuNR conjugate, can be deconvoluted into chemically distinct components. The peaks at 285.0 and 286.40 eV that were observed for **3** can be attributed to the C=C and C-C and/or C-N bonds, respectively (Figure 3.8). The C_{1s} XPS spectrum of **3**-AuNRs contains peaks at 285.1 and 286.5 eV, which can be attributed to the C=C and C-C and/or C-N bonds [185]. The small peak shifts towards larger binding energies can be attributed to conjugation of **3** onto the AuNRs [186].

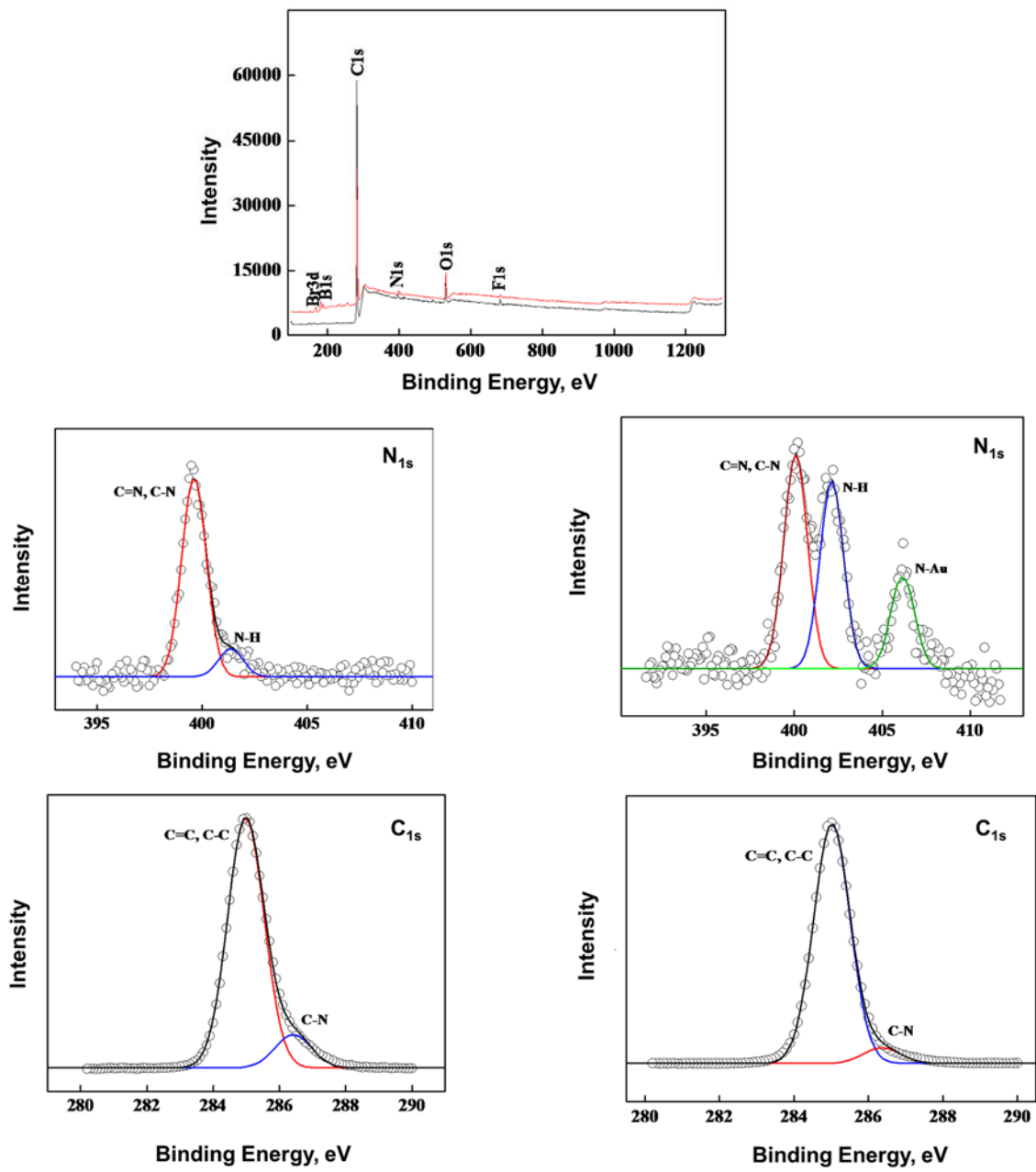


Figure 3.8. XPS spectra for the, (A) wide scans for (i) BODIPY 3 and (ii) 3-AuNRs, and (B) and (C) expanded wide scans for (i) BODIPY 3 and (ii) 3-AuNRs, and wide scans for (i) BODIPY 3 and (ii) 3-AuNRs.

Generally, BODIPY dyes are insoluble in water; however introduction of substituents on the ring enhances their solubility. The quaternized and zwitterionic BODIPY dyes **4(a)** and **4(b)** exhibit excellent solubility in DMF and DMSO and good solubility in water, especially for **4(a)**. The instrumental analyses are consistent with the predicted structures as shown in the experimental section in Chapter 2. The presence of the $-\text{SO}_3$ group in **4(b)** gave rise to strong absorptions at 1142 cm^{-1} ($\nu_{\text{asy}}, \text{SO}_2$) and 1030 cm^{-1} ($\nu_{\text{asy}}, \text{SO}_2$) and these are indicative of the formation of zwitterionic complexes (Figure 3.9A). Furthermore the presence of the bands associated with the C-N bond and the aromatic protons, respectively, between $3000\text{--}2900$ and $1300\text{--}1200\text{ cm}^{-1}$ in the regions highlighted in Figure 3.9A confirm successful quaternization of **2(b)**. The structures of both **4(a)** and **4(b)** were further confirmed by ^1H NMR. All of the substituent and ring protons were observed in the anticipated regions, including those for the propyl chain, and the $-\text{CH}_2-\text{SO}_3$, $-\text{N}-\text{CH}_2$ and $-\text{N}-\text{CH}_3$ groups. Figure 3.9B shows the mass spectrum of **4(a)** which further confirms the predicted structure, since the calculated molecular mass is 540.08 [M+H] .

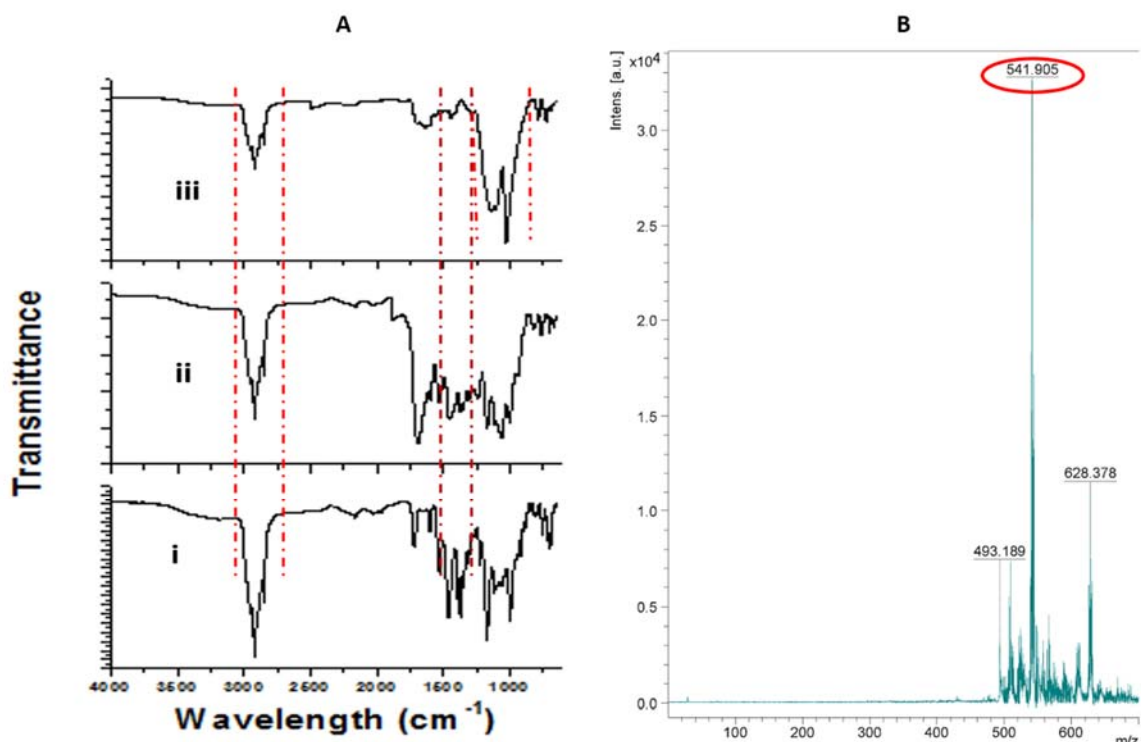


Figure 3.9. A: IR spectra of BODIPY dyes (i) **2(b)**, (ii) **4(a)** and (iii) **4(b)** showing the presence of aromatic and aliphatic alkanes, aromatic amines and the SO₂ group. B: MALDI-TOF mass spectrum of **4(a)** highlighting the expected mass.

Amongst other analytical methods, MALDI-TOF mass spectrometry was used to confirm proposed structures **5(a)** and **5(b)**, based on molecular masses at 795.8 [M+3H]⁺ and 831.1 [M+2H]⁺ (Figure 3.10). FT-IR spectroscopy was used to confirm the presence of the -OH groups in **6(a)** and **6(b)**, Figure 3.11, based on the presence of the broad band in the 3000 cm⁻¹ region. The ¹H NMR spectra of **5(a)-(b)** and **6(b)** contained peaks for the aromatic protons from the pyrene substituent as multiplets between 8 and 7 ppm. The OH groups of BODIPY **6** appeared as a singlet at ca. 9 ppm.

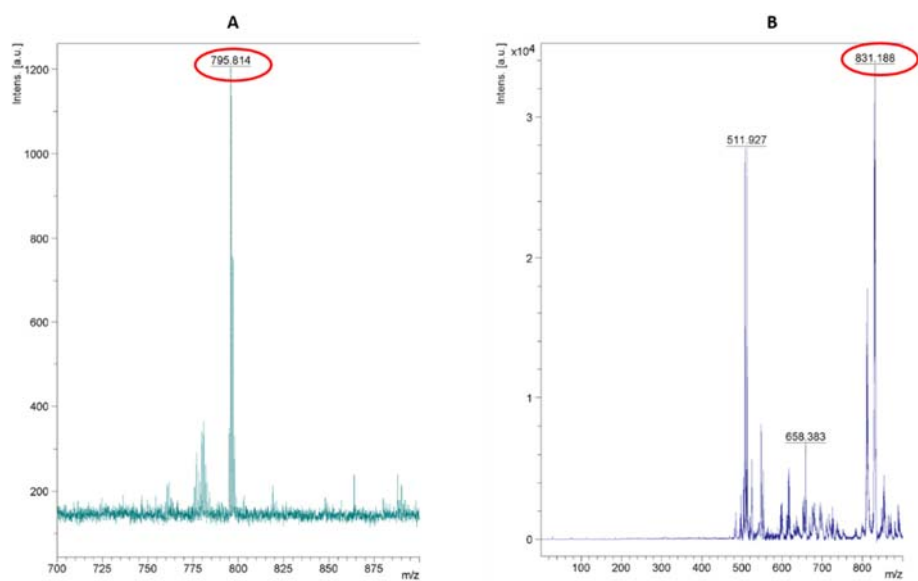


Figure 3.10. MALDI-TOF mass spectrum of A: **5(a)** and B: **5(b)** highlighting the expected mass.

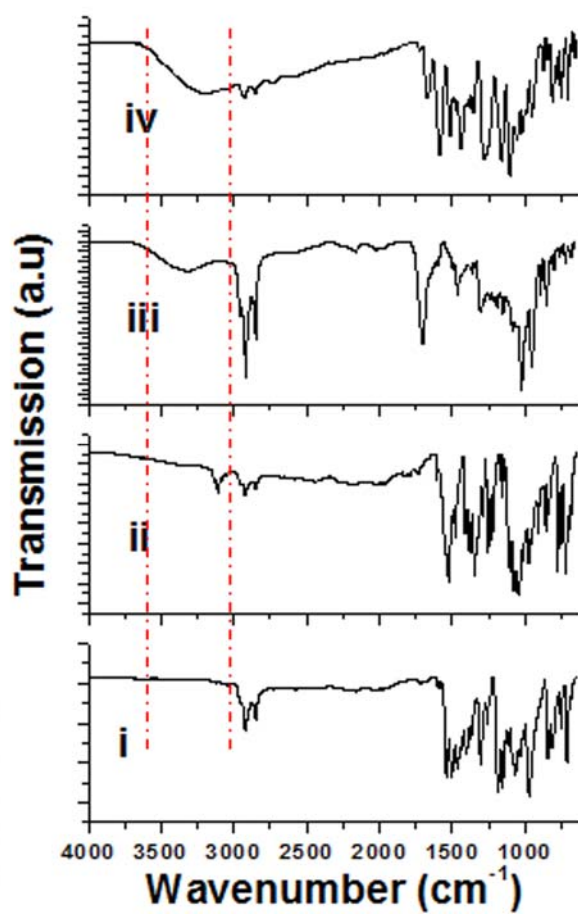


Figure 3.11. IR spectra of BODIPY dyes (i) **2(c)**, (ii) **2(a)** (iii) **6(a)** and (iv) **6(b)** showing the presence and absence of the OH group.

3.1.3 Optical spectroscopy

The absorption spectrum of BODIPY **3** contains the typical BODIPY absorption features, with a strong band in the 500–550 nm region corresponding to the $S_0 \rightarrow S_1$ transition (Figure 3.12A and Table 3.2) and a shoulder of vibrational intensity on the higher energy side, with a weaker band corresponding to the $S_0 \rightarrow S_2$ transition at ca. 420 nm (Figure 3.12A).

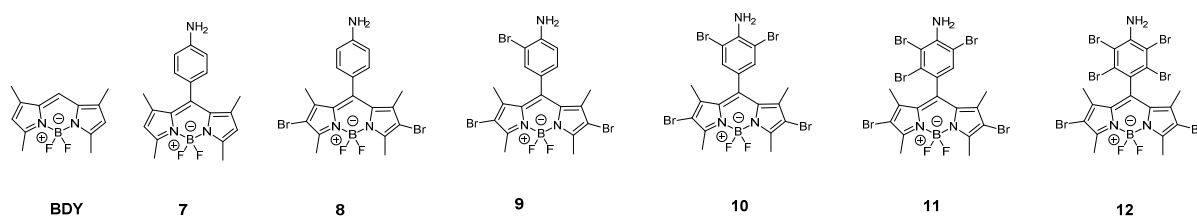


Figure 3.12. Molecular structures for a series of BODIPY dyes studied by TD-DFT.

Figure 3.12 shows the series of BODIPY dyes which were selected to analyze trends in the energies of the HOMO and LUMO of varied number of bromines and hence in the magnitude of the HOMO–LUMO gaps and the wavelengths of the main spectral bands. Despite the presence of the aniline ring at the meso-position, the series of brominated BODIPY dyes have similar electronic absorption spectra with the main BODIPY absorption band centered between 529 and 536 nm for BODIPY **3**, depending on the solvent used (Table 3.4 and Figure 3.13A). The red shift observed upon bromination (Figure 3.13A) can be attributed to a narrowing of the HOMO–LUMO gap due to the effect of the lone pairs on the bromine atoms, since there are significant molecular orbital coefficients in the HOMO and LUMO at the 2, 6-positions of the BODIPY core (Table 3.2 and Figure 3.14).

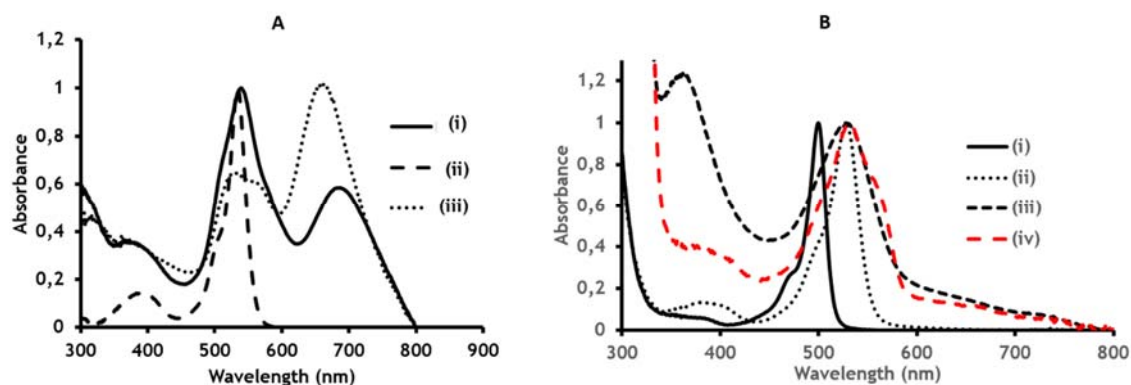


Figure 3.13. Normalized absorption spectra of, A: (i) **3**-AuNR in DMSO: H₂O (1:1), (ii) BODIPY **3** in DMSO and (iii) AuNRs in H₂O; B: (i) **1(b)**, (ii) **2(b)** in DCM (iii) BODIPY **4(a)** and (iv) BODIPY **4(b)** in acetone.

Table 3.2. Calculated and observed electronic excitation wavelengths of 1,3,5,7-tetramethyl-meso-phenyl-BODIPY (BDY), 2(a) and 4 (in chapter 2), 3 and 11 and calculated oscillator strengths and wavefunctions.

		λ_{\max} [nm]		f^a	Wavefunction = ^b
		Exp	Calc		
BDY	S ₀ →S ₁	500 ^c	411	0.55	H→L (96%); ...
2(a)	S ₀ →S ₁	497 ^c	413	0.53	H→L (98%); ...
4	S ₀ →S ₁	500	411	0.53	H→L (96%); ...
11	S ₀ →S ₁	---	434	0.61	H→L (97%); ...
3	S ₀ →S ₁	533	439	0.61	H→L (97%); ...

^a - Calculated oscillator strength. Only bands predicted to have oscillator strengths greater than 0.2 to the red of 350 nm are included. ^b - The wavefunctions based on the eigenvectors predicted by a TD-DFT calculation for the B3LYP optimized geometries with 6-31G(d) basis sets. H and L are used to denote the HOMO and LUMO, respectively. ^c - Experimental values for BDY and 1 are taken from references 187(a)-(c).

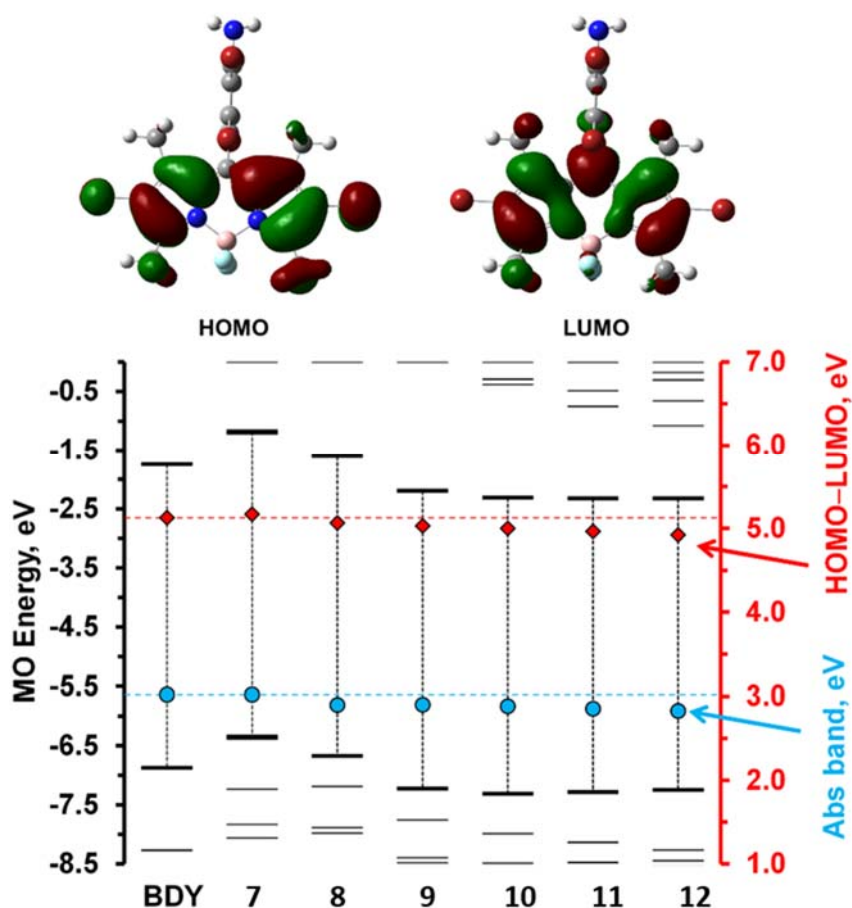


Figure 3.14 The HOMO and LUMO of the B3LYP optimized geometry of **3** at an isosurface values of 0.02 a.u. MO energies in TD-DFT calculations (Bottom) at the CAM-B3LYP/6-31G(d) level of theory for the B3LYP/6-31G(d) optimized geometries of 1,3,5,7-tetramethyl-mesophenyl-BODIPY (BDY), and model structures **7-12** (Fig. 3.12). The HOMO and LUMO for each compound are highlighted with thicker black lines. The calculated HOMO–LUMO gaps and energies for the main BODIPY absorption bands are plotted against a secondary axis.

The surface plasmon resonance (SPR) bands of AuNR are characterised by longitudinal and transverse band at 657.5 and 525 nm, respectively (Figure 3.13A). The transverse band is split into two which may be a result of the bone-shaped AuNRs observed. The electronic absorption spectrum of **3**-AuNR is slightly red shifted from 532 to 539 nm in the complex in

DMSO (Table 3.3 and Figure 3.13A) and broadened relative to the $S_0 \rightarrow S_1$ absorption band of BODIPY **3**. This could be due to the longitudinal dipole moment arrangement of both, which is known to result in red shifts for other chromophores [188]. The presence of the SPR bands confirms the functionalization of the AuNRs with BODIPY **3**. Furthermore, as a result of surface complexation in the AuNRs surface, the SPR band is diminished (Figure 3.13A).

Figure 3.13(B) shows the absorption spectra of BODIPY (i) **1(b)**, (ii) **2(b)** in DCM (iii) **4(a)** and (iv) **4(b)**. BODIPY **1(b)** and **2(b)** showed monomeric behaviour evidenced by a single absorption band. However, absorption band of the quaternized BODIPY dye derivatives **4(a)-(b)** showed an aggregated behaviour. In acetone, the absorption spectrum of the zwitterionic quaternization **4(b)** led to cofacial aggregation as evidenced by the presence of two non-vibrational peaks in the absorption region (Figure 3.13B). The lone pair electrons of the nitrogen atom of the substituent in **2(b)** are delocalized into the ring, thereby raising the highest occupied molecular orbital (HOMO) energy, and ultimately leading to a red shift of the main spectral band. However, when these lone pair electrons are engaged as in quaternized complexes **4(a)-(b)**, its mesomeric contribution to the ring electron density is lost [189]. Accordingly, the absorption band positions of **4(a)-(b)** relative to **2(b)** in acetone are blue-shifted by 1 or 8 nm, respectively (Table 3.3).

In comparison to non-styrylated BODIPYs **1(a)**, **1(c)**, **2(a)** and **2(c)**, introduction of styryl group(s) in the 3, 5-positions induces a significant red shift in the absorption wavelength (Figures 3.15A-3.16 and Table 3.3). This is attributed to the high molecular orbital coefficient at the 3, 5-positions of the BODIPY dyes which leads to the destabilization of the HOMO,

thereby reducing the HOMO–LUMO gap and consequently resulting in a marked red shifting of the absorption band. The behaviour of the absorption spectra of BODIPY **5** embedded in PBD as a thin film remained the same as the one in solution, this indicates that the BODIPY dye is stable even in the solid state (Figure 3.15B).

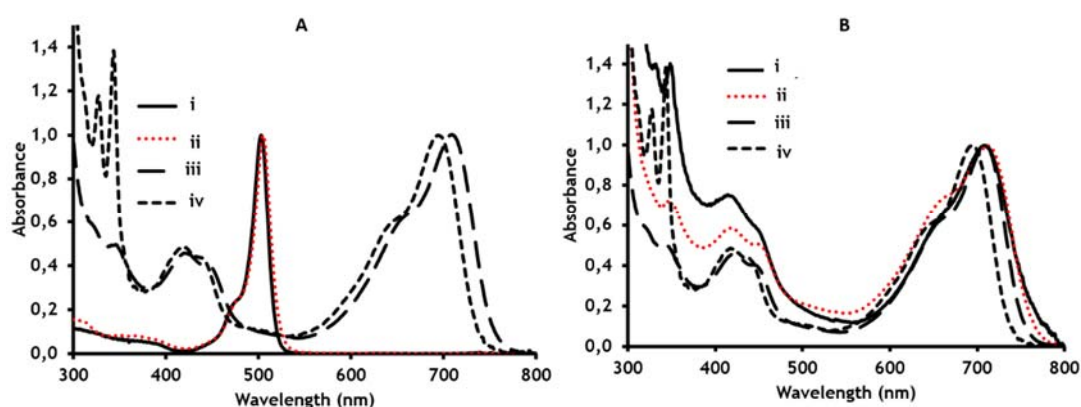


Figure 3.15. Normalized absorption spectra of various BODIPYs, A: (i) **1(a)**, (ii) **1(c)**, (iii) **5(a)** and (iv) **5(b)** in DCM; B: (i) **5(b)**, (ii) **5(a)** embedded in PBS as a thin film, (iii) **5(b)** and (iv) **5(a)**.

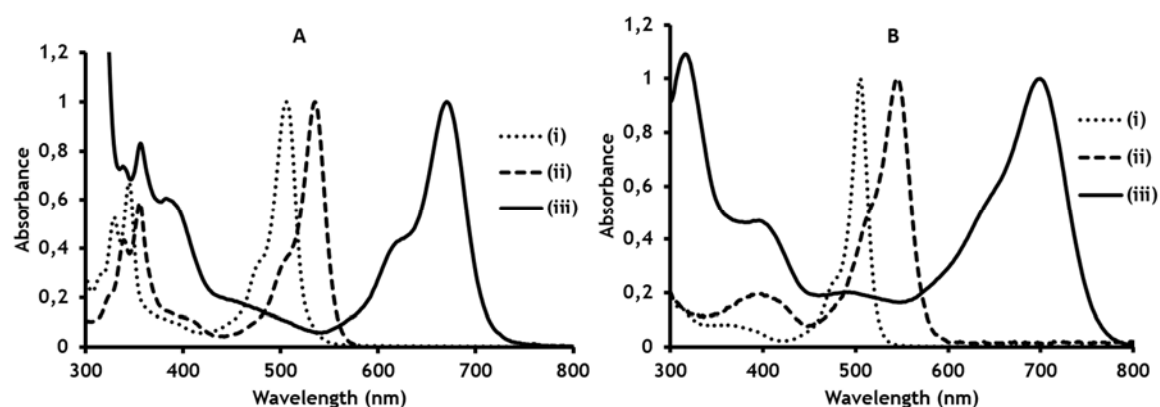


Figure 3.16. Normalized absorption spectra of various BODIPYs, A: (i) **1(d)**, (ii) **2(c)** and (iii) **6(b)**; B: (i) **1(a)**, (ii) **2(a)** and (iii) **6(a)** in DCM.

Plots of absorbance at the main absorption maxima against concentration of the targeted molecules were linear for concentrations below $1 \times 10^{-5} \text{ mol.L}^{-1}$ confirming that the dyes follow the Beer-Lambert law with no aggregation detected below this concentration. Molar extinction coefficients ($\log \epsilon$) were calculated from these plots and the values obtained are shown in Table 3.3.

Table 3.3. Absorption wavelengths of BODIPYs **1-6** and molar extinction coefficient ($\log \epsilon$) values calculated for the target BODIPY dyes.

Sample	Solvent	λ_{abs} [nm]	Log ϵ
1(a)	DCM	505.5	-
1(b)	DCM	501.5	-
1(c)	DCM	503	-
1(d)	DCM	508	-
2(a)	DCM	537.5	-
2(b)	DCM	535	-
2(c)	DCM	538	-
3	DMSO	532	4.45
AuNRs	Aqueous	525, 657.5	-
3-AuNRs	Aqueous-DMSO (1:1)	539, 688	-
4(a)	acetone	527	4.52
4(b)	acetone	534	4.71
5(a)	DCM	710.5	4.76
5(b)	DCM	695	5.21
5(a)-PBS	DCM	708	-
5(b)-PBS	DCM	710.5	-
6(a)	DCM	700	4.98
6(b)	DCM	670	4.89

3.2 Physicochemical properties

3.2.1 Fluorescence studies

The fluorescence spectra of the BODIPY target compounds and the **3**-AuNRs complex are near mirror images of the $S_0 \rightarrow S_1$ absorption band (Figures 3.17-3.20), as would normally be anticipated for complexes with rigid π -conjugation systems. The shape of the fluorescence band is independent of the excitation wavelength indicating that the emission is from the lowest vibrational level of the S_1 excited state [108].

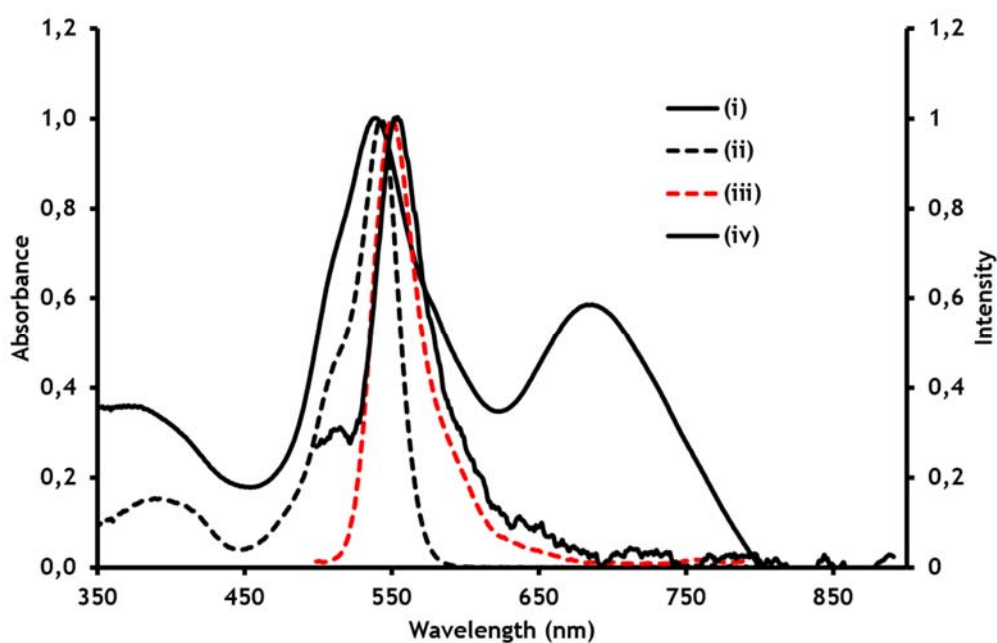


Figure 3.17. Normalized absorption spectra of BODIPYs (i) **3**-AuNRs in DMSO:H₂O (1:1) and (ii) **3** in DMSO), and normalized emission spectra of BODIPYs (iii) **3** in DMSO and (iv) **3**-AuNRs in DMSO:H₂O (1:1).

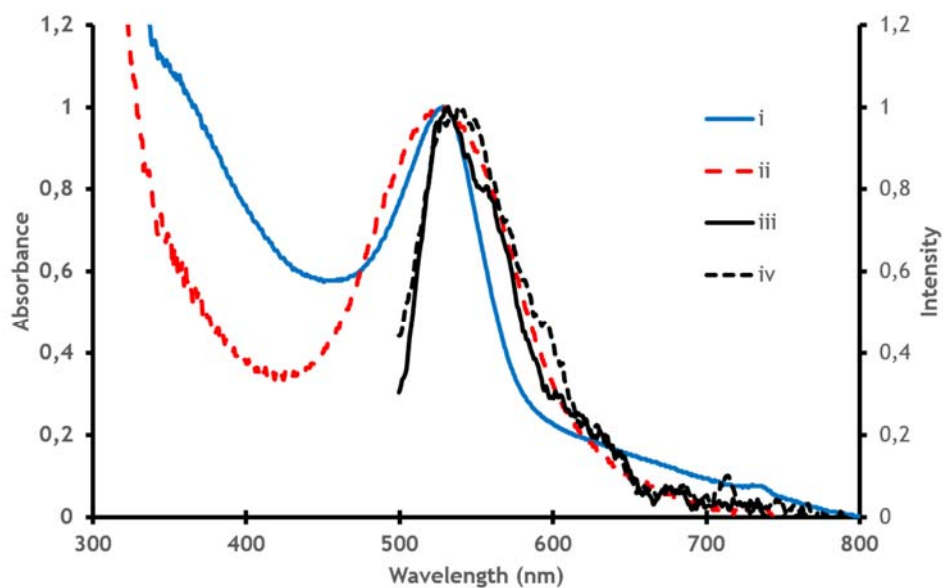


Figure 3.18. Normalized absorption spectra of BODIPYs (i) **4(a)** and (ii) **4(b)**, and normalized emission spectra of BODIPYs (iii) **4(a)** and (iv) **4(b)** in DMSO.

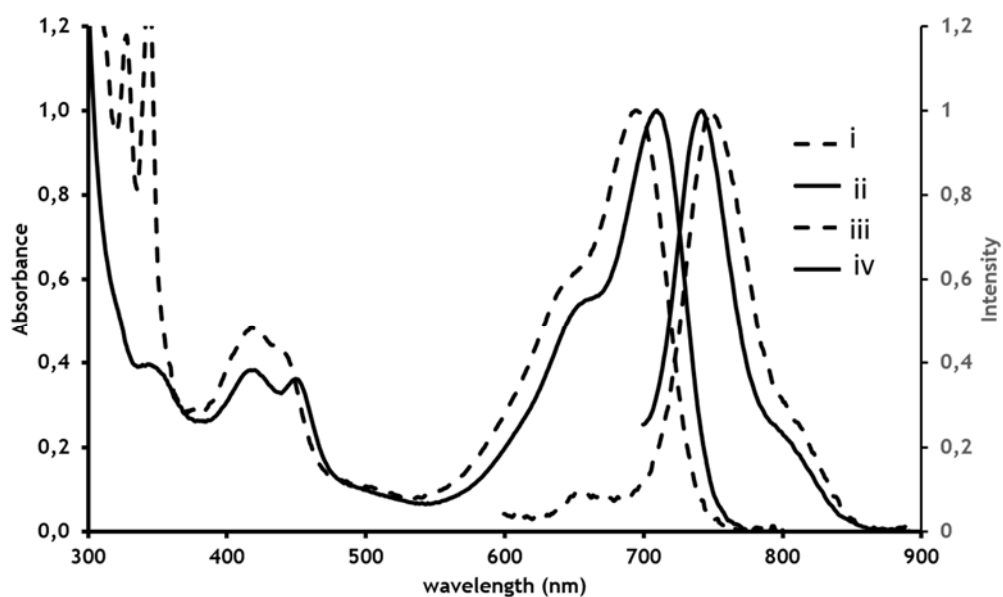


Figure 3.19. Normalized absorption spectra of BODIPYs (i) **5(b)** and (ii) **5(a)**, and normalized emission spectra of BODIPYs (iii) **5(b)** and (iv) **5(a)** in DMSO.

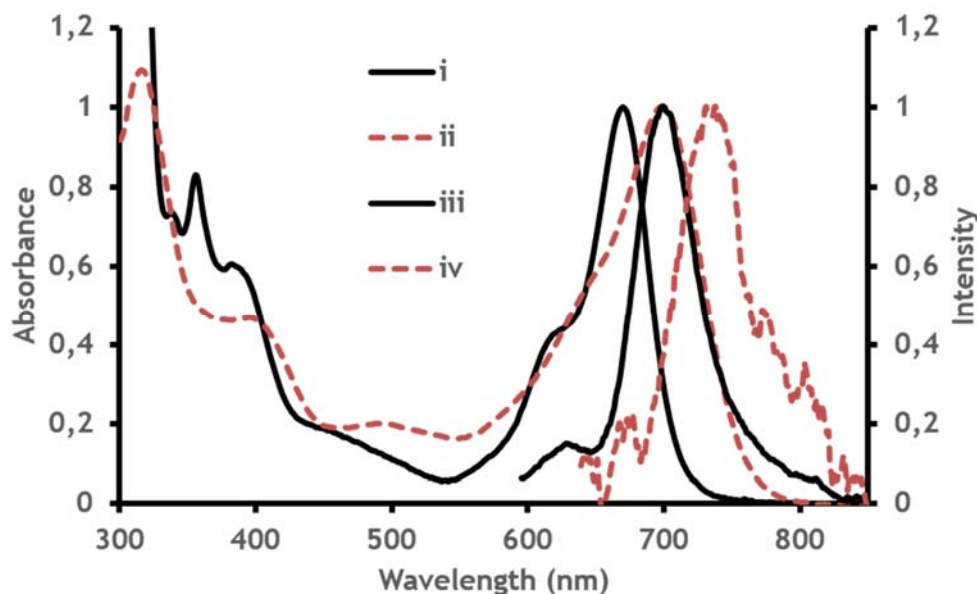


Figure 3.20. Normalized absorption spectra of BODIPYs (i) **6(b)** and (ii) **6(a)**, and normalized emission spectra of BODIPYs (iii) **6(b)** and (iv) **6(a)** in DCM.

The fluorescence quantum yield values (ϕ_F) of BODIPYs can be very high, reaching values of close to unity for some dyes in certain solvents [108, 188]. The calculated ϕ_F values for these BODIPY dyes in different solvents are reported in Tables 3.4 and 3.5. The photophysical properties of **3-6** were measured in dilute solutions (0.05–0.10 absorbance) at excitation wavelengths of 480 and 577 nm for BODIPY **3** and **4**, and **5** and **6**, respectively. The attachment of heavy atoms to the 2, 6-positions of the BODIPY core decreases the fluorescence quantum yield due to the heavy atom effect, which facilitates the $S_1 \rightarrow T_1$ intersystem crossing process. However, there was a decrease in fluorescence for BODIPY **5** which had no bromine atoms, this was attributed to the effect of energy transfer from the BODIPY to the pyrene moiety of the styryl substituent (Table 3.5). In addition, the fluorescence quenching observed for BODIPY **4** was also attributed to aggregation.

A further decrease in the fluorescence quantum yield upon conjugation to form **3**-AuNR, can be attributed to the external heavy atom effect caused by the Au atoms. Therefore, in the case of BODIPYs **3** and **4**, the low fluorescence quantum yields provide an indication of the potential utility of this BODIPY dye and its AuNR conjugate as photosensitizers for APDT. Low fluorescence quantum yields could also be indicative of a good optical limiter in the case of BODIPYs **5** and **6**. Most studies have reported a linear relationship between the fluorescence quantum yield, the wavelength emission band, and the solvent polarity [191-197]. However, in this study a minor blue shift of the emission band was observed with increasing solvent polarity in BODIPY **3** (Table 3.4).

The fluorescence lifetime is independent of the excitation and the emission wavelengths, confirming that emission occurs from the locally excited state [108]. Hence, with regards to BODIPY **3** there was no trend observed in this study. The changes in the emission wavelength in various solvent are shown in Table 3.4. However, the fluorescence lifetime decreases with increasing solvent polarity (Table 3.4). Mono- and bi-exponential fluorescence decay curves (Figures 3.21-3.22) were determined for BODIPYs **3** and **5**, and the **3**-AuNR conjugate, respectively. The bi-exponential curves for **3**-AuNR may be related to the relative orientation of the BODIPY and the nanoparticle. As shown in Figure 3.21, the **3**-AuNR conjugate was found to decay faster than BODIPY **3**, possibly due to enhanced rates of intersystem crossing and non-radiative decay. Furthermore, BODIPY **5(b)** decayed faster than **5(a)** which could be due to the external heavy atom effect induced by the bromine substituent in the phenyl group at the meso-carbon (Figure 3.21).

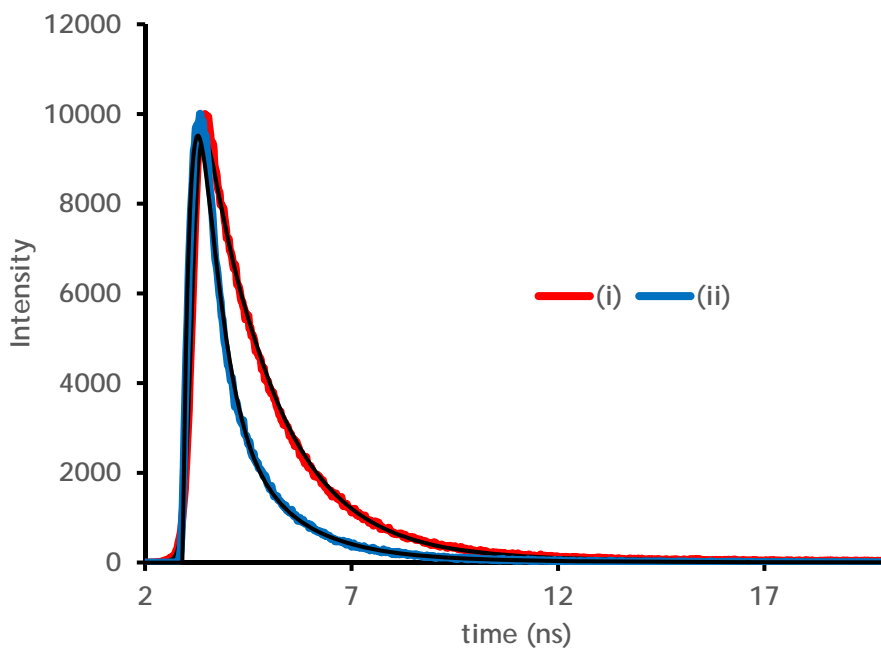


Figure 3.21. Fluorescence decay curves of (i) BODIPY **3** in DMSO and (ii) **3**-AuNRs in DMSO:H₂O (1:1).

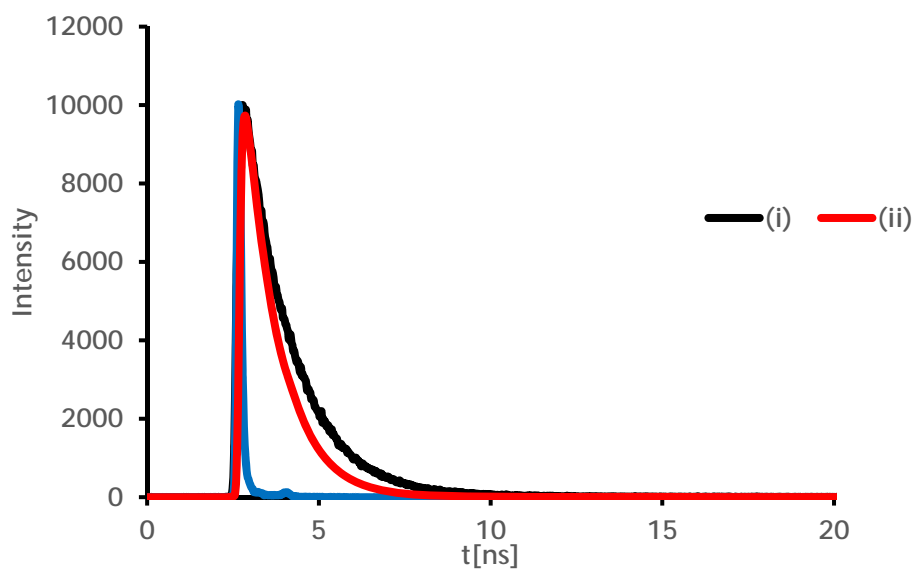


Figure 3.22. Fluorescence decay curves of BODIPYs (i) **5(b)** and (ii) **5(a)** in DMSO.

3.2.2 Photochemical studies

A chemical method has been used to determine the $^1\text{O}_2$ values of BODIPYs **3** and **4** in DMSO, with diphenylisobenzofuran (DPBF) used as the singlet oxygen scavenger. Singlet oxygen quantum yields, ϕ_Δ , provide an important parameter, which can be used to assess the potential of molecules for use as photosensitizers in singlet oxygen applications (e.g., for the Type II mechanism in PDT) [189]. A highly efficient transfer of energy between the excited triplet state of the BODIPY dye and the oxygen ground state is required to generate the high concentrations of singlet oxygen that are required for APDT [189]. Figures 3.22-3.23 shows the rate of DPBF consumption at the initial stage, which corresponds to the efficiency of $^1\text{O}_2$ generation. The calculated values show that BODIPY **3** has a very high $^1\text{O}_2$ quantum yield in DMSO relative to BODIPY **4** (Table 3.4). The low ϕ_Δ values of BODIPY **4** in DMSO could be due to aggregation effects. Moreover, the ϕ_Δ value is enhanced from 0.64 to 0.76 upon conjugation to form **3**-AuNR (Table 3.4) due to the heavy atom effect. The absence of spectral changes in the 450–600 nm region during the $^1\text{O}_2$ measurement demonstrates that both BODIPY **3** and **4** exhibit high photostability (Figures 3.23-3.24) and are resistant to photobleaching. Therefore, on the basis of the singlet oxygen quantum yields, it can be concluded that BODIPY **3** performs better as a photosensitizer than BODIPY **4** (Table 3.6).

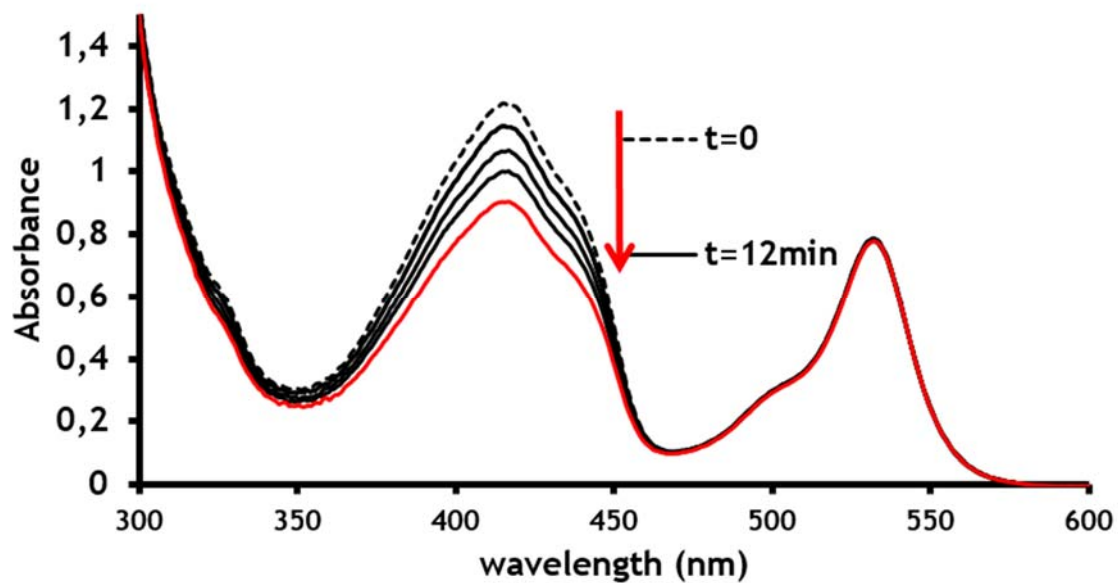


Figure 3.23. Photodegradation of DPBF in the presence of BODIPY **3** in DMSO in an interval of 3 min.

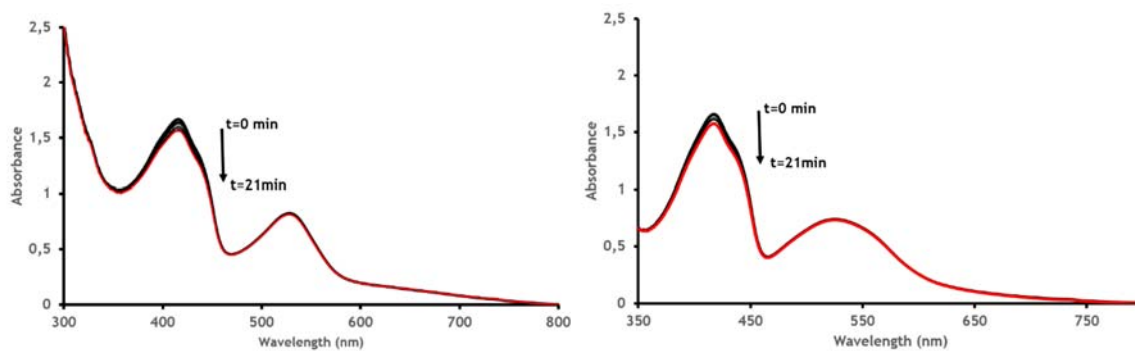


Figure 3.24. Photodegradation of DPBF in the presence of BODIPYs (i) **4(a)** and (ii) **4(b)** in DMSO in an interval of 3 min.

Table 3.4. Physicochemical properties of the short wavelength BODIPY dye photosensitizers.

Sample	Solvent	λ_{abs} [nm]	λ_{em} [nm]	Φ_f	τ_1 (ns)	τ_2 (ns)	χ^2	Φ_{Δ}
3	Toluene	536	554	0.05	1.82	-	0.991	-
	DMSO	531.5	547.9	0.09	1.63	-	0.987	0.64
	DMF	530.5	545	0.02	1.65	-	1.135	-
	DCM	534	550	0.07	1.70	-	0.945	-
3-AuNRs	DMSO	539	557	0.02	1.42	0.33	1.002	0.76
4(a)	DMSO	528.5	531.5	0.02	-	-	-	0.15
4(b)	DMSO	530	538.5	0.05	-	-	-	0.13

Table 3.5. Physicochemical properties of the distyryl-BODIPY dye derivatives.

Sample	Solvent	λ_{abs} [nm]	λ_{em} [nm]	Φ_f	τ_1 (ns)	χ^2
5(a)	DMSO	710	743	0.040	0.91	1.075
5(b)	DMSO	706	735	0.10	1.30	1.006
5(a)-PBS	DCM	710.5	-	-	-	-
5(b)-PBS	DCM	695	-	-	-	-
6(b)	DCM	670	699	0.020	-	-
6(a)	DCM	700	738	0.004	-	-

3.4. Summary

Substitution of bromines as a heavy atom enhanced the production of singlet oxygen for the BODIPY dyes studied for potential use as photosensitizers. The high singlet oxygen quantum yield and low fluorescence quantum yield makes the dyes studied potentially suitable for use as photosensitizers in APDT. Further research on the possible applications of BODIPY-AuNR conjugates is clearly merited.

Chapter 4

4.1. Nonlinear optical (NLO) parameters

According to Hambir and Ortiz *et al.*, π -conjugated systems possess characteristically large electronic polarizabilities, and it is reasonable to expect conjugated molecules to possess substantial hyperpolarizabilities [198, 199]. In addition, it is generally accepted in the literature that molecules with donor and acceptor moieties that are separated by a π -conjugation system exhibit large $\chi^{(3)}$ values [200]. Distryl-BODIPY dyes fused with pyrene and phenol rings were synthesized and studied to assess their potential for optical limiting applications. The styryl substituents were expected to provide the donor moieties, while the BODIPY core acts as the acceptor, to enhance the $\chi^{(3)}$ values. The extension of the π -conjugation system also shifts the main spectral bands to longer wavelength and this leads to weak absorption at 532 nm, making the dyes potentially suitable for OL where the second harmonic of Nd/YAG lasers is concerned.

The nonlinear optical parameters were determined using the Z-scan technique and setup described in Chapter 2. All studies were carried out in solution as well as in the solid state for BODIPY **5(a)-(b)**. The efficacy of an optical limiter cannot be described by a single parameter, hence, a number of optical limiting parameters are summarised in Table 4.1. The parameters reported in this work are the nonlinear absorption coefficient (β_{eff}), the imaginary third order susceptibility ($\text{Im}[\chi^{(3)}]$), the second order hyperpolarizability (γ), and the limiting intensity (I_{lim}).

4.1.1. *Nonlinear absorption coefficients (β_{eff}) and sequential photon (RSA) mechanism*

The nonlinear absorption coefficient (β_{eff}) is an important parameter for assessing the suitability of materials for optical limiting. It measures the degree of nonlinear absorptivity and depends on the population of molecules in the excited state. Generally, this parameter depends on two-photon absorption (2PA) processes, which can be sequential or simultaneous [201, 202]. In such a case, β_{eff} becomes a 2PA coefficient referred to as β_2 . On the other hand, when the absorption of two photons by the excited states is more prominent than in the ground states, a process called ESA, or more expansively, ESA from two-photon pumped state, leads to the RSA that is required for optical limiting. This mechanism results in materials with a positive nonlinear absorption coefficient and a decrease in transmittance as the material approaches the zero position of the Z-scan instrument at high-intensity levels, and such material are said to function as optical limiters [203]. To the best of our knowledge, BODIPY dyes have not been studied to any significant extent for the aforementioned application. As a result, the actual process which is responsible for their nonlinear optical response is not well understood, hence the response could be due to either of the two processes mentioned above. However, it appears safe to assume that the dominant mechanism is nonlinear absorption, since the experimental data fitted the 2PA function.

Measurements were carried out in DMSO and DCM for BODIPY **5** and **6**, respectively. The concentrations at which the studies were conducted are reported in Table 4.1. Figures 4.1-4.5 show the representative open-aperture Z-scans at 532 nm using 10 ns pulses of distyryl-

derivitized BODIPY **5**, **5** embedded in PBS as a thin film and **6**. The measurements demonstrate the strong nonlinear absorption (NLA) behaviours in both samples, with the shapes of the Z-scan profile exhibiting RSA signatures [204]. Analyses of the Z-scan results to obtain β_{eff} values were carried out by fitting the data to the 2PA function described in Chapter 1. The representative fitting plot is shown in Figures 4.1, 4.3 and 4.5. For a material to be a good optical limiter, the transmittance must be reduced by least 50%. Accordingly, based on this parameter BODIPYs **6(a)-(b)** can be viewed as constituting good optical limiting materials as they were able to reduce the intensity of the visible light well below 50%, which is very impressive for an organic dye in solution (Figure 4.5). Most organic materials reported in literature have to be conjugated to nanomaterials or embedded in polymer thin films for this to be achieved. This response of BODIPYs **6(a)-(b)** can be attributed to the increased polarizability due to the enhanced dipole moment within the molecule due to the presence of the hydroxyl substituents as well as bromine contributing to the heavy atom effect. BODIPY **6(b)** significantly reduced the transmittance compared to **6(a)**. This could be due to the increased π -conjugation introduced by the pyrene moiety at the meso-position (Figure 4.1). Although the transmittance was not reduced to below 50% by BODIPYs **5(a)-(b)** in solution, Figure 3.24, they still possess some optical limiting character. For BODIPYs **5(a)-(b)**, the optical limiting behaviour improved with increasing concentration, Figure 3.25. When the two dyes are compared, BODIPY **5(b)** behaves slightly better but there is no significant difference.

The optical limiting behaviour of BODIPYs **5(a)-(b)** was significantly improved when the dyes were embedded into PBC thin films (Figures 4.3-4.4). This can be attributed primarily to

aggregation of the molecules in the thin film. In previous studies aggregates have shown better activity, but the reason for this is not yet fully understood [205]. The β_{eff} values obtained lie within the range previously reported values for other organic compounds [206].

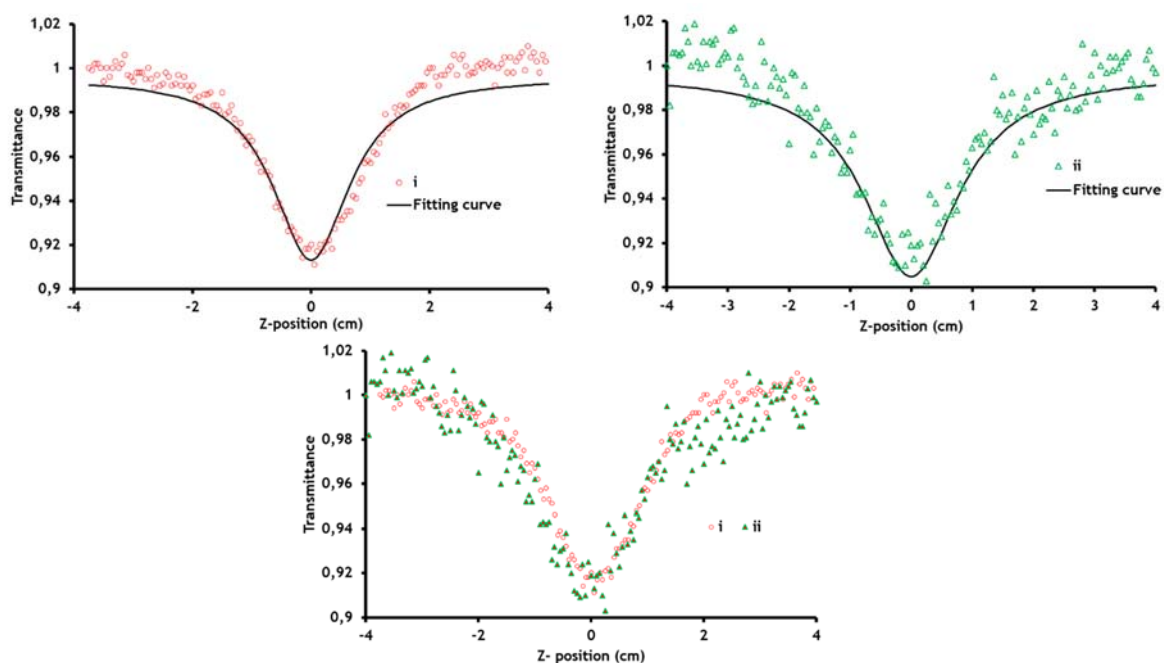


Figure 4.1. Open aperture z-scan profiles of BODIPYs (i) **5(a)** and (ii) **5(b)** in DMSO.

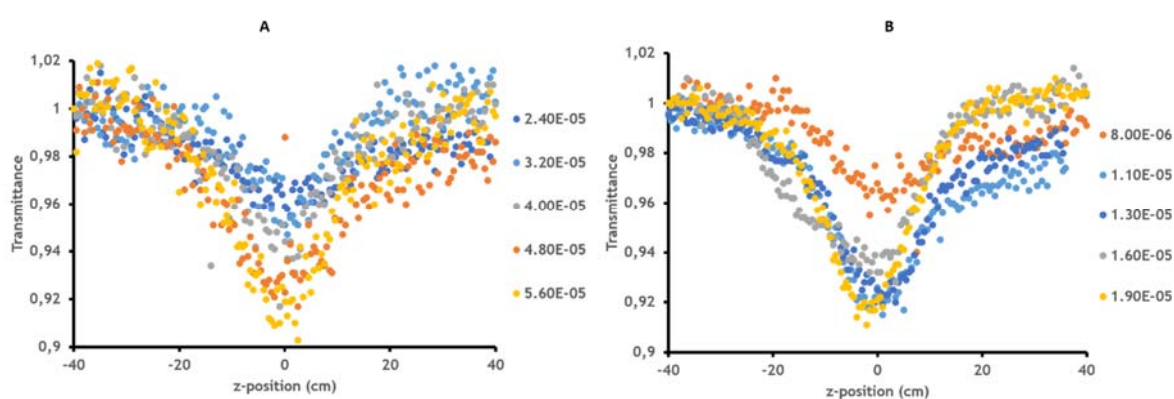


Figure 4.2. Open aperture z-scan profiles of BODIPYs (A) **5(a)** and (B) **5(b)** in DMSO at different concentrations.

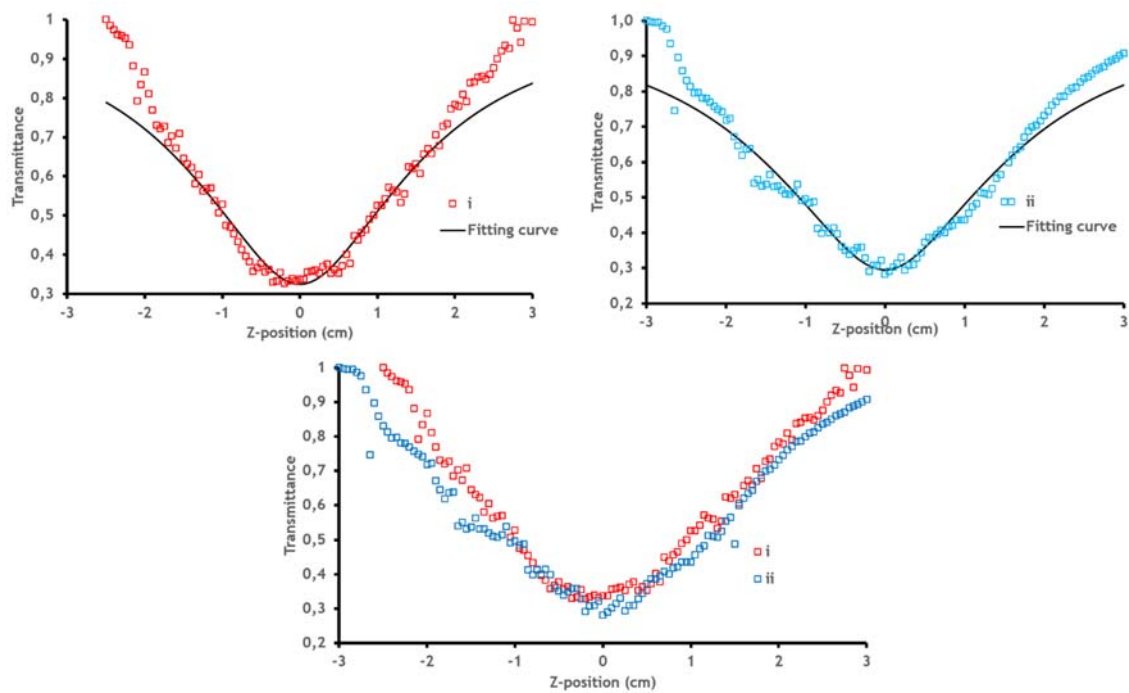


Figure 4.3. Open aperture z-scan profiles of BODIPY (i) **5(b)** and (ii) **5(a)** embedded in PBS thin films.

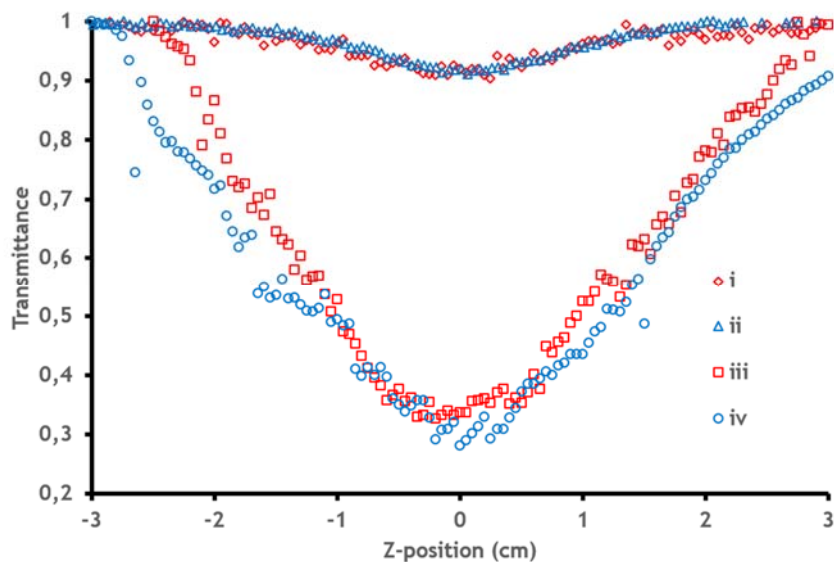


Figure 4.4. Open aperture z-scan profiles of BODIPYs (i) **5(a)**, (ii) **5(b)** in DMSO, (iii) **5(a)** and (iv) **5(b)** embedded in PBS thin films.

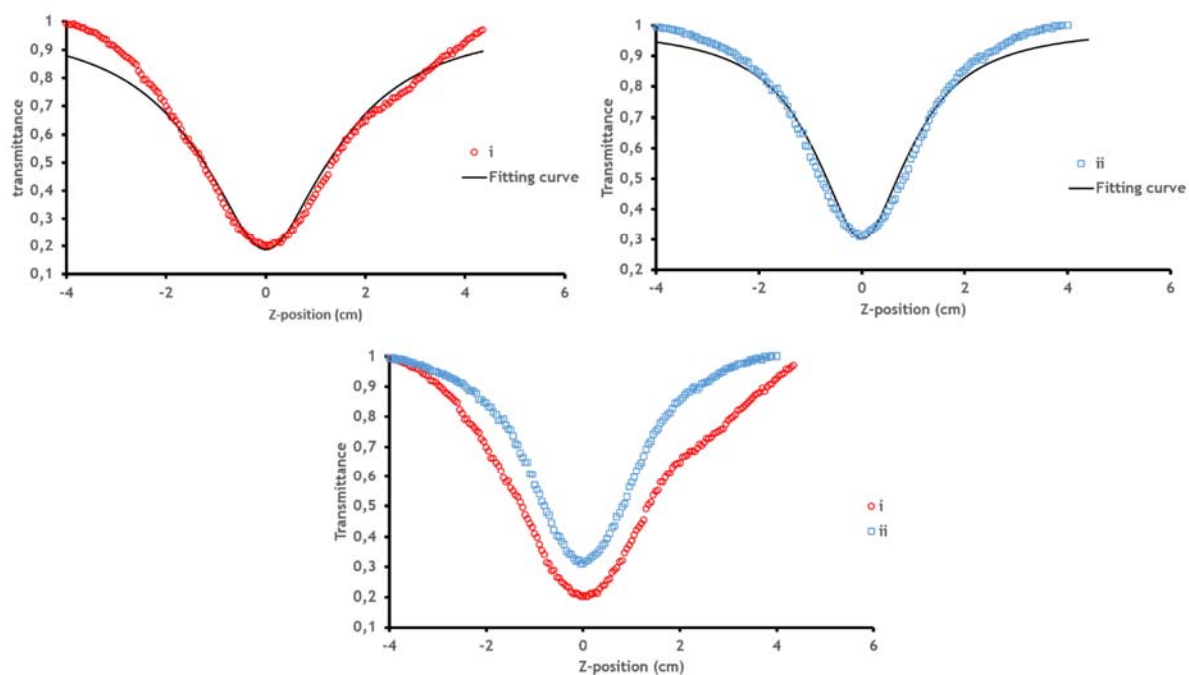


Figure 4.5. Open aperture z-scan profiles of BODIPYs (i) **6(b)** and (ii) **6(a)** in DCM.

4.1.2. Second-order hyperpolarizability (γ) and third-order nonlinear susceptibility

$$(I_m[\chi^{(3)}])$$

The estimated γ and $I_m[\chi^{(3)}]$ values for the samples are given in Table 3.6. γ measures the interaction of the incident photon with the permanent dipole moments of BODIPY dye derivatives. Good optical limiting materials must exhibit high absorbance as the intensity of the incident light is increased. On the other hand, $I_m[\chi^{(3)}]$ measures the fast response of a nonlinear optical material to the perturbation initiated by intense laser pulses. The reported limits range from 10^{-9} to 10^{-15} for $I_m[\chi^{(3)}]$ and from 10^{-29} to 10^{-34} for γ [207]. Accordingly, the values obtained fall well within this range, and relatively high values are obtained both in

solution and in the solid state (Table 3.6). Again, this shows that these BODIPY derivatives have good optical limiting properties, in accordance with the β_{eff} and RSA results that were obtained.

Table 4.1. Nonlinear optical limiting parameters for the distyryl-BODIPY dye derivatives upon 532 laser excitation.

Sample	Solvent	Conc. (M)	$B_{\text{eff}}(\text{cm/GW})$	$I_{\text{lim}}/\text{J}\cdot\text{cm}^{-2}$	$\text{Im}[\chi^{(3)}]/10^{-10} \text{ esu}$	$\gamma \text{ esu}$
5(a)	DMSO	0.0565	90	0.22	2.11	1.64×10^{-30}
5(b)	DMSO	0.0187	110	0.20	2.58	6.04×10^{-30}
5(a)-PBS	DCM	0.0134	409	0.12	8.90	3.40×10^{-29}
5(b)-PBS	DCM	0.00166	177	0.139	3.85	1.19×10^{-28}
6(a)	DCM	0.072721	300	0.034	6.53	4.59×10^{-30}
6(b)	DCM	0.263	179	0.032	3.89	7.57×10^{-31}

4.1.3. Optical limiting threshold (I_{lim})

The limiting threshold intensity or fluence (I_{lim}) is an important parameter in optical limiting measurements. It is defined as the input fluence (or energy) at which the nonlinear transmittance is 50% of the linear transmittance [208]. The value of I_{lim} was determined using plots of input vs. output intensity (Figures 4.6A-4.7A). The limiting threshold for damage to the human eye is $0.95 \text{ J}\cdot\text{cm}^{-2}$. Thus, low values for I_{lim} (below 0.95) is an indication of a good NLO response to the input intensity. The results obtained for all of the BODIPY dyes are below the limiting threshold. Saturation fluence (F_{sat}) curves for all of the BODIPY dyes are compared

by plotting transmittance (T) against the input fluence (I_0) (Figures 4.6B-4.7B). The plots showed a decrease in transmittance as the input fluence increases. Similar observations ascribed to 2PA for organic compounds have been reported previously [209, 210].

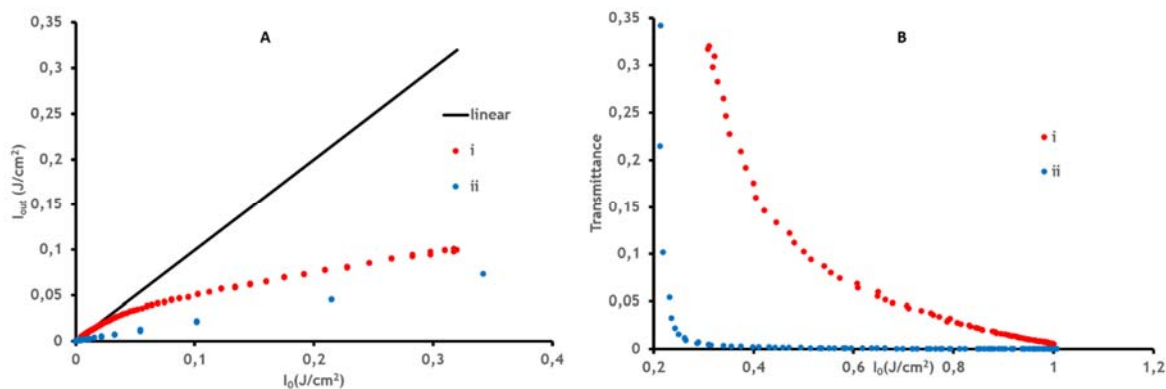


Figure 4.6. A: Input intensity vs output intensity plot for BODIPY (i) **6(a)** and (ii) **6(b)** in DCM. B: Transmittance vs input fluence (I_0) curves for (i) **6(a)** and (ii) **6(b)** in DCM. The black solid line represents linear transmission.

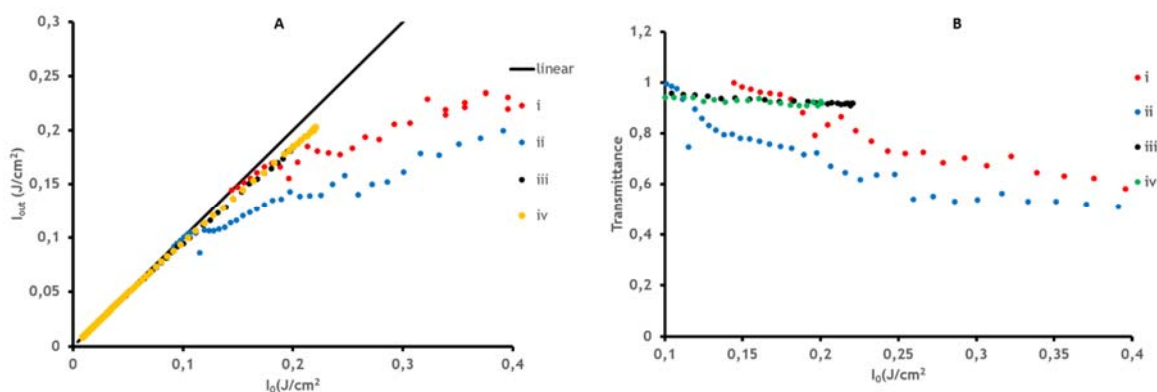


Figure 4.7. A: Input intensity vs output intensity plot for BODIPY (i) **5(a)**, (ii) **5(b)** embedded in PBS as thin films, (iii) **5(b)** and (iv) **5(a)** in DMSO. B: Transmittance vs input fluence (I_0) curves for (i) **5(b)**, (ii) **5(a)** embedded in PBS as thin films, (iii) **5(a)** and (iv) **5(b)** in DMSO. The black solid line represents linear transmission.

Since the concentration was not held constant, it cannot be concluded which BODIPY dye derivative behaved better. However, they all of the dyes proved to be excellent candidates for optical limiting and further investigations in this regard are merited.

4.2. Summary

Substitution with styryls at the 3, 5-positions shifted the main absorption band to longer wavelengths, so that there is only limited absorption at 532 nm. Dyes with pyrene and phenol ring moieties were found to have significant NLO activity for the second harmonic of Nd:YAG lasers. Further research in this regard is merited.

Chapter 5

This chapter describes the UV-visible absorption, fluorescence, and circular dichroism spectroscopy of BODIPY dye inclusion complexes with cyclodextrins in aqueous solution.

5.1. Introduction

An inclusion compound is a chemical complex, in which one molecule “the guest”, is enclosed within another molecular structure, “the host”. Covalent or ionic bonds are not necessary to form these complexes. Only weak Van der Waals forces or hydrogen-bonds play a role during the inclusion process between the host and guest molecules. Since there is no formation of chemical bonds between the functional groups that are involved, the following requirements are of importance in inclusion complex formation [211]:

- i. The host molecule should be able to form void spaces of a certain molecular dimension.
- ii. The guest molecule has to fit or at least partially fit into these void spaces.
- iii. The stereochemical structures and polarities of the guest and host molecules should enhance the formation of the inclusion complexes.

Although the guest molecule is not chemically modified upon inclusion, its physicochemical properties are affected and are often dominated by those of the host molecule. Frank [211] proposed the following classification for the host molecules into polymolecular, monomolecular, and macromolecular inclusion compounds, and the products of the blue-iodine reactions. The main focus in this chapter will be on monomolecular inclusion compounds. As the name implies, this type of inclusion results in the inclusion of each guest molecule by a host molecule. However, it should be noted that compounds consisting of two, three or four host molecules for each guest, are also considered to belong to this class of

inclusion compounds, if the host is known to form 1:1 inclusion compounds with other guests. From the above definition it is clear that the host molecules in this group have to be relatively large to contain void spaces of molecular dimensions [211]. Amongst crown ethers [212] and cryptates [213], cyclodextrin complexes are one of the most important representatives of this class [214]. Cyclodextrins (CDs) are naturally occurring cyclic oligosaccharides composed of six (α -CDx), seven (β -CDx), or eight (γ -CDx) D-glucopyranose residues (Figure 5.1). CDs are naturally occurring products of the degradation of starch by the glycosyltransferase enzyme of *Bacillus macerans* [215].

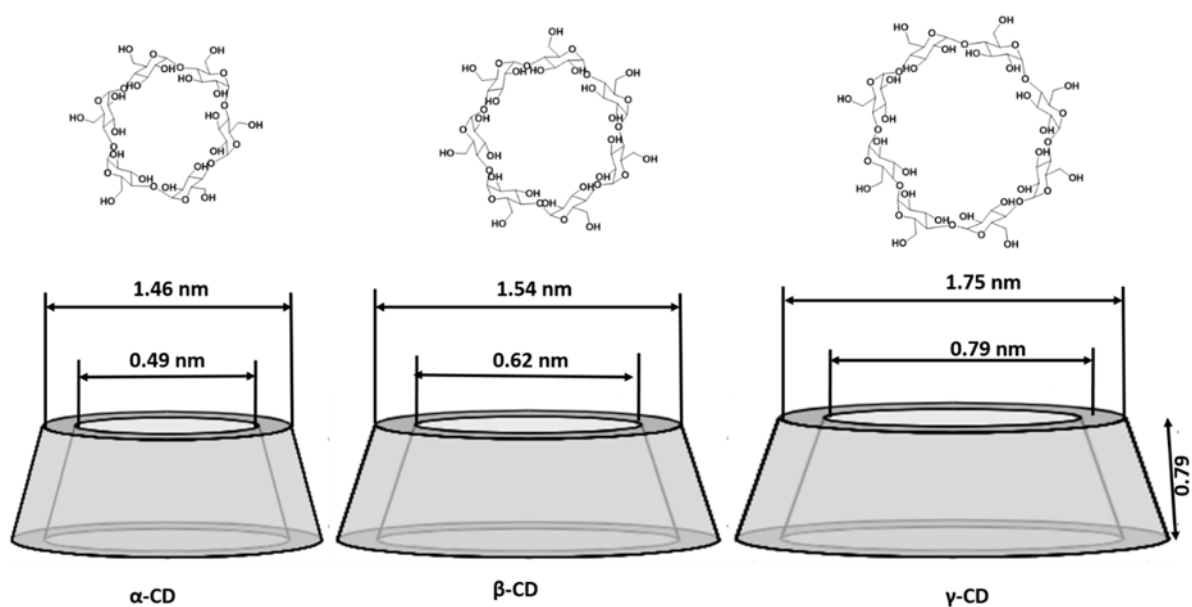


Figure 5.1. The structures of α , β , and γ -CDs and their molecular dimensions.

Due to the hydrophilic nature of their outer surfaces, CDx can be dissolved in water. When dissolved in aqueous solution, their apolar cavities provide a hydrophobic matrix, which has been described as a “microheterogeneous environment” [216]. As a result of the apolar nature of the cavity, the CDx are able to form inclusion compounds with a variety of guest molecules. Generally these inclusion compounds are called complexes [217, 218]. CDx complexes are relatively stable in aqueous solution. One, two or three cyclodextrin molecules

generally entrap one or two guest molecules [52]. The formation of such inclusion complexes can have certain advantages that facilitate a wide range of applications. The advantages of the complexation of drugs by CDx include; increased aqueous solubility, the prevention of unwanted side effects, the stabilization of the drug molecules, the transformation of liquid drugs into solids, the mixing of incompatible drugs and lastly, the masking of bad tastes and odours [216]. As a result of these advantages, possible applications for CDxs and their derivatives are being studied in various areas of chemistry, including the sensing of organic molecules and use as delivery agents for pharmaceuticals [219].

Although CDxs are almost spectroscopically transparent in the 300–1100 nm range, the movement of a guest from bulk water to the hydrophobic cavity may have a large influence on its spectroscopic properties due to the change in polarity. UV-visible absorption and fluorescence spectroscopy have long been used to study complexation by CDxs. Because the cavity is chiral, it induces circular dichroism intensity upon complexation of non-chiral guest molecules. In addition to providing direct spectroscopic evidence for the inclusion of the guest molecule, this induced circular dichroism (ICD) signal can also provide definitive information about the orientation of the guest molecule in the cavity [220-222].

The stability of the inclusion complexes depends both on the size and the redox properties of the guest molecule, as well as on the particular CDx that is used [216]. The impact of the steric requirements can be readily understood. A guest molecule that is too large to fit into the cavity (even partially) will usually not form an inclusion complex, whereas a molecule that is too small will provide insufficient binding towards the inside of the cavity. It should be noted that molecules that are too large to fit completely into the cavity can still be complexed

if part of the molecule is able to penetrate into the cavity. The main consideration in selecting guest and host molecules for study is that the size of the host cavity is appropriate to trap the guest molecules to form an inclusion complex [223].

This chapter is an exploratory work which aims to study the inclusion complexes formed between charged (**i** and **ii**) and π -conjugated (**iii** and **iv**) BODIPY dyes with α , β , and γ -CDx to gauge the possible utility of this approach for applications. The BODIPY dyes studied are shown in Figure 5.2. As mentioned in chapter 1, BODIPY dyes have many excellent properties for different applications and also some drawbacks which limits their suitability for use in other applications. A key goal of this study was to find a way to enhance the water solubility of BODIPY dyes. Although, BODIPY dyes are soluble in almost all organic solvents, solubility in aqueous solution remains challenging with most BODIPY dyes. Their incorporation into CDxs is likely to significantly enhance the water solubility of these dyes. To the best of our knowledge, no studies of the UV-visible absorption, fluorescence and circular dichroism spectroscopy of BODIPY-CDx inclusion complexes have been reported previously. It has long been known that CDxs can trap aromatic compounds, alkyl halides and gas molecules as guest molecules in their central cavities, resulting in the formation of inclusion complexes and a CD signal can be induced when a suitable chromophore is involved in this regard. Hence, the most commonly studied inclusion complexes have involved organic compounds such as phthalocyanines, porphyrins [224-231], pyrenes [232-234], and pharmaceutical drugs. UV-visible absorption, fluorescence, and induced circular dichroism measurements were performed to confirm that host-guest interactions occur between the BODIPY dye and the CDx and to study their binding geometries.

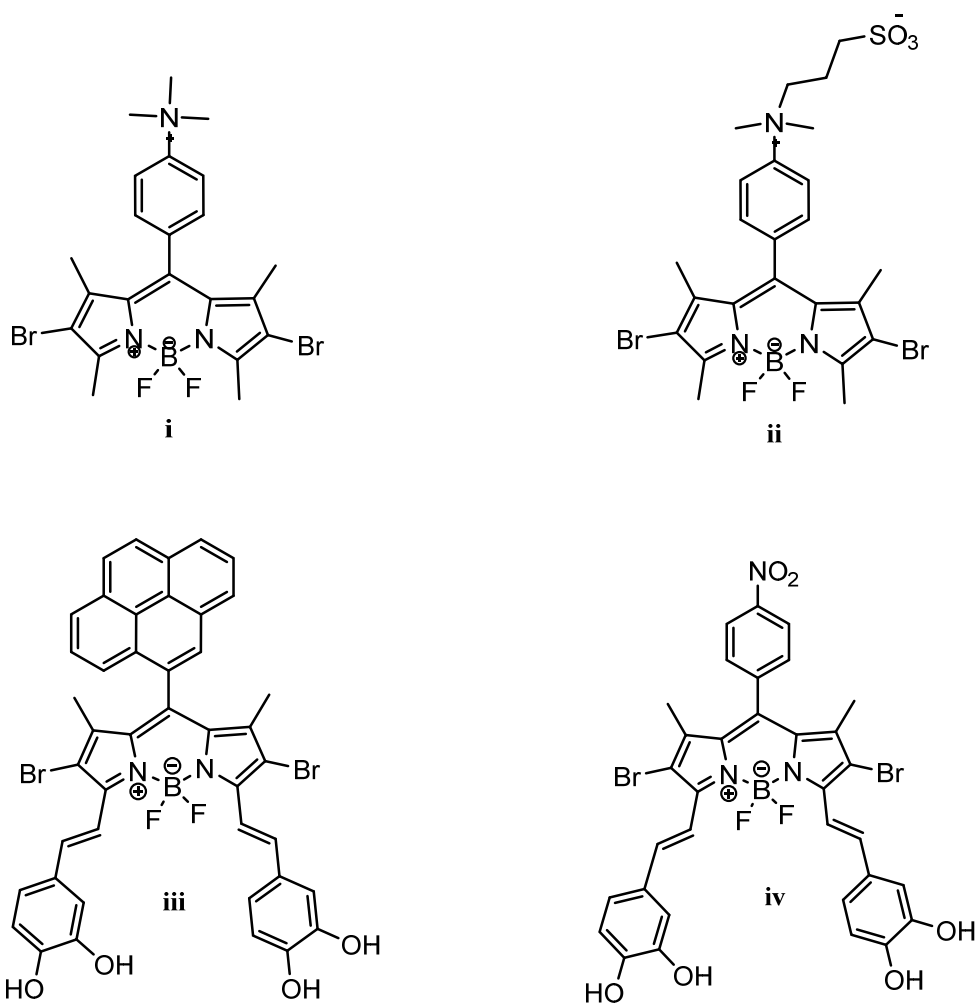


Figure 5.2. BODIPY dyes synthesised in this work to form inclusion complexes with CDXs.

5.2. Experimental section

5.2.1. Materials

The materials used for the synthesis of BODIPY **i-iv** were reported in Chapter 2. α - and β -CDx were purchased from Wako. 3, 4-dihydroxybenzaldehyde was purchased from the Kanto Chemical Company. Highly purified γ -CDx was provided by Prof. Nagao Kobayashi of Shinshu University and was recrystallized in an aqueous solution twice prior to use.

5.2.2. Instrumentation

- i. Ultraviolet-visible (UV-vis) absorption spectra were measured at room temperature on a Shimadzu UV-C636 spectrophotometer using a 1 cm path length cuvette for solution studies.
- ii. Fluorescence emission spectra were measured on a Jasco FP-8600 spectrofluorimeter.
- iii. Circular dichroism spectra were recorded on a Jasco J-720 spectrodichrometer in water at room temperature. All samples were prepared from aqueous stock solutions. The following conditions were used: bandwidth, 1.0 nm; slit width, 1.0 nm; autosensitivity, 10 mdeg; time constant, 1.0 s; step resolution, 0.2 nm; scan speed, 20 nm/min; number of scans, 4.

5.2.3. Preparation of BODIPY-cyclodextrin inclusion complexes

A series of stock solutions for BODIPYs **i**, **ii** and **iii**, **iv** were prepared in 3 or 4 ml of deionized water with concentrations of 6.37×10^{-6} , 2.82×10^{-6} and 4.56×10^{-6} , 1.68×10^{-6} M, respectively. A weighed quantity of α , β or γ -CDx was added, with stirring. The concentrations of α -, β - and γ -CDx ranged from 0.011–0.051, 0.009–0.049 and 0.008–0.040 M, respectively, while the concentrations of BODIPY dyes were held constant in all of the experiments. All solutions were allowed to equilibrate for 5 min prior to analysis.

5.3. Results and discussion

5.3.1. UV-visible absorption studies

Figures 5.4-5.6 provide the absorption spectra of the BODIPY dye **i-iv** in aqueous solutions in the absence and in the presence of CDxs. The bands in the 200–400 nm region correspond to those of the aromatic substituents attached to the BODIPY core, such as pyrene, phenol, nitrobenzene and phenyl groups. Moreover, the band at around 300–450 nm in the spectrum of **iii** can be assigned to the pyrene moiety. The blue shifted bands in the spectra of **iii** and **iv** can be attributed to the phenol and the red shifted band to the nitrobenzene in **iv** based on the electron donating and withdrawing of these moieties, respectively. On the other hand, the broad bands in Figures 5.3, 5.4 and 5.6, respectively, at 533.5, 534.5, 723 and 719 nm can be assigned to the $S_0 \rightarrow S_1$ transition of BODIPY dyes.

BODIPYs **i**, **ii**, **iii** and **iv** showed an aggregated monomeric behaviour in aqueous solution, signified by the broadened absorption bands at 533.5, 534.5, 723 and 719 nm, respectively

(Figures 5.3-5.6). The absorption spectra of **i** and **ii** are scarcely altered by the addition of both α - and β -CDx. The addition of α - and β -CDx to **i** results in a decrease in absorbance in the bands that lie at 267 and 533 nm. Similarly, there is an increase in the absorbance of **ii** for the bands that lie at 258, 319 and 534.5 nm.

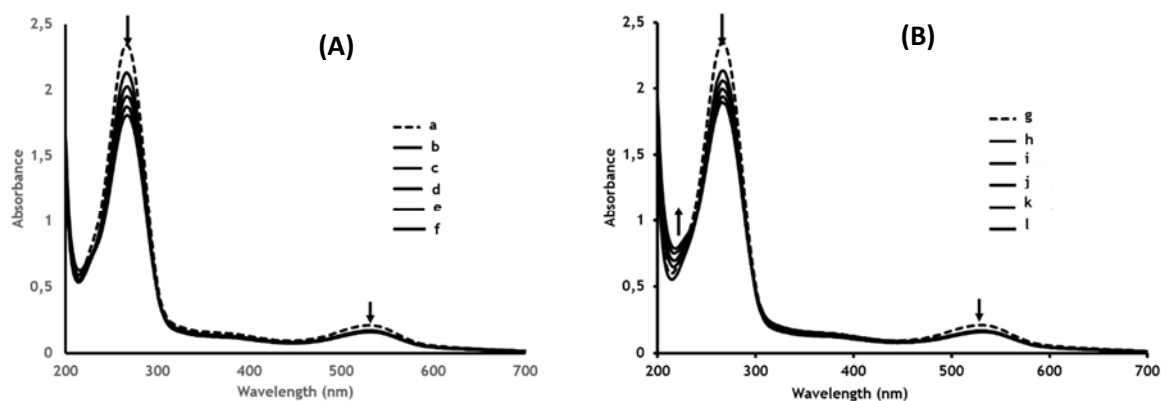


Figure 5.3. Absorption spectra of BODIPY **i** in aqueous solution in the absence (a) and (g) and in the presence of α - (A) and β - (B) CDxs: (b) $[\alpha\text{-CDx}] = 0.014$, (c) 0.028, (d) 0.056, (f) 0.112 and (h) $[\beta\text{-CDx}] = 0.012$, (i) 0.024, (j) 0.048, (k) 0.096, (l) 0.192 mol dm⁻³.

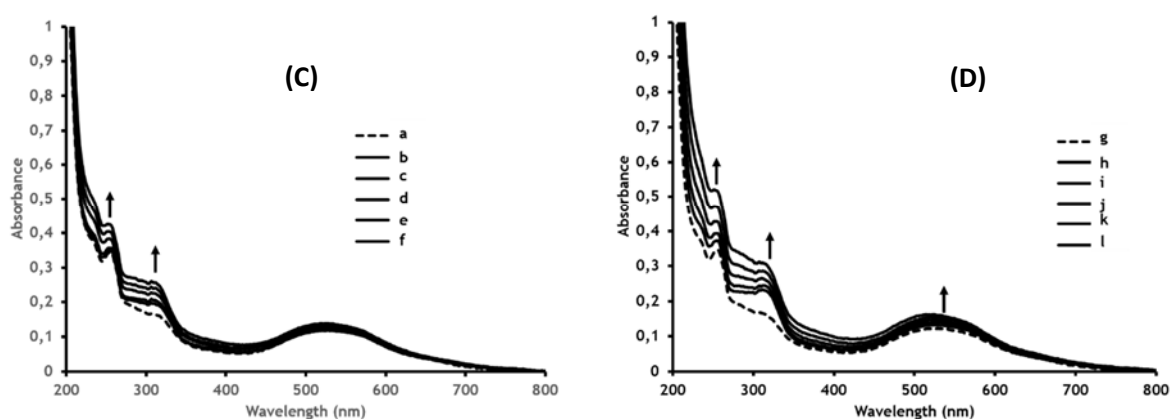


Figure 5.4. Absorption spectra of BODIPY **ii** in aqueous solution in the absence (a) and (g) and in the presence of α - (C) and β - (D) CDxs: (b) $[\alpha\text{-CDx}] = 0.014$, (c) 0.028, (d) 0.056, (f) 0.112 and (h) $[\beta\text{-CDx}] = 0.012$, (i) 0.024, (j) 0.048, (k) 0.096, (l) 0.192 mol dm⁻³.

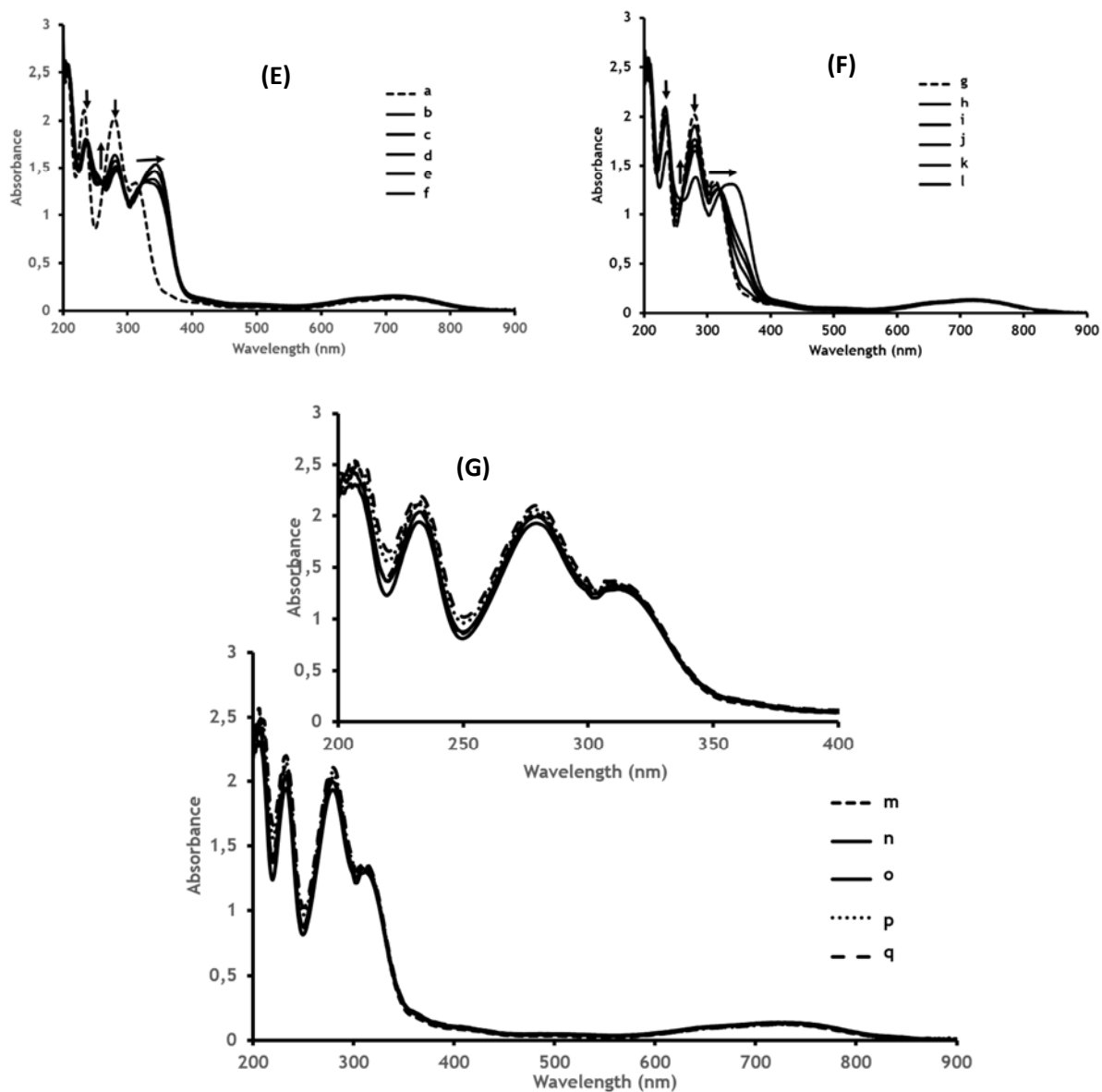


Figure 5.5. Absorption spectra of BODIPY **iii** in aqueous solution in the absence (a), (g) and (m) and in the presence of α - (E), β - (F) and γ - (G) CDxs: (b) $[\alpha\text{-CDx}] = 0.011$ (c) 0.022 , (d) 0.044, (f) 0.088; (h) $[\beta\text{-CDx}] = 0.009$, (i) 0.018, (j) 0.036, (k) 0.072, (l) 0.144 and (m) $[\gamma\text{-CDx}] = 0.008$ (n) 0.016 , (o) 0.032, (p) 0.064, (q) 0.128 mol dm⁻³.

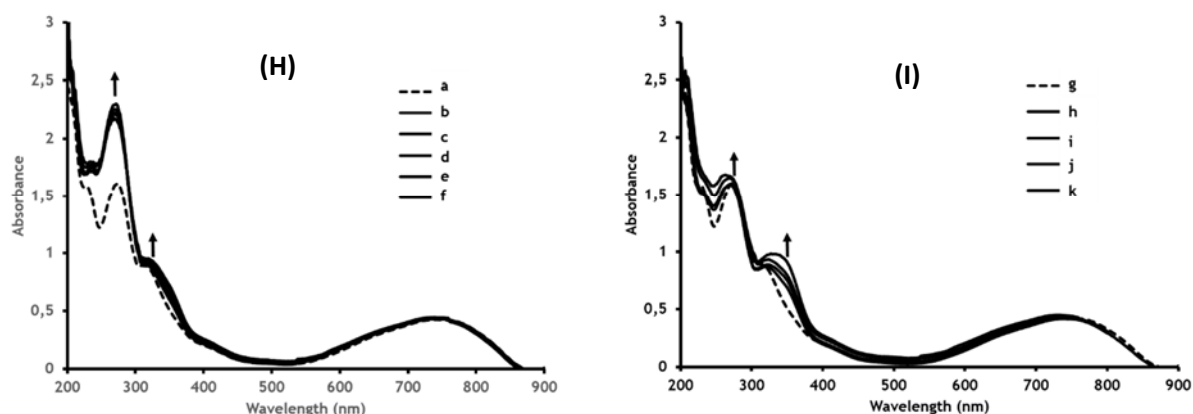
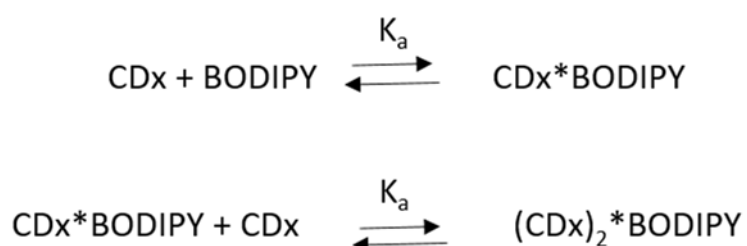


Figure 5.6. Absorption spectra of BODIPY **iv** in aqueous solution in the absence (a), (g) and (m) and in the presence of α - (E), β - (F) and γ - (G) CDxs: (b) $[\alpha\text{-CDx}] = 0.011$ (c) 0.022 , (d) 0.044, (f) 0.088 and (h) $[\beta\text{-CDx}] = 0.009$, (i) 0.018, (j) 0.036, (k) 0.072 mol dm⁻³.

Furthermore, addition of CDx to solutions of monomeric BODIPYs **iii** and **iv** results in a significant increase in the intensity of the absorption bands as well as noticeable shifts in their band centres at higher CDx concentrations (Figures 5.5-5.6). There was less or no significant change in the absorption peaks at 723 and 719 nm, respectively, for BODIPY dyes **iii** and **iv** on CDx addition. On the other hand, addition of α -CDx and β -CDx to a solution of BODIPY **iii** resulted in a decrease in the absorption intensity of the bands between 200–300 nm. There is a significant red shift of the absorption band in the 300–400 nm region with increasing concentration of α -CDx. However upon addition of β -CDx, the spectral change occurred only at a concentration of 0.144 mol dm⁻³ where the absorption band in the 300–400 nm region was broadened and red shifted. Addition of γ -CDx, resulted in a minor increase in intensity in the bands between 200–300 nm (Figure 5.5). Moreover, addition of both α -CDx and β -CDx to the solution of BODIPY **iv** scarcely altered the absorption bands in the 200–400 nm region

shown in Figure 5.6. There was only an increased broadening of the absorption bands in this region.

In previous studies, changes such as an enhancement or decrease in the intensity of the absorption and fluorescence bands have been ascribed to the formation of an inclusion complex between CDx and porphyrins [235, 236]. Therefore, the blue shifts and hyperchromic effects (change in the intensity of the bands) observed, respectively, in the spectra of BODIPYs **i** and **iii** on the one hand, and **ii** and **iv** on the other, as well as the blue shift of the main spectral bands of BODIPY **iii** are consistent with the formation of BODIPY-CDx inclusion complexes. The minor changes observed for the interaction between BODIPY **iii** and γ -CDx can be attributed to a weak interaction between the two because of the large diameter of this CDx (0.79 nm), this BODIPY dye may be partially fitted into the cavity of the γ -CDx. The absorption spectra of BODIPYs **i-iv** were used to calculate binding constants (K_a). The binding constant is a quantitative description of the affinity between the CDx and the BODIPY dye that binds to it [237]. The equations showing the equilibrium constants (K_a) for 1:1 and 1:2 (BODIPY:CDx) associations between the BODIPY dye and CDxs are depicted in Scheme 5.1.



Scheme 5.1. Simplified equilibria of CDx/BODIPY systems (K_a values are reported in Table 5.1).

The K_a values were obtained following a method previously described in literature [237]:

$$K_a = \frac{[CDx*BODIPY]}{[CDx][BODIPY]} \quad (10)$$

$$K_a = \frac{[CDx]_2*BODIPY]}{[CDx*BODIPY][CDx]} \quad (11)$$

Equations (10) and (11) describe the equilibrium constants for 1:1 and 1:2 associations, respectively. $CDx*BODIPY$ and $(CDx)_2*BODIPY$ are the complexes at equilibrium.

The data obtained for all of the CDxs are summarized in Table 5.1. The K_a values reported were calculated using the bands associated with the BODIPY core (i.e. the main absorption bands around 500 and 700 nm for BODIPYs **i** and **ii** on the one hand, and BODIPYs **iii** and **iv** on the other, respectively). The K_a values for the other bands in the 200–400 nm range were also calculated and they ranged between $1 \times 10^2 - 1 \times 10^4 \text{ M}^{-1}$. According to Muñoz de la Peñia *et al.* large binding constants are indicative of strong complex formation and *vice versa* [238]. Accordingly, the obtained K_a values demonstrate that the CDxs bind significantly more strongly with the aromatic substituents (i.e. the charged phenyl groups in BODIPYs **i** and **ii** as well as the phenol, nitrobenzene and pyrene in BODIPYs **iii** and **iv**) than with the BODIPY core. The reason for the difference is that the association constant is highly dependent on the environment of the test including sensitivity to pH, ionic strength, temperature, etc. [239]. In this case, the weak interaction with the BODIPY core could be viewed as being a result of the large diameter sizes of CDxs compared to the small size of the bromine atoms directly attached to the BODIPY core.

In addition, the presence of amino, hydroxyl and carbonyl groups in the guest molecules enables interactions with the hydrophilic parts of the outer surface of the CDxs via hydrogen

bonding, providing further stabilization to the hydrophobic interactions. Consequently, quite large values (ca. 1000 M^{-1} or higher) would be expected for the binding constant for such complexes [232]. This explains the main trends observed in the binding constant values that were obtained for the CDx interaction with the BODIPYs that contained these substituents.

5.3.2. Fluorescence studies

Figure 5.8 (A, B, C and D, respectively) provides the fluorescence spectra of BODIPY **i**, **ii**, **iii** and **iv** in aqueous solution in the absence and the presence of CDx excited at 480 nm for BODIPY **i** and **ii**, and 577 nm for BODIPY **iii** and **iv**. Only one emission band was observed for fluorescence, which is typical for monomeric species. It is widely known that aggregates generally do not fluoresce; thus the fluorescence in Figure 5.8 can be attributed to the presence of monomeric BODIPY dyes. The fluorescence spectra of the monomeric complexes were mirror images of the excitation spectra, as would normally be anticipated for monomeric BODIPY species.

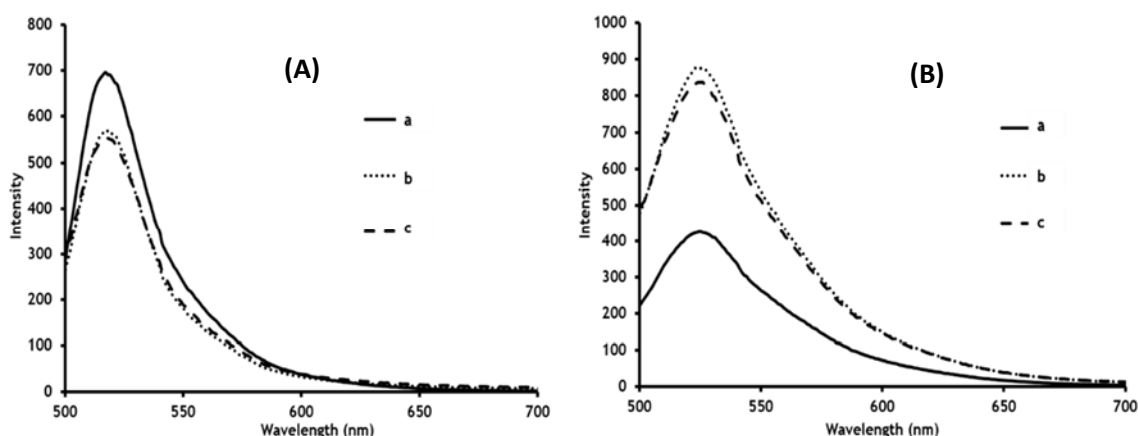


Figure 5.7. Fluorescence spectra of BODIPY **i** (A) and **ii** (B) in aqueous solution in the absence (a) and in the presence of α - (b) and β - (c) CDx rings (0.112 and $0.192 \text{ mol dm}^{-3}$, respectively).

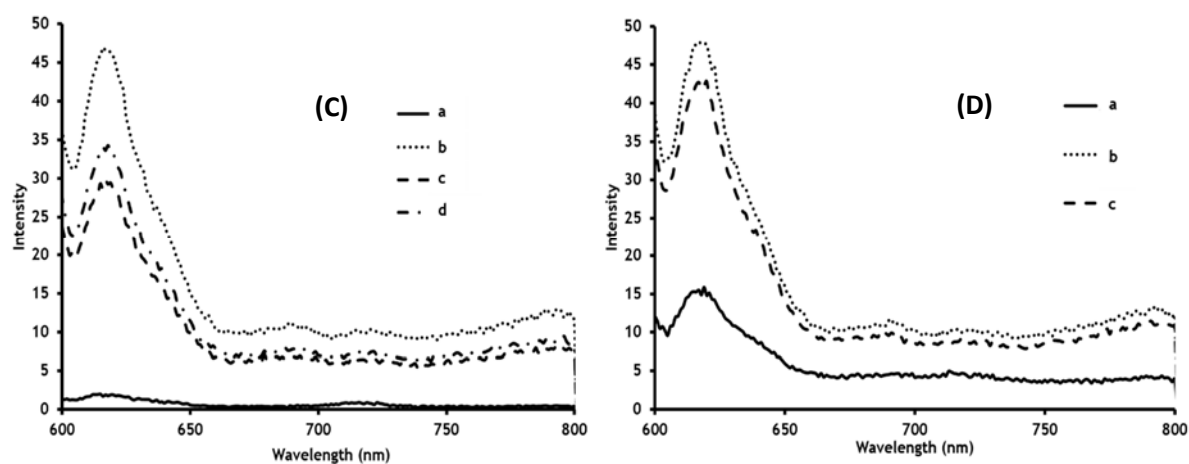


Figure 5.8. .Fluorescence spectra of BODIPY i (C) and ii (D) in aqueous solution in the absence (a) and in the presence of α - (b), β - (c) and γ - (d) CDx rings (0.088, 0.144 and 0.128 mol dm⁻³, respectively).

Changes in fluorescence can often be more sensitively detected than changes in the UV-visible absorption spectra. The fluorescence is sensitive to a change in the polarity of the microenvironment. When the polarity of the microenvironment changes, fluorescence can be shifted to longer or shorter wavelength or a change in quantum yield may occur. Therefore, this can be used as a mechanism to prove the formation of the inclusion complex. A significant blue shift was observed in the emission bands of all of the BODIPY dyes. In a study reported for *N,N*-dimethyl dansylamide- β -CDx [252], a similar blue shift was attributed to the change in the environment of the dansyl moiety to a less polar environment than water. Accordingly, these changes may indicate that the BODIPY dyes are in a less hydrophobic (less polar) environment due to the formation of inclusion complexes. The fluorescence quantum yield values were in accordance with the observed increases and decreases in the fluorescence intensity (Table 5.1). From the calculated fluorescence quantum yield values, Table 5.1, it can be concluded that there is a better interaction between CDx and BODIPYs ii,

iii and **iv** as opposed to BODIPY **i**. Therefore, as stated previously the changes in the fluorescence quantum yield and the spectral shift can be an indicative of the inclusion complex formation.

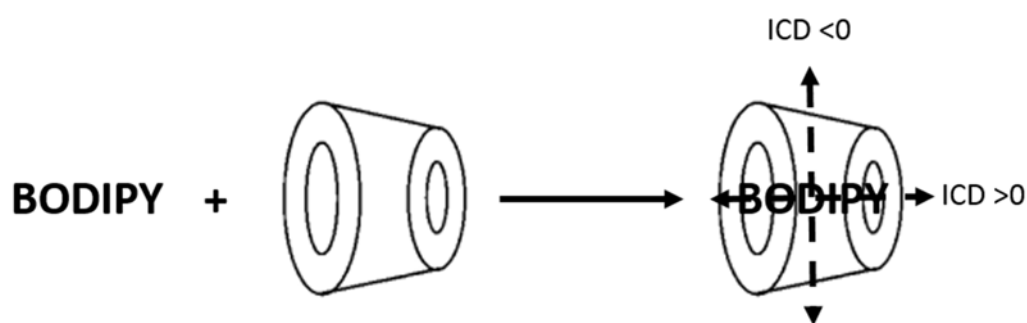
Decreases [240] and increases [235] in fluorescence intensity upon addition of CDx has been reported for porphyrins. The fluorescence intensity may increase or decrease upon addition of a guest, depending on very restrained variations in complex geometry. A decrease in intensity is observed in the spectrum of BODIPY **i**, while increases are observed in those of BODIPYs **ii**, **iii** and **iv**. According to Kano *et al.*, fluorescence enhancement in this context is probably due to the dissolution of guest molecules adsorbed to the walls of the container [235] and/or a destabilization of a non-emissive intramolecular charge-transfer state due to an increase in the hydrophobicity of the environment [241-250]. The decrease in fluorescence intensity observed for BODIPY **i** can be an indicative of BODIPY moieties being removed from the cavity. This removal results in the interaction of BODIPY moieties with the hydrophilic part of the CDx, hence the resultant quenching of fluorescence observed in Figure 5.7A [237]. Therefore, in both cases, these changes can be attributed to the formation of an inclusion complex. The increased fluorescence intensity observed for **ii-iv** is indicative of efficient hydrophobic interactions between the host and the guest molecule [251].

5.3.3. Circular dichroism studies

The orientation of the chromophore can be elucidated by analyzing the CD spectra, or alternatively, if the inclusion type has been established, the direction of the electric dipole transition moment (edtm) can be determined instead. It has been established both

experimentally and theoretically that electronic transitions parallel to the molecular axis of CDxs produce positive ICD, while those normal to the axis show negative ICD to form an axial and equatorial inclusion, respectively [253,254] (Scheme 4.2).

Furthermore, a lid type inclusion has been identified as a possibility where both the short and long axis polarised transitions are normal to the molecular axis of CDx. For this type of inclusion only negatively signed bands can be observed in the CD spectrum. Conversely, the orientation of guest molecules trapped in the CDx cavity can be inferred from the sign of the ICD spectra, if the polarisations of the bands of the guest molecules are known. Accordingly, if the band is associated with a $\pi \rightarrow \pi^*$ transition, the sign of the ICD band should be positive for an equatorial inclusion and negative for an axial inclusion as in the aromatic substituents in the BODIPY dye. Figures 5.10 and 5.12 shows the UV region of the absorption and ICD spectra of BODIPY **ii** and **iv**, respectively in β - and α -CDx.



Scheme 5.2. Schematic representation of inclusion types showing electronic transitions parallel to the molecular axis of CDxs to produce positive ICD, and those normal to the axis producing negative ICD.

The wavelengths of the peaks and troughs in the ICD spectrum lie close to the band centres observed in the electronic absorption spectrum. A consideration of the size and geometry of the guest molecule makes it clear that axial inclusion is the only possible structure for BODIPY dyes **i** and **iii**. Accordingly, this means that the long axis of the BODIPY dye lies parallel to the CDx molecular axis. In the ICD spectra of BODIPY **i** and **iii**, the negatively signed ICD bands can only be assigned to the short axis polarised transitions and the other positively signed ICD bands are polarised along the long axis of the molecule (Figures 5.9 and 5.11, respectively).

The inclusion structure in BODIPY **iii**- α -CDx, can be inferred to be of the lid type based on the sign of the ICD spectrum [254b]. The macrocyclic plane of the aromatic substituents lie on the rim of the α -CDx ring or a similar arrangement. There is an exception to the rule described above for the signs of ICD bands upon lid type inclusion, when the aromatic guest molecules lie above the rim of the CDx by more than ca. 0.3 Å along the CDx axis [254]. This analysis is based on the small size of the α -CDx compared to the substituents of BODIPY **iii**.

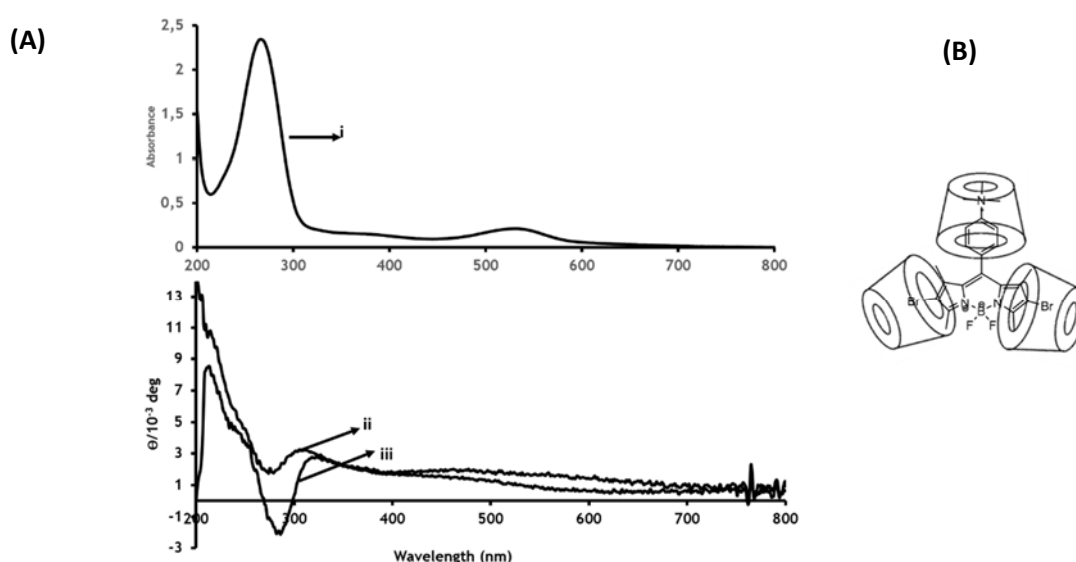


Figure 5.9. (A) Absorption (i) and CD spectra of BODIPY **i** in the presence of (ii) β -CDx and (iii) α -CDx (0.0615 and 0.07 mol.dm⁻³, respectively). (B) Schematic configurations of **i**-CDx inclusion complex.

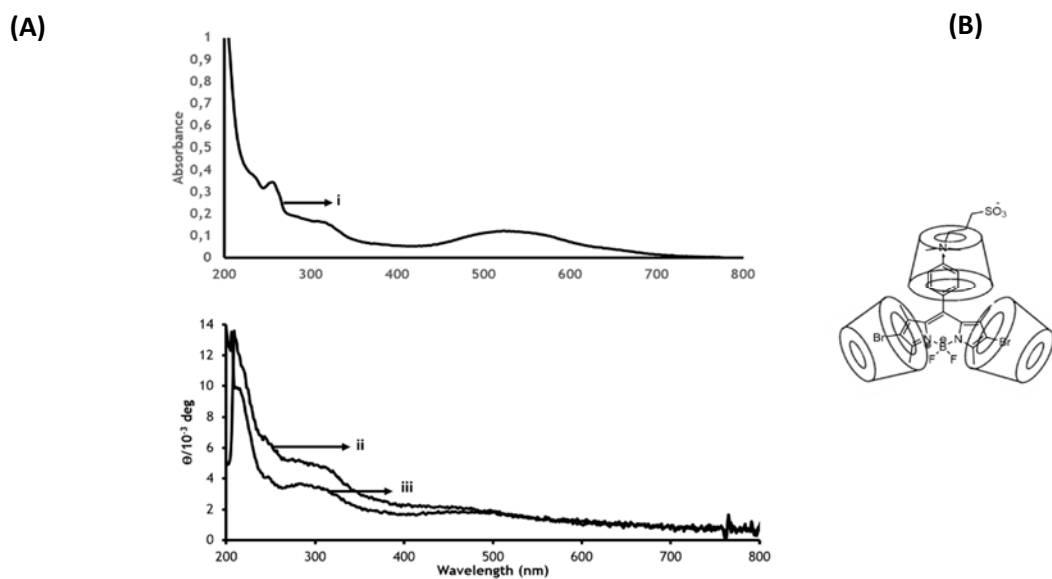


Figure 5.10. (A) Absorption (i) and CD spectra of BODIPY **ii** in the presence of (ii) β -CDx and (iii) α -CDx (0.0615 and 0.07 mol.dm⁻³, respectively). (B) Schematic configurations of **ii**-CDx inclusion complex.

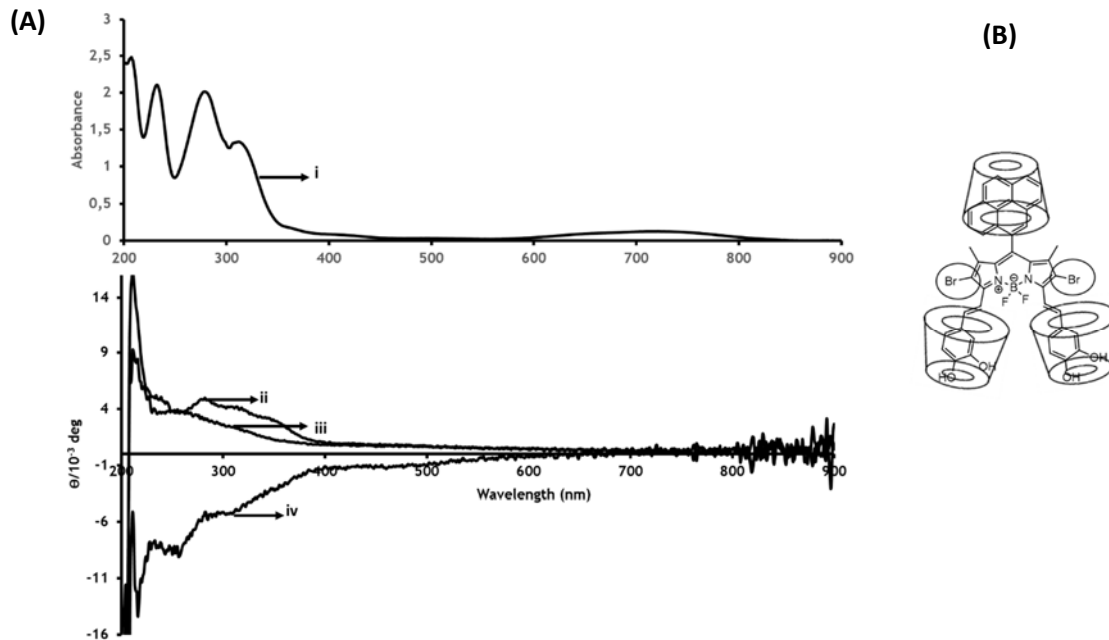


Figure 5.11. (A) Absorption (i) and CD spectra of BODIPY **iii** in the presence of (ii) β -CDx, (iii) γ -CDx and (iv) α -CDx (0.04655, 0.0399 and 0.0532 mol.dm⁻³, respectively) (B) Schematic configurations of **iii**-CDx inclusion complex.

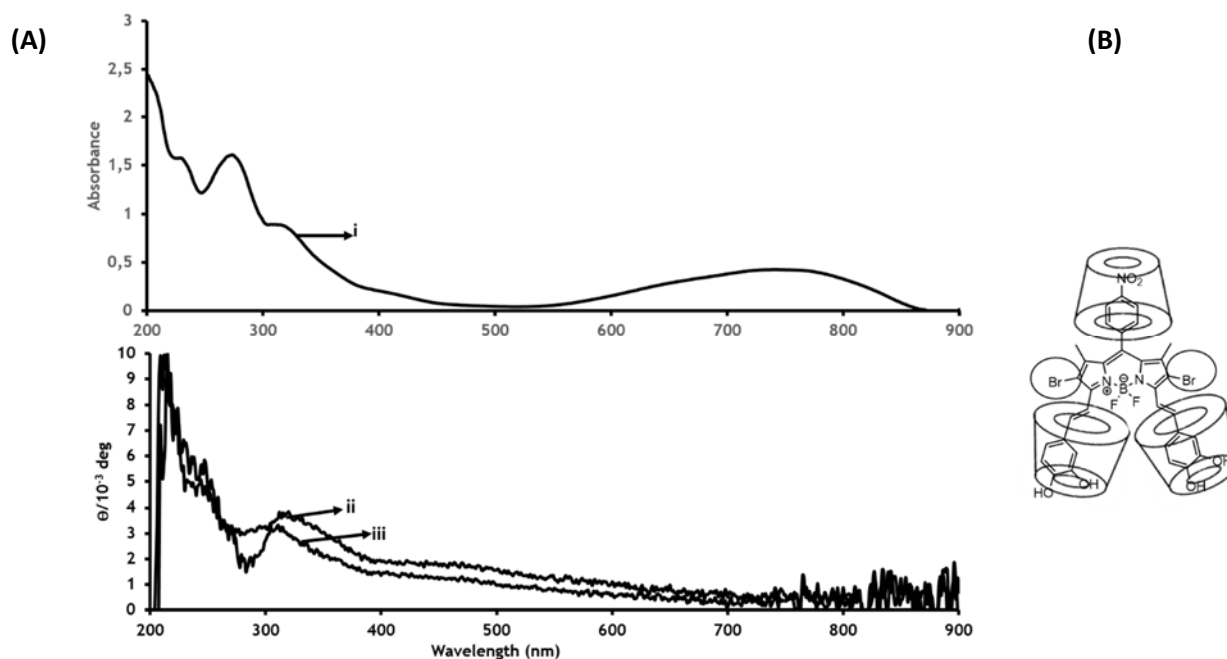


Figure 5.12. (A) Absorption (i) and CD spectra of BODIPY **ii** in the presence of (ii) β -CDx and (iii) α -CDx. (0.0458 and 0.0528 mol.dm⁻³, respectively) (B) Schematic configurations of **ii**-CDx inclusion complex.

The driving force for the inclusion of guest molecules by CDx rings is the hydrophobic interaction [253]. Accordingly, in solvents containing water, hydrophobic aromatic guest molecules tend to penetrate deep into the hydrophobic CDx cavity, and this provides the rationale for the predicted inclusion structures in Figures 5.9-5.12. All these BODIPY dyes exhibit a better interaction with β -CDx, since their medium size may provide a better fit for the aromatic substituents. Because of the diameter of γ -CDx, the interaction with the BODIPY dye appears to be weak. Weak and broad ICD band intensity is observed.

Table 5.1. Photophysical data for the BODIPY-CDx inclusion complexes and their binding constants (K_a).

Sample	CDx type	λ_{abs} (nm)	$^a\lambda_{\text{em}}$ (nm)	Conc. (mol dm ⁻³)	K_a (M ⁻¹)	$^b\Phi_F$
BODIPY i	α	533.5	518	0	2.28	0.093
		533.5	519	0.0138	14.55	0.065
		533.5		0.028	8.20	
		534.5		0.0421	5.45	
		535.5		0.0561	4.09	
		535.5		0.07	3.55	
	β	533.5		0	0.20	
		533.5	519	0.0121	18.97	0.060
		533.5		0.0243	9.45	
		534.5		0.0365	6.29	
		536		0.049	5.07	
		534.5		0.0615	4.04	
BODIPY ii	α	523.5	526	0	0.009	0.08
		525	526	0.0138	0.036	0.12
		524.5		0.0278	0.018	
		524.5		0.0418	0.027	
		524.5		0.0561	0.031	
		525		0.07	0.036	
	β	523.5		0	0.84	
		525	526	0.012	0.11	0.10

		524.5		0.0246	0.09	
		524.5		0.0366	0.08	
		524.5		0.049	0.08	
		525		0.0615	0.08	
BODIPY iii	α	720.5	618	0	0.02	0.013
		720.5	618	0.010562	0.22	0.12
				0.021226	0.08	
				0.0319556	0.06	
				0.042542	0.10	
				0.0532	0.03	
	β			0	0.02	
		720.5	618	0.009226	0.26	0.077
				0.01842	0.10	
				0.02767	0.07	
				0.0371	0.12	
				0.04655	0.04	
	γ			0	0.02	
		720.5	618	0.00785	0.30	0.088
				0.0158	0.11	
				0.0237	0.08	
				0.0318	0.13	
				0.0399	0.05	
BODIPY iv	α	742.5	616	0	0.978	0.092

			618	0.0106	0.004	0.14
				0.0213	0.002	
				0.0318	0.012	
				0.0422	0.022	
				0.0528	0.018	
	β			0	0.978	
		742.5	618	0.009	0.005	0.064
				0.0182	0.002	
				0.0274	0.014	
				0.0368	0.025	
				0.0458	0.021	

^a Excited at 577. ^b Zn-tButyl Pc in benzene as reference ($\phi_F=0.37$) [255]

5.4. Summary

A study of the inclusion complexes formed between the BODIPY dyes and CDx was successfully carried out. It can be concluded that the aromatic substituents in the BODIPY dyes were trapped in all of the CDx rings used in this study. However, absorption and fluorescence studies showed a weak interaction of CDx with the BODIPY core, mainly with an alkyl halide bond (C-Br) directly attached to the BODIPY core. The binding constants are consistent with stable 1:1 inclusion complexes of the aromatic substituents with CDx. The predicted stoichiometry was deduced based on a consideration of the geometry of the BODIPY dyes. The interaction with the BODIPY core is weak as shown by the low K_a values

reported in Table 4.1. At higher CDx concentrations, the interaction is even weaker which could be attributed to CDx interacting with each other resulting in greater complex instability.

Chapter 6

6. GENERAL CONCLUSIONS AND FUTURE PROSPECTS

6.1. *Conclusions*

The versatility and ease of synthesis of BODIPY dyes have promoted them to be used in a wide range of applications such as APDT and NLO, which were studied in this work. Herein, the newly derived BODIPY dyes were successfully synthesized using reaction mechanisms such as the acid catalysed condensation, electrophilic substitution and the Knoevenagel condensation reactions. These reactions were used to synthesize the aniline, quaternized and distyryl BODIPY dyes, respectively. The desired properties for the proposed applications such as improving water solubility, red shifting of the absorption band, and decreased fluorescence and enhanced singlet oxygen quantum yields were successfully achieved. The results obtained demonstrate that these BODIPY derivatives are suitable for these applications.

The functionalization of AuNRs to the aniline BODIPY significantly improved the physicochemical properties of this dye for APDT purposes. The singlet oxygen quantum yield was increased from 0.64 to 0.76. The solvent variation studies also showed that the fluorescence and absorption spectrum are independent of the solvent polarity. Furthermore, the quaternized BODIPY dye derivatives also showed improved water solubility. On the other hand, the addition of the styryl group significantly shifted the maximum of the absorption band to longer wavelength. Attaching a pyrene moiety as a substituent to the styryl in the 3, 5-positions of BODIPY dye 5 (in Chapter 3) resulted in an optical limiting response at 532 nm with fairly good γ and $(I_m[\chi^{(3)}])$ values. However, embedding these dye to PBC improved the optical properties of these dyes significantly due to aggregation. In addition, attachment of

phenol groups to the styryl as a substituent resulted in even better results in solution. The data obtained for all of the BODIPY dyes studied for NLO demonstrate that these dyes have potential candidates for optical limiting where the second harmonic of Nd/YAG lasers is concerned.

6.2. *Future prospects*

Although, the physicochemical properties of BODIPY 3 (in Chapter 3) were greatly improved, there is still a need to improve the spectroscopic properties of this dye. The improved spectroscopic properties include a red shift of the absorption band to longer wavelength. On the other hand, the aggregation observed in the quaternized BODIPY dyes may limit their utility for APDT, since this results in a decrease of the singlet oxygen quantum yield. Therefore, attachment of larger groups like polymers may be required. Red shifting of the absorption band may also be a necessity for these dyes. Furthermore, the concentration of the distyryl derivatives studied for NLO should be kept constant so that a better comparison can be made to study the effect of concentration, solvent and the substituents on the BODIPY core.

REFERENCES

1. M. Maeda, *Laser Dyes*, Academic Press, Tokyo, 1984.
2. F. P. Schäfer, *Dye Lasers*, 3rd Ed., Springer-Verlag, Berlin, 1990.
3. A. P. de Silva, H. Q. N. Gunaratne, T. Gunnlaugsson, A. J. M. Huxley, C. P. McCoy, J. T. Rademacher, T. E. Rice, *Chem. Rev.*, 97 (1997) 1515.
4. B. Valeur, I. Leray, *Coord. Chem. Rev.*, 205 (2000) 3.
5. K. Rurack, U. Resch-Genger, *Chem. Soc. Rev.*, 31 (2002) 116.
6. H. Zollinger, *Color Chemistry*, 3rd Ed., Wiley-VCH, Zurich, 2003.
7. J. R. Lakowicz, *Principles of Fluorescence Spectroscopy*, 3rd Ed., Springer, Singapore, 2006.
8. M. Alexiades-Armenakas, *Clin. Dermatol.*, 24 (2006) 16.
9. M. Bhatti, A. MacRobert, S. Meghji, B. Henderson, M. Wilson, *Photochem. Photobiol.*, 68 (1998) 370.
10. T. Ito, K. Kobayashi, *Photochem. Photobiol.*, 25 (1977) 399.
11. R. F. Donnelly, P. A. McCarron, M. M Tunney, *Microbiol. Res.*, 163 (2008) 1.
12. L. W. Tutt, T. F. Boggess, *Prog. Quantum Electron.*, 17 (1993) 299.
13. Y. Barkana, M. Belkin, *Surv. Ophthalmol.*, 44 (2000) 459.
14. A. T. Byrne, A. E. O'Connor, M. Hall, J. Murtagh, K. O'Neill, K. M. Curran; K. Mongrain, J. A. Rousseau, R. Lecomte, S. McGee, J. J. Callanan, D. F. O'Shea, W. M. Gallagher, *B. J. Cancer.*, 101 (2009) 1565; (b) H. He, P.C. Lo, S.L. Yeung, W.P. Fong, D. K. P. Ng, *J. Med. Chem.*, 54 (2011) 3097; (c) A. Gorman, J. Killoran, C. O'Shea, T. Kenna, W. M. Gallagher, D. F. O'Shea, *J. Med Chem.*, 54 (2011) 3097.
15. (a) R. Ziessel, G. Ulrich, A Harriman, *New J. Chem.*, 31 (2007), 496; (b) A. Loudet, K. Burgess, *Chem Rev.*, 107 (2007), 4891.

16. A. Treibs, F.-H. Kreuzer, *Lieb. Ann. Chem.*, 718, (1968), 208.
17. K. Yamada, T. Toyota, K. Takakura, M. Ishimaru, T. Sugawara, *New J. Chem.*, 25, (2001), 667.
18. J. Karolin, L. B.-A. Johansson, L. Strandberg, T. Ny, *J. Am. Chem. Soc.*, 116 (1994) 7801.
19. F. López Arbeloa, T. L. Arbeloa, I. L. Arbeloa, *J. Photochem. Photobiol.*, 3 (1999) 35.
20. R. Y. Lai, A. J. Bard, *J. Phys. Chem. B*, 107 (2003) 5036.
21. Z. Shen, H. Röhr, K. Rurack, H. Uno, M. Spieles, B. Schulz, G. Reck, N. Ono, *Chem. Eur. J.*, 10 (2004) 4853.
22. W. Qin, M. Baruah, M. Van der Auweraer, F.C. De Schryver, N. Boens, *J. Phys. Chem. A*, 109 (2005) 7371.
23. A. D. Quartorolo, N. Russo, E. Sicilia, *Chem. Eur. J.*, 12 (2006) 6797.
24. S. Badré, V. Monnier, R. Méallet-Renault, C. Dumas-Verdes, E. Y. Schmidt, B. A. Trofimov, R. B. Pansu, *J. Photochem. Photobiol. A*, 183 (2006) 238.
25. A. Cui, X. Peng, J. Fan, X. Chen, Y. Wu, B. Guo, *J. Photochem. Photobiol. A*, 186 (2007) 85.
26. T. G. Pavlopoulos, M. Shah, J. H. Boyer, *Appl. Opt.*, 27 (1988) 4998.
27. M. Shah, K. Thangaraj, M.-L. Soong, L. T. Wolford, J. H. Boyer, I. R. Politzer, T. G. Pavlopoulos, *Heteroat. Chem.*, 1 (1990) 389.
28. T. G. Pavlopoulos, J. H. Boyer, M. Shah, K. Thangaraj, M.-L. Soong, *Appl. Opt.*, 29 (1990) 3885.
29. J. H. Boyer, A. M. Haag, G. Sathyamoorthi, M.-L. Soong, K. Thangaraj, T. G. Pavlopoulos, *Heteroat. Chem.*, 4 (1993) 39.
30. Y. Assor, Z. Burshtein, S. Rosenwaks, *Appl. Opt.*, 37 (1998) 4914.
31. M. S. Mackey, W. N. Sisk, *Dyes Pigments*, 51 (2001) 79.

32. G. Jones II, O. Klueva, S. Kumar, D. Pacheco, *Int. Soc. Opt. Eng.*, 4267 (2001) 24.
33. T. G. Pavlopoulos, M. Shah, J. H. Boyer, *Appl. Opt.*, 27 (1988) 4998.
34. M. Shah, K. Thangaraj, M.-L. Soong, L. T. Wolford, J. H. Boyer, I. R. Politzer, T. G. Pavlopoulos, *Heteroat. Chem.*, 1 (1990) 389.
35. T. G. Pavlopoulos, J. H. Boyer, M. Shah, K. Thangaraj, M-L. Soong, *Appl. Opt.*, 29 (1990) 3885.
36. J. H. Boyer, A. M. Haag, G. Sathyamoorthi, M.-L. Soong, K. Thangaraj, T. G. Pavlopoulos, *Heteroat. Chem.*, 4 (1993) 39.
37. I. D. Johnson, H. C. Kang, R. P. Haugland, *Anal. Biochem.*, 198 (1991) 228.
38. M. L. Metzker, J. Lu, R. A. Gibbs, *Science*, 271 (1996) 1420.
39. S. A. Farber, M. Pack, S.-Y. Ho, I. D. Johnson, D. S. Wagner, R. Dosch, M. C. Mullins, H. S. Hendrickson, E. K. Hendrickson, M E. Halpern, *Science*, 292 (2001) 1385.
40. R. Reents, M. Wagner, J. Kulhmann, H. Waldmann, *Angew. Chem. Int. Ed.*, 43 (2004) 2711.
41. C. Sun, J. Yang, L. Li, X. Wu, Y. Liu, S. Liu, *J. Chromatogr. B*, 203 (2004) 173.
42. L. Gai, J. Mack, H. Lu, H. Yamada, G. Lai, Z. Li, Z. Shen, *Chem. Eur. J.*, 20 (2014) 109.
43. T. Werner, C. Huber, S. Heinl, M. Kollmannsberger, J. Daub, O. S. Wolfneis, *Fresenius J. Anal. Chem.*, 359 (1997) 150.
44. M. Baruah, W. Qin, N. Basaric, W. M. De Borggraeve, N. Boens, *J. Org. Chem.*, 70 (2005) 4152.
45. M. Baruah, W. Qin, C. Flors, J. Hofkens, R. A. L. Vallée, D. Beljonne, M. Van der Auweraer, W. M. De Borggraeve, N. Boens, *J. Phys. Chem. A*, 110 (2006) 5998.
46. H. Sunahara, Y. Urano, H. Kojima, T. Pagano, *J. Am. Chem. Soc.*, 129 (2007) 5597.

47. Y. Ando, S. Iino, J. Yamada, K. Umezawa, N. Iwasawa, D. Citterio, K. Suzuki, *Sensors Actuators B*, 121 (2007) 74.
48. K. Rurack, M. Kollmannsberger, U. Resch-Genger, J. Daub, *J. Am. Chem. Soc.*, 122 (2000) 968.
49. A. Coskun, B. T. Baytekin, E. U. Akkaya, *Tetrahedron Lett.*, 44 (2003) 5649.
50. C. Goze, G. Ulrich, L. Charbonnière, M. Cesario, T. Prangé, R. Ziessel, *Chem. Eur. J.*, 9 (2003) 3748.
51. Y. Gabe, Y. Urano, K. Kikuchi, H. Kojima, T. Nagano, *J. Am. Chem. Soc.*, 126 (2004) 3357.
52. R. Méallet-Renault, R. Pansu, S. Amigoni-Gerbier, C. Larpent, *Chem. Commun.*, (2004) 2344.
53. S. Y. Moon, N. R. Cha, Y. H. Kim, S-K. Chang, *J. Org. Chem.*, 69 (2004) 181.
54. H. Koutaka, J. Kosuge, N. Fukasaku, T. Hirano, K. Kikuchi, Y. Urano, H. Kojima, T. Nagano, *Chem. Pharm. Bull.*, 52 (2004) 700.
55. J. L. Bricks, A. Kovalchuk, C. Trieflinger, M. Nofz, M. Büschel, A. I. Tomalchev, J. Daub, K. Rurack, *J. Am. Chem. Soc.*, 127 (2005) 13522.
56. K. Yamada, Y. Nomura, D. Citterio, N. Iwasawa, K. Suzuki, *J. Am. Chem. Soc.*, 127 (2005) 6956.
57. N. Basaric, M. Baruah, W. Qin, B. Metten, M. Smet, W. Dehaen, N. Boens, *Org. Biomol. Chem.*, 3 (2005) 2755.
58. T. Kálai, K. Hideg, *Tetrahedron*, 62 (2006) 10352.
59. J. Bañuelos, L. Arbeloa, T. Arbeloa, V. Martinez, I. L. Arbeloa, *Applied Science Innovations Pvt. Ltd.*, (2012) 641. [<http://www.applied-science-innovations.com/CHAPTER-19.pdf>]
60. Y. W. Wang, A. B. Descalzo, Z. Shen, X. Z. You, K. Rurack, *Chem. Eur. J.*, 16 (2010) 2887.

61. N. Boens, V. Leen, W. Dehaen, *Chem. Soc. Rev.*, 41 (2012) 1130.
62. G. Ulrich, R. Ziessel, A. Harriman, *Angew. Chem. Int. Ed.*, 47 (2008) 1184.
63. K. Tram, H. Yan, H. A. Jenkins, S. Vassiliev, D. Bruce, *Dyes Pigments*, 82 (2009) 392.
64. I. J. Arroyo, R. Hu, G. Merino, B. Z. Tang, E. Pena-Cabrera, *J. Org. Chem.*, 74 (2009) 5719.
65. A. Schmitt, B. Hinkeldey, M. Wild, G. Jung, *J. Fluoresc.*, 19 (2009) 755.
66. T. E. Wood, A. Thompson, *Chem. Rev.*, 107 (2007) 1831-1861.
67. T. V. Goud, A. Tutar, J.-F. Biellmann, *Tetrahedron*, 62 (2006) 5084-5091.
68. (a) A. H. Jackson, R. K. Pandey, K. R. Nagaraja Rao, E. Roberts, *Tetrahedron Lett.*, 26 (1985) 793-796; (b) S. E. Bari, J. Iturraspe, B. Frydman, *Tetrahedron*, 51 (1995) 2255-2266.
69. L. J. Jiao, J. L. Li, S. Z. Zhang, C. Wei, E. H. Hao, M. G. H. Vicente, *New J. Chem.*, (2009) 33, 1888.
70. T. Uppal, X. K. Hu, F. R. Fronczek, S. Maschek, P. Bobadova-Parvanova, M. G. H. Vicente, *Chem. Eur. J.*, 18 (2012) 3893.
71. L. J. Jiao, C. J. Yu, T. Uppal, M. M. Liu, Y. Li, Y. Y. Zhou, E. H. Hao, X. K. Hu, M. G. H. Vicente, *Org. Med. Chem. Lett.*, 8 (2010) 2517.
72. A. Loudet, Y. Ueno, L. Wu, J. Jose, J. R. Barhoumi, R. Burghardt, K. Burgess, *Bioorg. Med. Chem. Lett.*, 21 (2011) 1849.
73. N. Boens, V. Leen, W. Dehaen, *Chem. Soc. Rev.*, 41 (2012) 8212.
74. M. Baruah, W. W. Qin, C. Flors, J. Hofkens, R. A. L. Vallee, D. Beljonne, M. Van der Auweraer, W. M. De Borggraeve, N. Boens, *J. Phys. Chem. A*, 110 (2006) 5998.
75. T. Yogo, Y. Urano, Y. Ishitsuka, F. Maniwa, T. Nagano, *J. Am. Chem. Soc.*, 127 (2005) 12162.
76. S. Atilgan, Z. Ekmekci, A. L. Dogan, D. Guc, E. U. Akkaya, *Chem. Commun.*, (2006) 4398.

77. J. Murtagh, D. O. Frimannsson, D. F. O'Shea, *Org. Lett.*, 11 (2009) 5386.
78. K. Rurack, M. Kollmannsberger, J. Daub, *Angew. Chem. Int. Ed.*, 40 (2001) 385.
79. W. L. Zhao, E. M. Carreira, *Angew. Chem. Int. Ed.*, 44 (2005) 1677.
80. L. Li, B. Nguyen, K. Burgess, *Bioorg. Med. Chem. Lett.*, 18 (2008) 3112.
81. S. L. Niu, G. Ulrich, R. Ziessel, A. Kiss, P.-Y. Renard, A. Romieu, *Org. Lett.*, 11 (2009) 2049.
82. H. J. Worries, J. H. Koek, G. Lodder, J. Lugtenburg, R. Fokkens, O. Driessen, G. R. Mohn, *J. R. Neth. Chem. Soc.*, 104 (1985) 288.
83. T. Yogo, Y. Urano, Y. Ishitsuka, F. Maniwa, T. Nagano, *J. Am. Chem. Soc.*, 127 (2005) 12162.
84. C. Goze, G. Ulrich, M. L. J. Mallon, B. D. Allen, A. Harriman, R. Ziessel, *J. Am. Chem. Soc.*, 128 (2006) 10231.
85. G. Ulrich, C. Goze, M. Guardigli, A. Roda, R. Ziessel, *Angew. Chem. Int. Ed.*, 44 (2005) 3694.
86. T. Rohand, W. Qin, N. Boens, W. Dehaen, *Eur. J. Org. Chem.*, (2006) 4658.
87. L. J. Jiao, C. J. Yu, J. L. Li, Z. Y. Wang, M. M. Wu, E. H. Hao, *J. Org. Chem.*, 74 (2009) 7525.
88. G. Ulrich, R. Ziessel, A. Harriman, *Angew. Chem. Int. Ed.*, 47 (2008) 1184.
89. G. Ulrich, R. Ziessel, *J. Org. Chem.*, 69 (2004) 2070.
90. S. Zrig, P. Remy, B. Andrioletti, E. Rose, I. Asselberghs, K. Clays, *J. Org. Chem.*, 73 (2008) 1563.
91. L. Wu, A. Loudet, R. Barhoumi, R. C. Burghardt, K. Burgess, *J. Am. Chem. Soc.*, 131 (2009) 9156.
92. I. Moczar, P. Huszthy, Z. Maidics, M. Kadar, K. Toth, *Tetrahedron*, 65 (2009) 8250.
93. A. Gossauer, F. Nydegger, T. Kiss, R. Slezniak, H. Stoeckli-Evans, *J. Am. Chem. Soc.*, 126 (2004) 1772.

94. S. L. Niu, C. Massif, G. Ulrich, R. Ziesel, P.-Y. Renard, A. Romieu, *Org. Biomol. Chem.*, 9 (2011) 66.
95. C. Thivierge, R. Bandichhor, K. Burgess, *Org. Lett.*, 9 (2007) 2135.
96. B. Raymer, M. Kavana, A. Price, B. Wang, L. Corcoran, R. Kulathila, J. Groarke, T. Mann, *Bioorg. Med. Chem. Lett.*, 19 (2009) 2804.
97. S. O. McDonnell, D. F. O'Shea, *Org. Lett.*, 8 (2006) 3493.
98. V. F. Donyagina, S. Shimizu, N. Kobayashi, E. A. Lukyanets, *Tetrahedron Lett.*, 49 (2008) 6152.
99. G. Ulrich, S. Goeb, A. De Nicola, P. Retailleau, R. Ziesel, *J. Org. Chem.*, 76 (2011) 4489.
100. Z. Shen, H. Rohr, K. Rurack, H. Uno, M. Spieles, B. Schulz, G. Reck, N. Ono, *Chem. Eur. J.*, 10 (2004) 4853.
101. M. Wada, S. Ito, H. Uno, T. Murashima, N. Ono, T. Urano, Y. Urano, *Tetrahedron Lett.*, 42 (2001) 6711.
102. L. Bonardi, G. Ulrich, R. Ziesel, *Org. Lett.*, 10 (2008) 2183.
103. Y. Ni, W. Zeng, K.-W. Huang, J. Wu, *Chem. Commun.*, 49 (2013) 1217.
104. C. C. Zhao, Y. Zhou, Q. N. Lin, L. Y. Zhu, P. Feng, Y. L. Zhang, J. A. Cao, *J. Phys. Chem. B*, 115 (2011) 642.
105. A. Harriman, G. Izzet, R. Ziesel, *J. Am. Chem. Soc.*, 128 (2006) 10868.
106. C. Goze, G. Ulrich, R. Ziesel, *J. Org. Chem.*, 72 (2007) 313.
107. Funda Yükrük, *PhD thesis*, Middle East Technical University, 2005.
108. F. L. Arbeloa, J. Bañuelos, V. Martínez, T. Arbeloa, I. L. Arbeloa, *Int. Rev. Phys. Chem.*, 24 (2005) 339.
109. F. L. Arbeloa, T. L. Arbeloa, I. L. Arbeloa, I. García-Moreno, A. Costela, R. Sastre, F. Amat-Guerri, *Chem. Phys.*, 236 (1998) 331.

110. J. Bañuelos, F. L. Arbeloa, V. Martínez, I. L. Arbeloa, *Chem. Phys.*, 296 (2004) 13.
111. S. Frey-Forgues, D. Lavabre, *J. Chem. Ed.*, 76 (1999) 1260.
112. R. F. Kubin, A. N. Fletcher. *J. Luminesc.*, 27 (1982) 455.
113. A. Ogunsipe, J. Y. Chen, T. Nyokong, *New J. Chem.*, 28 (2004) 822.
114. C.D Geddes, J.R. Lakowicz, in *Topics in Fluorescence Spectroscopy*, Springer, New York, 2005.
115. T. G. Pavlopoulos, *Prog. Quantum Elect.*, 26 (2002) 193.
116. F. P. Schäfer, *Dye Lasers*, 3rd Ed., Springer-Verlag, Berlin, 1990.
117. A. A. Gorman, I. Hamblett, T. A. King, M. D. Rahn, *J. Photochem. Photobiol.*, 130 (2000) 127.
118. L. Jiao, W. Pang, J. Zhou, Y. Wei, X. Mu, G. Bai, E. Hao. *J. Org. Chem.*, 76 (2011) 9988
119. I. Seotsanyana-Mokhosi, T. Nyokong, *J. Porphyrins Phthalocyanines*, 8 (2004) 1214.
120. A. O. Ogunsipe, T. Nyokong, *J. Porphyrins Phthalocyanines*, 9 (2005) 121.
121. R. W. Redmond, J. N. Gamlin. *Photochem. Photobiol.*, 70 (1999) 391.
122. J. Rosenthal, S. J. Lippard, *J. Am. Chem. Soc.*, 132 (2010) 5536.
123. J.-Y. Liu, M. E. El-Khouly, S. Fukuzumi; D. K. P. Ng, *Chem. Eur. J.*, 17 (2011) 1605.
124. G. Jori, S. B. Brown, *Photochem. Photobiol. Sci.*, 3 (2004) 403.
125. G. Jori, C. Fabris, M. Soncin, S. Ferro, O. Coppellotti, D. Dei, L. Fantetti, G. Chiti, G. Roncucci, *Lasers Surg. Med.*, 38 (2006) 468.
126. D. A. Caminos, M. B. Spesia, P. Pons, E. N. Durantini, *Photochem. Photobiol. Sci.*, 7 (2008) 1071.
127. M. Wainwright, *J. Antimicrob. Chemother.*, 42 (1998) 13.
128. P. W. Taylor, P. D. Stapleton, J. P. Luzio, *Drug Discov. Today*, 7 (2002) 1086.
129. B. Bagchi, S. Basu, *Photochem. Photobiol.*, 29 (1979) 403.

130. M. Bhatti, A. MacRobert, S. Meghji, B. Henderson, M. Wilson, *Photochem. Photobiol.*, 68 (1998) 370.
131. T. Ito, K. Kobayashi, *Photochem. Photobiol.*, 25 (1977) 399.
132. R. F. Donnelly, P. A. McCarron, M. M. Tunney, *Microbiol. Res.*, 163 (2008) 1.
133. F. H. E. Schagen, A. C. E. Moor, S. C. Cheong, S. J. Cramer, H. Ormond, A. J. Eb, T. M. A. R. Dubbelman, R. C. Hoeben, *Gene Ther.*, 6 (1999) 873.
134. A. N. Vzorov, D. W. Dixon, J. S. Trommel, L. G. Marzilli, R. W. Compans, *Antimicrob. Agents Chemother.*, 46 (2002) 3917.
135. L. Latos-Grazynski, J. Lisowski, M. M. Olmstead, A. L. Balch, *Inorg. Chem.*, 28 (1989) 1183.
136. F. D'Souza, P. M. Smith, M. E. Zandler, A. L. McCarty, M. Itou, Y. Araki, O. Ito, *J. Am. Chem. Soc.*, 126 (2004) 7898; (b) A. de la Escosura, M. V. Martínez-Díaz, D. M. Guldi, T. Torres, *J. Am. Chem. Soc.*, 128 (2006) 4112; (c) A. Gouloumis, D. González-Rodríguez, P. Vázquez, T. Torres, S. Liu, L. Echegoyen, J. Ramey, G. L. Hug and D. M. Guldi, *J. Am. Chem. Soc.*, 128 (2006) 12674.
137. H. Lu, Z. Xue, J. Mack, Z. Shen, X. You, N. Kobayashi, *Chem. Commun.*, 46 (2010) 3565.
138. J. H. Boyer, A. M. Haag, G. Sathyamoorthi, M. L. Soong, K. Thangaraj, *Heteroat. Chem.*, 4 (1993) 39.
139. E. Paszko, C. Ehrhardt, D. P. Kelleher, J. V. Reynolds, *Photodiagnosis Photodyn. Ther.*, 8 (2011) 14.
140. L. Li, J. Han, B. Nguyen, K. Burgess, *J. Org. Chem.*, 73 (2008) 1963.
141. T. Bura, R. Ziesel, *Org. Lett.*, 13 (2011) 3072.
142. S. Atilgan, Z. Ekmecki, A.L. Dogan, D. Guc, E.U. Akkaya, *Chem. Commun.*, 42 (2006) 4398.

143. H. He, P.-C. Lo, S.-L. Yeung, W.-P. Fong, D. K. P. Ng, *J. Med. Chem.*, 54 (2011) 3097.
144. E. Caruso, S. Banfi, P. Barbieri, B. Leva, V. T. Orlandi, *J. Photochem. Photobiol. B*, 114 (2012) 44.
145. A. Gorman, J. Killoran, C. O'Shea, T. Kenna, W. M. Gallagher, D. F. O'Shea, *J. Am. Chem. Soc.*, 126 (2004) 10619.
146. T. Yogo, Y. Urano, Y. Ishitsuka, F. Maniwa, T. Nagano, *J. Am. Chem. Soc.*, 127 (2005) 12162.
147. S. Atilgan, Z. Ekmekci, A. L. Dogan, D. Guc, E. U. Akkaya, *Chem. Commun.*, (2006) 4398.
148. *IUPAC Compendium of Chemical Terminology*, Vol. 68, A. D. McNaught, A. Wilkinson (Eds.), Blackwell Scientific Publications, Oxford, UK, 2nd Ed., 1997, p 2245.
149. D. Bechet, P. Couleaud, C. Frochot, M.-L. Viriot, F. Guillemin, F. Barberi-Heyob, *Cell Press.*, 26 (2008) 612.
150. S. E. Choi, S. Sohn, J. W. Cho, E. A. Shin, P. S. Song, P. Kang, *J. Photochem. Photobiol. B*, 73 (2004) 101.
151. S. L. Haywood-Small, D. I. Vernon, J. Griffiths, J. Schofield, S. B. Brown, *Biochem. Biophys. Res. Comm.*, 339 (2006) 569.
152. E. Paszko, C. Ehrhardt, D. P. Kelleherd, J. V. Reynolds, *Photodiagn. Photodyn. Ther.*, 8 (2011) 14.
153. P. Calzavara-Pinton, M. Rossi, R. Sala, M. Venturini, *Photochem. Photobiol.*, 88 (2012) 512.
154. A. Rai, A. Prabhune, C. C. Perry, *J. Mater. Chem.*, 20 (2010) 6789.
155. P. Maillard, S. Gaspard, J. L. Guerquin-Kern, M. Momenteau, *J. Am. Chem. Soc.*, 111 (1989) 9125.

156. C.-F. Choi, J.-D. Huang, P.-C. Lo, W. P. Fong, D. K. P. Ng, *Org. Biomol. Chem.*, 6 (2008) 2173.
157. D. Dini, M. Hanack, in *The Porphyrin Handbook: Physical Properties of Phthalocyanine-Based Materials*, Vol. 17, K. M. Kadish, K. M. Smith, R. Guilard (Eds.), Academic Press, USA, (2003) pp. 1-36.
158. D. Young, *Computational Chemistry: A Practical Guide for Techniques to Real World Problems*, John Wiley and Sons, 2001.
159. Y. Barkana, M. Belkin, *Surv. Ophthalmol.*, 44 (2000) 459.
160. S. R. Marder, J. E. Sohn, G. D. Stucky, *Materials for Nonlinear Optics*, American Chemical Society, Washington, DC (1991), p. 71.
161. P. de la Torre, F. Vázquez, T. Agulló-López, T. Torres, *J. Mater. Chem.*, 8 (1998) 1671.
162. Q. Zheng, G. S. He, P. N. Prasad, *Chem. Phys. Lett.*, 475 (2009) 250.
163. P.-A. Bouit, K. Kamada, P. Feneyrou, G. Berginc, L. Toupet, O. Maury, C Andraud, *Adv. Mater.*, 21 (2009) 1151.
164. D. Potamianos, P. Giannakopoulou, A. Kaloudi-Chantzea, G. Pistolis, S. Couris, Third-order Nonlinear Optical Properties of Some Novel BODIPYs, Transparent Optical Networks (ICTON), IEEE Xplore Digital Library, 16th International Conference, 2014.
165. M. Zhu, *J. Polym. Sci. A*, 46 (2008) 7401.
166. M. Sheik-Bahae, A. A Said, E. W. Van Stryland, *Opt. Lett.*, 14 (1989) 955.
167. M. Sheik-Bahae, A. A. Said, T.-H. Wei, D. J. Hagan, E. W. Van Stryland, *IEEE J. Quantum Electron.*, 26 (1990) 760.
168. *Characterization Techniques and Tabulations for Organic Nonlinear Materials*, E. W. Van Stryland, M. Sheik-Bahae, M. G. Kuzyk, C. W. Dirk (Eds.), Marcel Dekker, Inc., 1998, pp. 655-692.

169. *Handbook of Nonlinear Optics*, 2nd Ed., R. L. Sutherland, D. G. Mclean, S. Kirkpatrick, (Eds.), Marcel Dekker, Inc., 2003.
170. D. Dini, M. Barthel, M. Hanack, *Eur. J. Org. Chem.*, (2000) 3759.
171. V. Chauke, M. Durmuş, T. Nyokong, *J. Photochem. Photobiol. A*, 192 (2007) 179.
172. J. Simon, C. Sirlin, *Pure Appl. Chem.*, 61 (1989) 1625.
173. M. Baruah, W. Qin, N. Basaric, W. M. De Borggraeve, N. Boens, *J. Org. Chem.*, 70 (2005) 4152.
174. B. N. Achar, G. M. Fohlen, J. A. Parker, J. Keshavayya, *Polyhedron*, 6 (1987) 1463.
175. K. A. Kozek, K. M. Kozek, W. Wu, S. R. Mishra, J. B. Tracy, *Chem. Mater.*, 25 (2013) 4537.
176. M. E. Wieder, D. C. Hone, M. J. Cook, M. M. Handsley, J. Gavrilovic, D. A. Russell, *Photochem. Photobiol. Sci.*, 5 (2006) 727.
177. E. Caruso, S. Banfi, P. Barbieri, B. Leva, V. T. Orlandi, *J. Photochem. Photobiol. B*, 114 (2012) 44.
178. H. He, P.-C. Lo, S.-L. Yeung, W.-P. Fong, D. K. P. Ng, *J. Med. Chem.*, 54 (2011) 3097.
179. S. Zhu, N. Dorh, J. Zhang, G. Vegesna, H. Li, F-T. Luo, A. Tiwari, H. Liu, *J. Mater. Chem.*, 22 (2012) 2781.
180. G. Meng, S. Velayudham, A. Smith, R. Luck, H. Y. Liu, *Macromolecules*, 42 (2009) 1995.
181. F. M. Veronese, G. Pasut, *Drug Discov. Today*, 10 (2005) 1451.
182. M. Durmuş, A. Erdögmus, A. Ogunsipe, T. Nyokong, *Dyes Pigments*, 82 (2009) 244.
183. D. C. Hone, P. I. Walker, R. Evans-Gowing, S. Fitzgerald, A. Beeby, I. Chambrier, M. J. Cook, D. A. Russell, *Langmuir*, 18 (2002) 2985.
184. K. Heister, M. Zharnikov, M. Grunze, *Langmuir*, 17 (2001) 8.
185. Y. W. Yang, L. J. Fan, *Langmuir*, 18 (2002) 1157.

186. (a) H. Lu, S. S. Zhang, H. Z. Liu, Y. W. Wang, Z. Shen, C. G. Liu, X. Z. You, *J. Phys. Chem. A*, 113 (2009) 14081; (b) T. Matsumoto, Y. Urano, T. Shoda, H. Kojima, T. Nagano, *Org. Lett.*, 9 (2007) 3375; (c) T. Ueno, Y. Urano, H. Kojima, T. Nagano, *J. Am. Chem. Soc.*, 128 (2006) 10640.
187. S. Vukovic, S. Corni, B. Mennucci, *J. Phys. Chem. C*, 113 (2009) 121.
188. M. Camur, V. Ahsen, M. Durmuş, *J. Photochem. Photobiol. A*, 219 (2011) 217.
189. F. Odobel, H. Zabri, *Inorg. Chem.*, 44 (2005), 5600.
190. E. Vos de Wael, J. A. Pardoën, J. A. Van Koeveringe, J. Lugtenburg, *Recl. Trav. Chim. Pays-Bas*, 96 (1977) 306.
191. M. Kollmannsberger, K. Rurack, U. Resch-Genger, J. Daub, *J. Phys. Chem. A*, 102 (1998) 10211.
192. T. L. Arbeloa, F. L. Arbeloa, I. L. Arbeloa, I. García-Moreno, A. Costela, R. Sastre, F. Amat-Guerri, *Chem. Phys. Lett.*, 299 (1999) 315.
193. A. Costela, I. García-Moreno, R. Gomez, C. Sastre, F. Amat-Guerri, M. Liras, F. L. Arbeloa, J. B. Prieto, I. L. Arbeloa, *J. Phys. Chem. A*, 106 (2002) 7736.
194. F. L. Arbeloa, J. B. Prieto, V. M. Martínez, T. A. López, I. L. Arbeloa, *Chem. Phys. Chem.*, 5 (2004) 1762.
195. J. B. Prieto, F. L. Arbeloa, V. M. Martínez, T. A. López, F. Amat-Guerri, M. Liras, I. L. Arbeloa, *Chem. Phys. Lett.*, 385 (2004) 29.
196. W. Qin, M. Baruah, A. Stefan, M. Van der Auweraer, N. Boens, *Chem. Phys. Chem.*, 6 (2005) 2343.
197. S. A. Hambir, D. Wolfe, G. J. Blanchard, G. L. Baker, *J. Am. Chem. Soc.*, 119 (1997) 7367.
198. A. Ortiz, B. Insuasty, M. R. Torres, M. R. Herranz, N. M. A. Herranz, N. Martin, R. Viruela, *Eur. J. Org. Chem.*, 1 (2008) 99.

199. S. R. Marder, D. N. Beratan, L. T. Cheng, *Science*, 252 (1991) 103.
200. R. L. Sutherland, *Handbook of Nonlinear Optics*, 2nd Edn, Marcel Dekker, New York, 2003.
201. L. W. Tutt, T. F. Boggess, *Prog. Quant. Electr.*, 17 (1993) 299.
202. G. de la Torre, P. Vázquez, F. Agulló-López, T. Torres, *Chem. Rev.*, 104 (2004) 3723.
203. B. E. A. Saleh, M. C. Teich, *Fundamentals of Photonics*, Wiley, New York, 1991.
204. J. Britton, C. Litwinski, E. Antunes, M. Durmuş, V. Chaukea, T. Nyokong, *J. Macromol. Sci. A*, 50 (2013) 110.
205. E. M. Antunes, T. Nyokong, *J. Porphyrins Phthalocyanines*, 13 (2009) 153.
206. D. Dini, M. Hanack, in *The Porphyrin Handbook*, K. M. Kadish, K. M. Smith, R. Guilard (Eds.), Academic Press, 1999, pp. 22-31.
207. R. W. Redmond, J. N. Gamlin, *Photochem. Photobiol.*, 70 (1999) 391.
208. T. Pritchett, in *Sensors and Electron Devices Directorate*, ARL, 2002, pp. 1-2.
209. S. H. Guang, R. Gvishi, P. N. Prasad, B. A. Reinhardt, *Opt. Commun.*, 117 (1995) 133.
210. S. G. Frank, *J. Pharm. Sci.*, 64 (1974) 1585.
211. I. Goldberg, in *Complexes of Crown Ethers with Molecular Guests: Inclusion Compounds*, Vol. 2, J. L. Atwood, J. E. D. Davies, D. D. MacNicol (Eds.), Academic Press, London, pp. 261-335.
212. B. Dietrich, in *Cryptate complexes: inclusion compounds*, Vol. 2, J. L. Atwood, J. E. D. Davies, D. D. MacNicol (Eds.), Academic Press, London, 1984, pp. 337-405.
213. M. A. Villiers, *Acad. Sci.*, 111 (1891) 536.
214. D. French, *Adv. Carbohydr. Chem.*, 12 (1957) 189.

215. W. Saenger, in *Structural aspects of cyclodextrins and their inclusion complexes: Inclusion compounds*, Vol. 2, J. L Atwood, J. E. D. Davies, D. D. MacNicol (Eds), Academic Press, London, 1984, pp. 231-259.
216. J. Szejtli, *Cyclodextrins and their Inclusion Complexes*, Akademiai Kiado, Budapest, 1982.
217. M. L. Bender, M. Komiyama, *Cyclodextrin Chemistry*, Springer, Berlin, 1978.
218. A. Ueno, *Supramol. Sci.*, 3 (1996) 31.
219. J. Bügler, J. F. J. Engbersen, D. N. Reinhoudt, *J. Org. Chem.*, 63 (1998) 5339.
220. D. D. Perrin, W. F. L. Armarego, *Purification of Laboratory Chemicals*, 3rd Ed., Pergamon Press, Oxford, 1989.
221. A. M. Groth, L. F. Lindoy, G. V. Meehan, *J. Chem. Soc.*, (1996) 1553.
222. Y. Xu, M. Guo, X. Li, A. Molkovski, C. Wedemiotis, Y. Pang, *Chem Commun.*, 47 (2011) 8883.
223. S. Hamai, T. Koshiyama, *J. Photochem. Photobiol. A*, 127 (1999) 135.
224. X. P. Wang, J. H. Pan, W. H. Li, Y. Zhang, *Talanta*, 54 (2001) 805.
225. X. P. Wang, J. H. Pan, S. M. Shuang, *Spectrochim. Acta. A*, 57 (2001) 2755.
226. T. Carofiglio, R. Fornasier, V. Lucchini, C. Rosso, U. Tonellato, *Tetrahedron Lett.*, 37 (1996) 8019.
227. J. S. Manka, D. S. Lawrence, *Tetrahedron Lett.*, 30 (1989) 7341.
228. F. Venema, A. E. Rowan, R. J. M. Nolte, *J. Am. Chem. Soc.*, 118 (1996) 257.
229. S. Hamai, H. Satou, *Spectrochim. Acta A*, 57 (2001) 1745.
230. J. Mosinger, M. Deumie, K. Lang, P. Kubat, D. M. Wagnerova, *J. Photochem. Photobiol. A*, 130 (2000) 13.
231. A. Muiioz de la Peiia, T. Ndou, J. B. Zung, I. M. Wamer, *J. Phys. Chem.*, 95 (1991) 3334.
232. Y. Kusumoto, *Chem. Phys. Lett.*, 136 (1986) 535.

233. T. Yorozu, M. Hoshino, M. Imamura, *J. Phys. Chem.*, 86 (1902) 4426.
234. S. Hamai, T. J. Koshiyama, *Photochem. Photobiol. A*, 127 (1999) 135.
235. X. P. Wang, J. H. Pan, S. M. Shuang, *Spectrochim. Acta A*, 57 (2001) 2755.
236. S. Silva, P. M. R. Pereira, P. Silva, F. A. A. Paz, M. A. F. Faustino, J. A. S. Cavaleiro, J. P. C. Tome, *Chem. Commun.*, 48 (2012) 3608.
237. Y. Dotsikas, Y. L. Loukas, *J. Am. Soc. Mass Spectrom.*, 14 (2003) 1123.
238. K. A. Connors, T. W. Rosanske, *J. Pharm. Sci.*, 69 (1980) 173.
239. K. Kano, I. Takenoshita, T. Ogawa, *Chem. Lett.*, (1980) 1035.
240. F. V. Bright, G. C. Catena, J. Huang, *J. Am. Chem. Soc.*, 112 (1990) 1343.
241. H. Kondo, H. Nakatan, K. Hiromi, *J. Biochem.*, 79 (1976) 393.
242. C. J. Seliskar, L. Brand, *J. Am. Chem. Soc.*, 93 (1971) 5405.
243. G. C. Catena, F. V. Bright, *Anal. Chem.*, 61 (1989) 905.
244. V. Crescenci, A. Gamini, A. Palleshi, R. Rizzo, *Gazz. Chim. Ital.*, 116 (1986) 435.
245. C. A. Haskard, C. J. Easton, B. L. May, S. F. Lincoln, *J. Phys. Chem.*, 100 (1996) 14457.
246. A. Harada, M. Furue, S. Nozakura, *Macromolecules*, 10 (1977) 676.
247. D. J. Jobe, R. E. Verrall, R. Palepu, V. C. Reinsborough, *J. Phys. Chem.*, 92 (1988) 3582.
248. H.-J. Schneider, T. Blatter, S. Simova, *J. Am. Chem. Soc.*, 113 (1991) 1996.
249. N. Sarkar, K. Das, D. Nath, K. Bhattacharyya, *Chem. Phys. Lett.*, 196 (1992) 491.
250. R. Shelli, McAlpine, A. Miguel, Garcia-Garibay, *J. Am. Chem. Soc.*, 120 (1998) 4269.
251. H. F. M. Nelissen, F. Venema, R. M. Uittenbogaard, M. C. Feiters, R. J. M. Nolte, *J. Chem. Soc., Perkin Trans. 2*, (1997) 2045.
252. *Cyclodextrin Fundamentals and Applications*, F. Toda, A. Ueno (Eds.), Sangyo-Tosho, Tokyo, 1995.

253. (a) N. Kobayashi, T. Osa, *Bull. Chem. Soc. Jpn.*, 64 (1991) 1878; (b) N. J. Kobayashi, *Chem. Commun.*, (1988) 918.
254. T. Hannappel, B. Burfeindt, W. Storck, F. Willig, *J. Phys. Chem.*, 101 (1997) 6799.